# JOURNAL OF TELECOMMUNICATIONS AND INFORMATION TECHNOLOGY

## 1/2002

Special issue edited by Józef Modelski

### Part 2

# Editorial Board

# Editorial Advisory Board

# JOURNAL OF TELECOMMUNICATIONS AND INFORMATION TECHNOLOGY

## *Preface*

In this special issue, consisting of two parts, the Reader will find papers, selected from over 180 ones, presented during the *13th International Conference on Microwaves, Radar and Wireless Communications* MIKON-2000, which was held at the Wroclaw Technical University, Wroclaw, Poland on 22–24 May 2000.

The MIKON conference has over 30 years history, however only for the fourth time it was being organised as an biannual international event. The first nine conferences were held under the auspices of Polish Academy of Sciences (PAN) on the national scale, with only a limited number of foreign invited speakers. Initially known as microwave solid state technology conference MECS, in 1983 it was transformed into MIKON. Those nine national conferences created a solid basis for the transforming MIKON into an international conference in 1994. Now it takes place regularly every two years in May in various Polish cities – the biggest research and cultural centres. The MIKON conference has become known as a regional conference in Central and Eastern Europe. The increasing participation of foreign attendees and their papers has resulted in the situation that last year, for the first time, they outnumbered the Polish contributions.

MIKON has been continuously modified and extended, to cover new areas of microwave research and engineering. Due to the fact that telecommunications and radar technology are the principal driving forces behind microwave research, recently MIKON has been transformed into the conference on microwaves, radar, and wireless communications. The MIKON-2000 Technical Program Committee has accepted 168 contributions in all, from 25 countries, mostly from the region of Eastern and Central Europe. We have also heard 20 invited speakers, the world leading experts. Many of the 27 topical sessions were focus on field traditionally addressed at MIKON, such as passive and active components, measurement techniques, CAD and antennas. However, in MIKON-2000 a greater proportion of papers was devoted to radar technology and polarimetry, as well as to microwave and optical communication systems. The strength of the MIKON-2000 was enhanced by covering almost full range of microwave activities from components, devices, systems, and networks up to applications.

The second part of this special issue comprises 12 papers from the areas of microwave active devices and technology, photonics, microwave-lightwave interaction, microwave measurements and CAD for active and passive devices. I hope this volume will find the Reader's interest and will prove to be for practical usage.

Józef Modelski
Guest Editor

# PHEMT transistor models
# for accurate CAD of MMIC amplifiers

Zbigniew Nosal

**Abstract** — **Selected models of PHEMT transistors are presented for the popular Philips D02AH process. The models are based on a set of measurements of transistor parameters and have been verified against measurements of fabricated MMIC amplifiers. The usefulness of particular models for the CAD of microwave circuits is discussed.**

*Keywords* — *monolithic microwave integrated circuits, transistor modeling.*

## 1. Introduction

Accurate modeling of microwave monolithic integrated circuits (MMICs) is very desirable for the reason of high fabrication costs of GaAs circuits. Designers are trying to achieve the "first trial success" to lower costs and accelerate the introduction of new products. Mature and reliable technology and accurate models of circuit components – active devices in particular – are crucial for the achievement of economic goals. The D0AH process from the Philips Microwave Limeil (PML) foundry has proven to provide reliable and repeatable circuits, as our 4 year experience indicates. The models presented here are based on many measurements of individual transistors and complete MMICs [1]. These results may aid other designers to select proper model and to adjust its parameters appropriately. The emphasis has been placed on nonlinear models capable of accurate prediction of intermodulation distortion. The level of the IM products is one of the most important parameters specified for modern telecommunication circuits.

## 2. HEMT transistor models
## for the D02AH process from Philips

Philips foundry provides several models for the PHEMT transistors in the D02AH technology (and the newer version ED02AH) [2]. Small signal linear models are given in the form of tables of circuit parameters versus bias point of a transistor. Nonlinear models are defined by the equations given in the manual as well as models distributed for the Microwave Design System and Cadence CAD systems.

A set of computer programs has been developed at the Institute of Electronic Systems (IES) to implement the linear and nonlinear models defined by the Philips data. The output from these programs provides tables of scattering and noise parameters for particular transistor geometry and selected bias point. Number of MMICs have been designed with these parameters in previous years. The agreement

between design and measurements was reasonably good, when typical bias points were used for transistors.
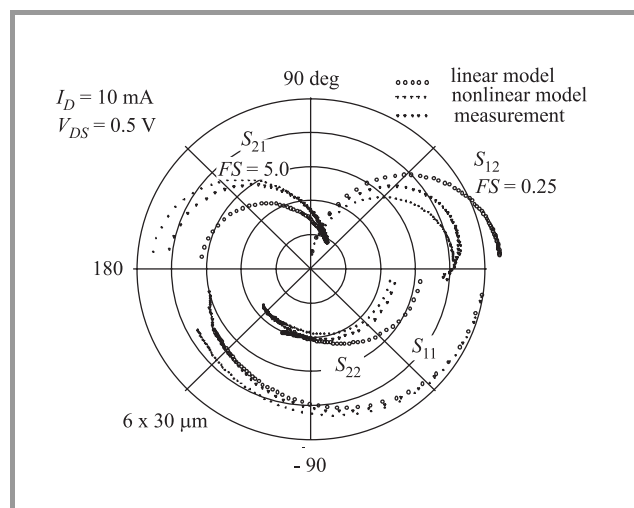


*Fig. 1.* Comparison of PML models of a FET with measurement.

Comparison of data measured for test transistors with the model parameters discloses discrepancies at low and high currents in particular. Typical results for a transistor with 6 gate segments of 30 $\mu$m width each (labeled $6 \times 30$) are shown in Fig. 1 for the bias point $I_D = 10$ mA, $V_{DS} = 0.5$ V. The relative error

$$\delta = \frac{S_{ij\,\text{measured}} - S_{ij\,\text{model}}}{S_{ij\,\text{measured}}}$$

can be as high as 30% at selected frequencies. Similar errors are encountered at low drain currents (below 0.1 $I_{DSS}$). Noise figures of amplifiers designed were typically higher then design by 0.2 dB at a level of 1 dB and as much as 0.5 dB at a level of $NF \approx 3$ dB (for feedback amplifiers). These differences initiated the research into more accurate model definition. The software used for the design of MMICs at the IES is usually the Serenade suite from Ansoft and the models for this software were investigated in more detail.

## 3. Nonlinear microwave FET models
## for the Serenade software

Nonlinear simulator (Microwave Harmonica – M-H) from the Serenade suite of CAD software [3] is implementing several nonlinear models of microwave FETs. Two models

have been selected for further use: a model by Kacprzak and Materka [4] (labeled K-M in subsequent text) and a model from the Triquint foundry [5] – labeled TOM2. These models are known to provide high accuracy in the computation of nonlinear properties of amplifiers (e.g. intermodulation).

General chip model – excluding package – of a microwave FET in the M-H program is shown in Fig. 2. Its internal nonlinear portion is specific to the model used.
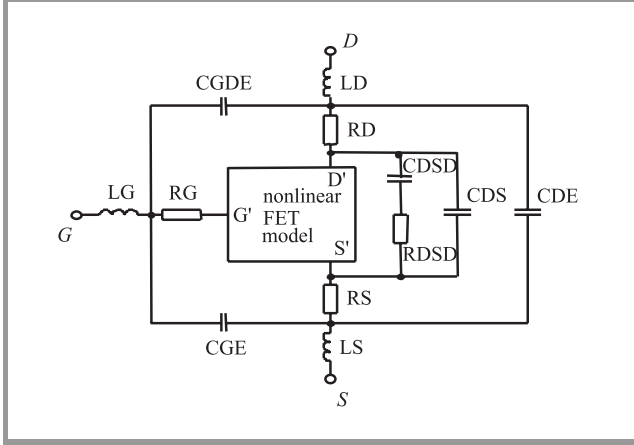


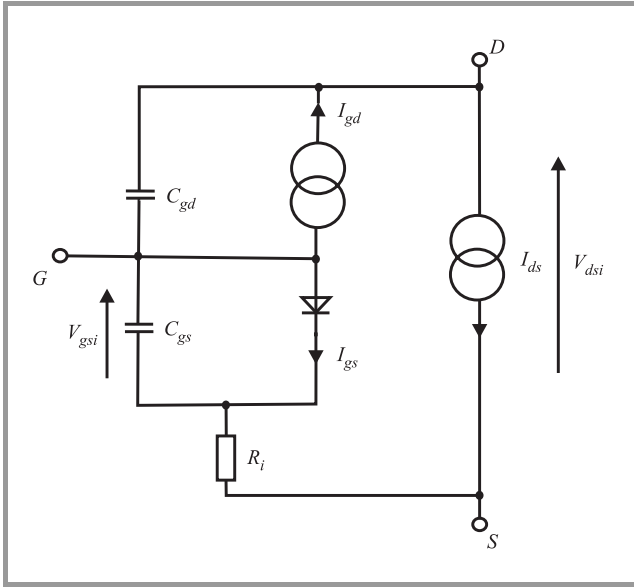**Fig. 2.** General FET transistor model in Microwave Harmonica.



**Fig. 3.** Kacprzak-Materka FET model.

The structure of the K-M model is presented in Fig. 3. Static response of a drain current versus internal voltages $V_{gsi}$, $V_{dsi}$ is characterized by a set of parameters listed below:

$IDSS$ – saturation current for $V_{GS} = 0$, $VP0$ – pinch-off voltage for $V_{DS} = 0$, $GAMA$ – slope parameter versus $V_{dsi}$ for $VP0$, $E$ – constant part of power law parameter $I_D(V_{gsi})$, $KE$ – dependence of power law on $V_{gsi}$, $SL$ – slope of the drain characteristic in the linear region, $KG$ – dependence

of $V_{gsi}$ on $V_{dsi}$ in the linear region, $SS$ – slope of the $I_D(V_{DS})$ char. in the saturated region.

Drain current for the K-M model is given by:

$$I_{ds} = IDSS \left(1 + SS \frac{V_{dsi}}{IDSS}\right) \times$$

$$\times \left(1 - \frac{V_{gsi}}{VPO + GAMA \cdot V_{dsi}}\right)^{(E + KE \cdot V_{gsi})} \times$$

$$\times \tanh\left(\frac{SL \cdot V_{gsi}}{IDSS(1 - KG \cdot V_{gsi})}\right). \tag{1}$$

Triquint TOM2 model is depicted if Fig. 4 and its set of DC parameters is explained below:

$BETA$ – transconductance coefficient, $VT0$ – pinch-off voltage, $U$ – mobility degradation fitting parameter, $GAMA$ – slope parameter of $VT0$ (versus $V_{dsi}$), $Q$ – power law parameter for $I_D(V_{gsi})$, $NG$, $ND$ – subthreshold slope parameters for $I_D(V_{gsi}, V_{dsi})$, $DELT$ – slope of $I_D(V)DS)$ in the saturated region, $ALFA$ – slope of $I_D(V_{DS})$ in the linear region.
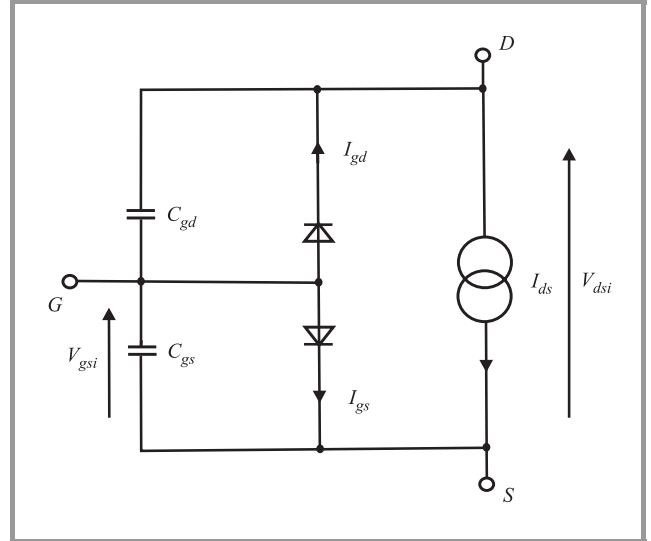


**Fig. 4.** TOM-2 model.

These parameters are used in a set of Eqs. (2) which define the drain current as a function of voltages $V_{dsi}$, $V_{gsi}$.

$$I_{ds} = \frac{I_{ds0}}{1 + DELT \cdot I_{ds0} \cdot V_{dsi}}$$

$$V_{gst} = V_{gsi} - VT0 + GAMA \cdot V_{dsi}$$

$$I_{ds0} = \frac{B}{1 + U \cdot V_{gsi}} V_g^Q KTanh$$

$$V_g = Q \cdot V_{st} \ln\left[\exp\left(\frac{V_{gst}}{Q \cdot V_{st}}\right) + 1\right]$$

$$V_{st} = (NG + ND \cdot V_{dsi})V_t$$

$$KTanh = \frac{ALFA \cdot V_{dsi}}{\sqrt{1 + (ALFA \cdot V_{dsi})^2}}. \tag{2}$$

A computer program was written to identify parameters of both models to fit the measured DC curves and also scattering parameters for a range of bias point values. The program first matches the DC characteristics of the model. Then the model parameters responsible for its DC properties (including $RS$ and $RD$ resistances) are fixed and the parameters relevant for the AC small signal response are found. These include the coefficients in capacitance equations, parasitic capacitances and inductances (see Fig. 2). Typical definitions of both models for the M-H program are given next.

For a transistor with the total gate width of 180 $\mu$m (6 segments 30 $\mu$m wide) the K-M model is as follows:

.model D02AH FET (IDSS=0.046077 SS=0.006156
+VP0=-0.744190 GAMA=-0.092446 E=1.141426
+KE=-2.508094 SL=0.334809 KG=0.455653
+RS=6.02 RD=3.790510 CLVL=2 CGS0=0.172254pF
+CGD0=0.0377342pF VBI=0.4454390
+CDS=0.0240132pF R10=1.9680642 KR=0.2275464
+RG=6.7097157 CGE=0.0270697pF CDE=0.0058621pF
+CGDE=0.0046914pF LG=0.0202468nH
+LD=0.0291279nH LS=0.0097873nH
T=0.1784086ps TJ=300 VMAX=0.5 VDMX=-3.0).

Triquint TOM2 model for the same transistor is as follows:

.model D02AH FET (BETA=0.138751
+VT0=-0.557976 U=0.002805 GAMA=0.053786
+Q=1.486948 NG=1.660377 ND=0.080267
+DELT=1.178524 ALFA=7.025695 RS=4.73-0066
+RD=3.888-889 CGS0=0.-12pF CGD0=0.048pF
+IS=1.5pA T=1E-12 LG=15pH LD=8.83pH
+LS=3.22pH CDE=21.514fF CGE=6.68fF
+CGDE=0.004pF +RDSD=903.4 CDSD=264.28pF
VDMX=3.0).

Selected measured characteristics of PHEMT transistors from the D02AH process are compared in Figs. 5 − 8 with various models evaluated. MDS denotes results from the *Microwave Design System* (HP) for the library models provided by PML.



**Fig. 6.** Low current range for $I_D(V_{DS})$ curves modeling.
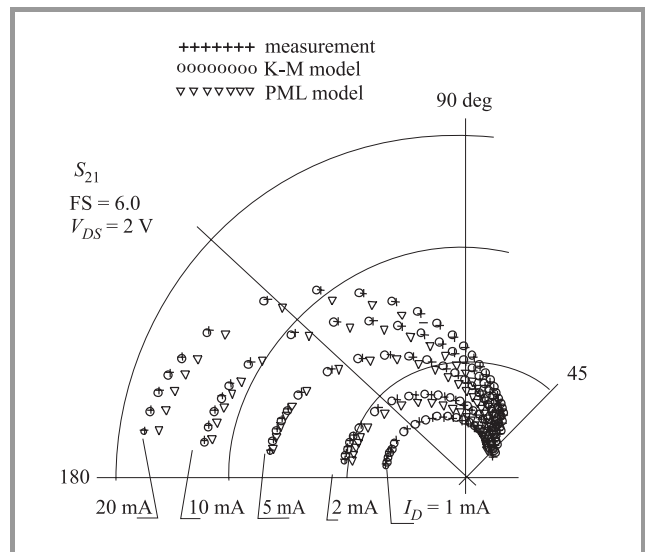


**Fig. 7.** $S_{21}$ versus frequency and drain current. Transistor $6 \times 30$ $\mu$m, frequency range: $1 - 40$ GHz.
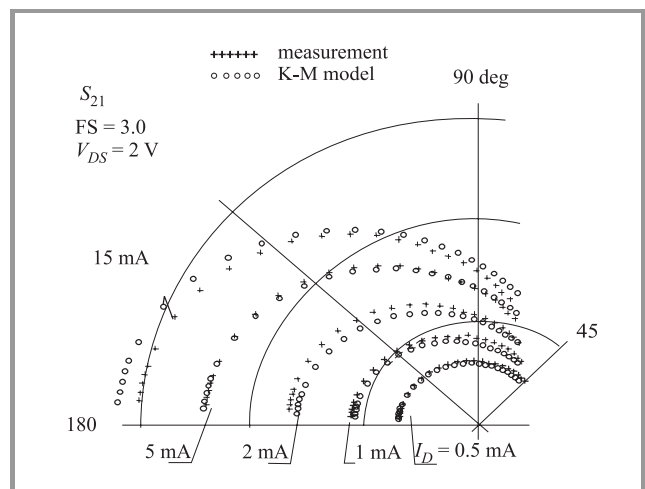


**Fig. 8.** $S_{21}$ versus frequency and drain current. Transistor $6 \times 15$ $\mu$m transistor: $f = 1 - 40$ GHz.



**Fig. 5.** Modeling of output characteristics of a $6 \times 30$ $\mu$m FET.

Both K-M and TOM2 models predict the DC characteristics very accurately over broad range of currents and voltages. TOM2 model is slightly more accurate in this respect. Philips model for MDS is not very accurate, particularly at low drain voltages. Small signal parameters generated from the K-M model provide average relative error $\delta$ on the order $2-4\%$, with slightly greater errors for high drain current. It has to be mentioned that none of the models makes provision for the dynamic changes in chip temperature. This is the main reason of discrepancies at higher $I_D$ and $V_{DS}$ bias points – both for DC and small signal characteristics. Such improved models could certainly be developed, but it was not the aim of this work to create new models, but to improve existing ones for the popular microwave CAD packages. Tests on real circuits presented next prove that very good agreement may be achieved with the models precisely identified.

# 4. Experimental verification of models

Several amplifiers designed at the IES have been evaluated with the models presented. An example of a simple two stage L-Band amplifier (Fig. 9) is presented below. Transmission parameters $S_{21}$ and $S_{12}$ are compared in Fig. 10 and IM distortion measurements and modeling are presented in Figs. 11 and 12. IM test were performed with two equal signals at input with frequencies $f_1 = 1000$ MHz and $f_2 = 1010$ MHz.
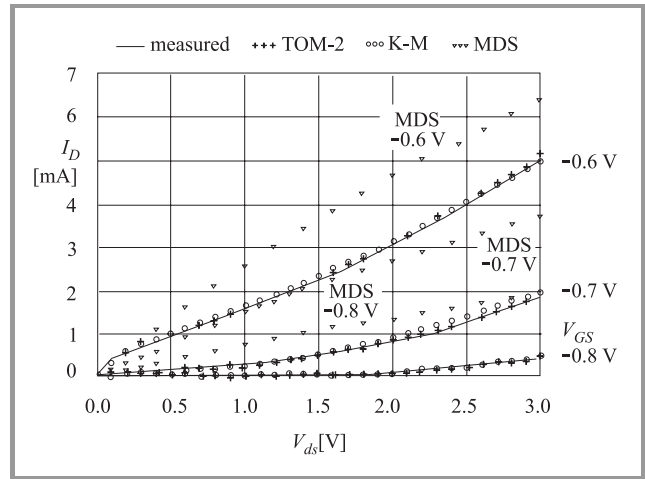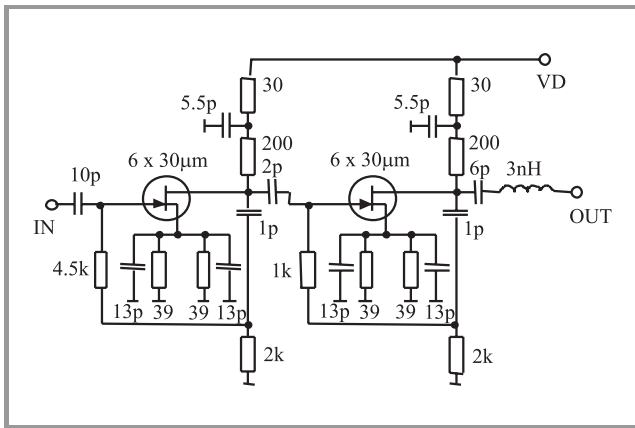


Fig. 9. Simplified circuit diagram of the LNAMP134 amplifier.

Both models (Kacprzak-Materka and TOM2) provide quite precise simulation of both small signal and nonlinear properties of MMIC amplifiers. When model parameters are appropriately identified, i.e. fitted to actual transistor parameters, accurate prediction is possible for operation in the saturation region as well as in the linear region of the FET bias. K-M model proved to be more accurate in prediction of the intermodulation distortion of microwave

amplifiers and therefore it has been subsequently used for the design of more advanced MMICs at the Warsaw University of Technology.
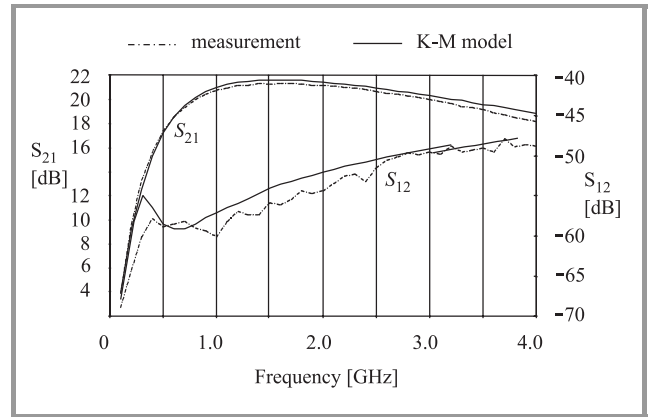


Fig. 10. Forward ($|S_{21}|$) and reverse ($|S_{12}|$) transmission modeling for the LNAMP134 MMIC.
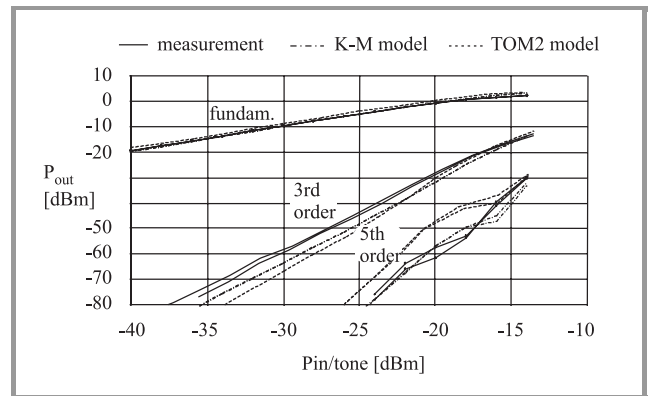


Fig. 11. Intermodulation distortion – measurement and modeling for $V_D = +6$ V.
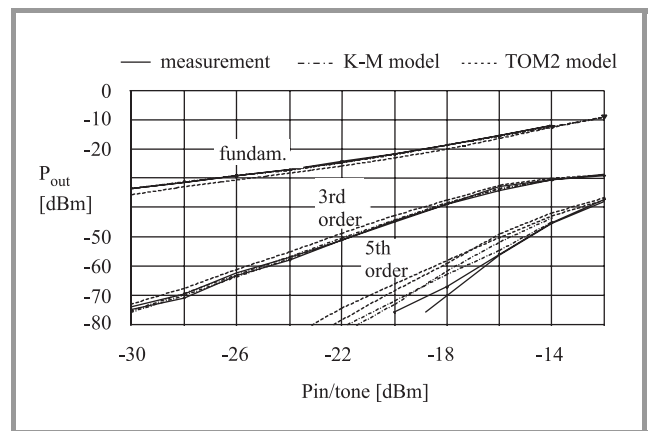


Fig. 12. Intermodulation distortion comparison for $V_D = +3$ V.

# Acknowledgement

# References

[1] "Monolithic microwave integrated circuits – modeling, design and measurements". Internal Report, Institute of Electronic Systems of the WUT, Warsaw, Jan. 1999 (in Polish).

[2] *GaAs IC design manual, foundry process D02AH (V2.0)*. Philips Microwave Limeil, Jan. 1997.

[3] *Serenade V.7.0 users guide and reference manual*. Ansoft Corp., 1997.

[4] A. Materka and T. Kacprzak, "Computer calculation of large-signal GaAs FET amplifier characteristics", *IEEE Trans. MTT*, vol. MTT-33, no. 2, pp. 129–135, 1985.

[5] D. Smith, "TOM-2: an improved model for GaAs MESFET". Internal Memorandum. Triquint Semiconductor Inc., Feb. 1995.

**Zbigniew Nosal** was born in 1947. He received the M.Sc. and Ph.D. degrees in electrical engineering from Warsaw University of Technology, in 1970 and 1980, respectively. In 1980–83 he has been with the National Radio Astronomy Observatory (New Mexico, USA) working on the low noise cryogenic receivers for radiotelescopes. At present he is with Inphi Corporation (California, USA) on leave from the WUT. His main areas of research include low noise microwave amplifier design and CAD algorithms for analysis and optimization of microwave circuits. Since 1995 he has been engaged in the GaAs MMIC design, modeling and optimization of low bias power circuits.
e-mail: z.nosal@ise.pw.edu.pl
Institute of Electronic Systems
Warsaw University of Technology
Nowowiejska st 15/19
00-665 Warsaw, Poland

# MOVPE InP based material for millimeter and submillimeter wave generation and amplification

Włodzimierz Strupiński, Kamil Kosiel, Agata Jasik, Rafał Jakieła, Andrzej Jeleński, Eric Kollberg, Larse Dillner, and Muhammat Nawaz

**Abstract** — **The potential of the MOVPE growth process for millimeter and submillimeter wave generation and amplification is presented. The increase in layer quality, the improved homogeneity and purity, the precision of mono-layers growth and wide spectrum III-V compounds makes MOVPE techniques very attractive for modern device applications. The characterisation results of the heterostructures dedicated for HBV varactors and 2-DEG transistors (HEMT) are described.**

*Keywords* — *epitaxy InP, MOVPE, microwave generation.*

## 1. Introduction

The rapid development in millimeter and submillimeter wave generation and amplification devices is connected to the new material requirements. MOVPE epitaxy of III-V semiconductors compounds gives the opportunity to realise the heterostructures of outstanding parameters. The heterostructure barrier varactor (HBV) has received considerable attention as a promising symmetric varactor element for frequency multiplier applications at millimeter and submillimeter wave. Heterostructure includes doped and undoped layers of binary and ternary compounds, lattice-matched and strained, relatively thick and very thin. HEMTs structures need very high purity level of undoped layers as well as high structural quality even in the case of pseudomorphic transistors.

## 2. Experimental

Epitaxial growth has been carried out in automatic controlled horizontal LP-MOVPE Aixtron system, model 200 R&D.

The reactor is a horizontal quartz tube with rectangular cross-section. A carbon susceptor coated with silicon carbide is infrared heated. The temperature of the susceptor is monitored by two thermocouples placed inside susceptor. The growth process is controlled automatically. The group III precursors were trimethylgallium, trimethylaluminum, trimethylindium. Phosphine and arsine were used for the group V elements. Laminar flow of high purity hydrogen as a carrier gas, high linear velocity of gases and low pressure (100 mbar) in the reactor enable the growth of the layers of the outstanding parameters. According to the type of deposited epilayers, in this case – InP:Fe (SI) and InP:S substrates were used. Typical orientation was (100) and diameter 2 inches.

In order to optimise the epitaxial growth considering purity of starting materials, substrates quality, growth parameters, etc, single layers of InP, InGaAs and InAlAs were deposited and characterised.

## 3. Results

The growth temperature was optimised very carefully considering surface morphology and electrical parameters of undoped InP layers. As the result of the above mentioned investigations InP undoped epilayers can be grown in temperature 655°C with very good electrical parameters. Figure 1 presents the results of our measurements of mobility versus carrier concentration compared with the results from literature. For undoped InP layers, $1.5 - 2.5$ mm thick, mobility $m_{77} = 70000$ cm$^2$/Vs was achieved for $n = 1.1 \cdot 10^{14}$ cm$^{-3}$. For the thicker layer – $m_{77} = 165000$ cm$^2$/Vs for $n = 2.4 \cdot 10^{14}$ cm$^{-3}$ and $m_{max} = 205000$ cm$^2$/Vs at 50 K where measured.
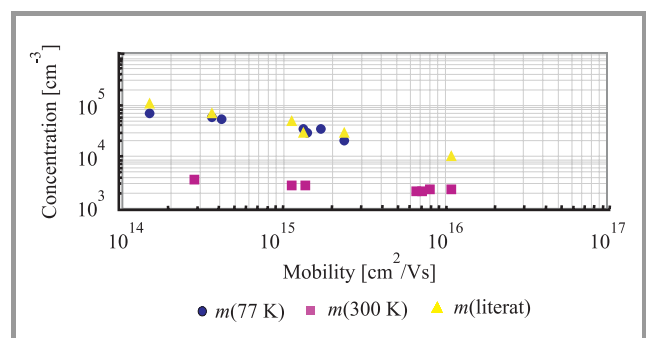


*Fig. 1.* Mobility versus carrier concentration in InP ($d = 2.5$ $\mu$m) undoped epilayer in comparison with data from literature.

The quality of InP layers was examined by photoluminescence. From Fig. 2 it is evident that the acceptor concentration is very low. High exciton peak in comparison to donor peaks ($D^0X$, $D^+X$) informs that layer is very pure. The main purpose of this part of work was the growth of lattice-matched InGaAs and InAlAs layer on InP buffer. The relation between partial pressures of TMIn, TMGa, TMAl and AsH$_3$ was crucial for the realisation of it. As
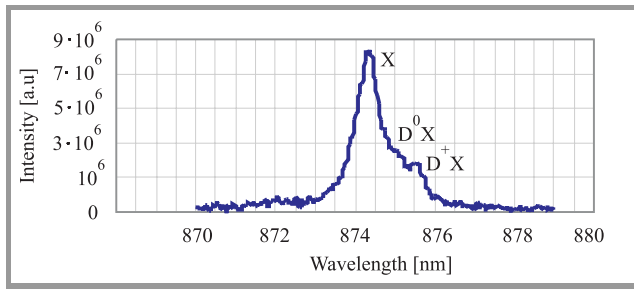
**Fig. 2.** Photoluminescence spectrum of InP undoped epilayer (thickness $-2\ \mu$m).

the consequence of many growth runs the ability of controlling lattice-mismatch (Da/a) with resolution $50-100$ ppm was achieved. This means that lattice-mismatch between InGaAs or InAlAs and InP can be intentionaly changed from region of tensile stress, through lattice-match to comprehensive stress region. Figure 3 presents X-ray diffraction results where rocking curve of the substrate and epilayer are practically in the same position ($\Delta a/a < 220$ ppm).
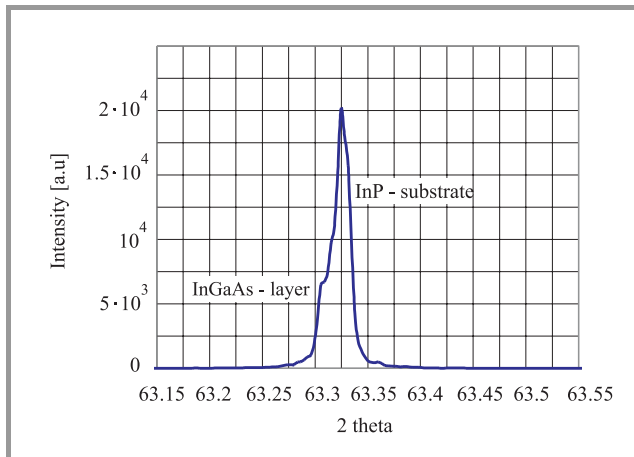


**Fig. 3.** X-ray diffraction result of lattice-matched InGaAs on InP substrate.

The varactors and transistors structures require strain layers grown on lattice-matched layers-sequences, like $In_{0.75}GaAs$ in HEMT or AlAs and InGaP in varactor.

The critical thickness of such layers, characteristic for the lattice-mismatch parameter, plays the key role in the growth of strain layers. Above the critical thickness, due to lattice relaxation processes, defects, mainly misfit dislocations, are created. However, in the case when the difference between lattice parameters of the substrate and the layer is too high, the deposited material crystalises in 3D mode. The islands of the dimensions, which depend on the growth parameters, are created on the very thin planar wetting layer. Further observations show that the driving force for the 2D-3D transition can be minimised by slowing the relaxation of misfit strain. As a result – the relatively smooth layer can be deposited in lower temperature for the optimal growth rate. The quality of the InGaAs, InGaP, AlAs strained layers de-

posited on InP substrate have been examined by the X-ray, AFM and SIMS methods. Atomic Force Microscopy allows to observe 3D growth mode even for very thin layers. Relatively strong relaxation effects are recognised by surface roughness. Two-dimensional diffraction measurements are much more sensitive tool for estimation of relaxation degree. Apart from the estimation of the lattice parameter in two perpendicular directions it is also possible to measure the diffusion scattering caused by linear density of misfit dislocations. Experimentally determined values of critical thickness were determined and compared to theoretical values calculated from formula of Matthews-Blakeslee for $In_xGa_{1-x}As$, for x up to 0.75.

# 4. Conclusions

The characterisation results of MOVPE heterostructures enable their optimisation for their application for millimetre and submillimetre devices for wave generation and amplification. New concepts of devices, in which the growth precision of mono-layers, accurate lattice-matching or intentional stress of layers, and high purity are needed, can be realised.

# References

[1] M. Nawaz, W. Strupiński, J. Stenarson, S. H. M. Persson, and H. Zirath, "Reliability evaluation of MOCVD grown AlInAs/GaInAs/InP HEMTs", in *1999 IEEE Int. Reliab. Phys. Proc.*, IEEE Catalog no. 99CH36296.

**Włodzimierz Strupiński** received the M.Sc. degree in material science from Technical University of Warsaw in 1981. In 1991, he received the Ph.D. degree in physics from Technical University of Warsaw. His thesis work involved developing GaP epitaxial layers doped with nitrogen for green LEDs. Since joining the Institute of Electronic Materials Technology in 1983 he has been working on vapor phase epitaxy and metallorganic vapor phase epitaxy of III-V semiconductors, GaAs and InP-related. His research interest includes epi-structures for HEMT transistors, HBV varactors, lasers, photodetectors, etc.
e-mail: strupi_w@sp.itme.edu.pl
Institute of Electronic Materials Technology
Wólczyńska st 133
01-919 Warsaw, Poland

**Kamil Kosiel**
Institute of Electronic Materials Technology
Wólczyńska st 133
01-919 Warsaw, Poland

Włodzimierz Strupiński, Kamil Kosiel, Agata Jasik, Rafał Jakieła, Andrzej Jeleński, Eric Kollberg, Larse Dillner, and Muhammat Nawaz

**Agata Jasik**
Institute of Electronic Materials Technology
Wólczyńska st 133
01-919 Warsaw, Poland

**Rafał Jakieła**
Institute of Electronic Materials Technology
Wólczyńska st 133
01-919 Warsaw, Poland

**Andrzej Jeleński**
e-mail: jelens_a@sp.itme.edu.pl
Institute of Electronic Materials Technology
Wólczyńska st 133
01-919 Warsaw, Poland

**Eric Kollberg**
Department of Microwave Electronics
Chalmers University of Technology
SE-41296 Gothenburg, United States of America

**Larse Dillner**
Department of Microwave Electronics
Chalmers University of Technology
SE-41296 Gothenburg, United States of America

**Muhammat Nawaz**
Department of Microwave Electronics
Chalmers University of Technology
SE-41296 Gothenburg, United States of America

# The 100 W class A power amplifier for L-band T/R module

Wojciech Wojtasiak, Daniel Gryglewski, and Edward Sędek

**Abstract — In the paper a balanced high power amplifier with class A silicon bipolar transistors for L-band T/R module is described. The amplifier was designed for maximum power and minimum transmitance distortions. The obtained parameters of the amplifier are as follow: output power at 1 dB compression $P_{1\,dB} > 49$ dBm, linear gain $|S_{21}| > 10$ dB, and transmitance deviations during the RF pulse: phase $\Delta arg(S_{21}) < 0.9°$ and $\Delta P_{out} < 0.2$ dB.**

*Keywords — modeling, MESFETs, finite difference time domain method, power transistors, microwave transistors.*

## 1. Introduction

For the last few years fast development of microwave power amplifier has been achieved. These devices are widely applied in radiocommunication and radiolocation systems [1]. The power amplifiers for T/R modules of active phased array radar should be characterized by small transmitance distortions. The recommended phase changes of transmitance during power pulse are less than $\Delta arg(S_{21}) < 1°$, between pulses $\Delta arg(S_{21}) < 0.1°$ at the power changes less than $\Delta P_{out} < 0.2$ dB [1].

The paper describes 100 W balanced power amplifier with two bipolar transistors designed at the Institute of Radio-electronics of the Warsaw University of Technology. The presented project is a continuation of a research work [2]. The significant improvement has been achieved.

## 2. The design method

The design procedure of power amplifiers has been exactly explained in the grant KBN report [3]. The described amplifier was designed with two silicon, bipolar transistors LFE15600X made by Philips. It's parameters are shown in the Table 1. These transistors are intended for use in common emitter, class AB amplifiers in CW conditions for professional applications. The amplifier described in the paper was worked in keyed class A mode.

The selected transistors, due to input and output inner matching sections, essentially are intended for amplifiers with a relative bandwidth less than 5% at $1.5 - 1.7$ GHz range. The outside input and output matching sections were

designed in such way to change the frequency range into desired range of $1.28 - 1.42$ GHz. The developed algorithm with aid of universal microwave circuits simulator as well as an original, self-made computer program was used for calculation [3]. As a substrate RT/Duroid 6010 (Rogers Corp.), $\varepsilon_r = 10.8$, $h = 0.635$ mm was used. The layout of the amplifier is shown in Fig. 1.

Table 1
Parameters of the class AB power amplifier

| Mode of operation | $f$ [GHz] | $U_{CE}$ [V] | $I_{CQ}$ [A] | $P_{out}$ [W] | $G_{po}$ [dB] | $\eta_c$ [%] |
|---|---|---|---|---|---|---|
| Class AB (CW) | 1.5 | 24 | 0.2 | 55 | 8 | 50 |

## 3. Measurement results

The amplifier worked in keyed class A mode. This kind of work permit to increase the supply conditions of transistors. Quiescent bias point was: $I_C = 6$ A and $U_{CE} = 24$ V at open state of the transistors. The open time was 50 $\mu$s, duty factor 0.3% and the width of power pulse was 24 $\mu$s. The linear gain and output power at 1 dB gain compression point versus frequency is shown in Fig. 2. The characteristic of output power versus input power are presented in Fig. 3.

The measurements of transmitance distortions during RF pulse were made. The self-invented measurement system was applied [3]. The measured transmitance phase changes were less than $\Delta arg(S_{21}) < 0.9°$. The "stability" of the output power was better than $\Delta P_{out} < 0.2$ dB during the RF pulse.

## 4. Conclusions

The measured amplifier parameters prove accuracy of used design procedure. The output power at 1 dB compression point exceeds 49 dBm, gain is better than 10 dB in band $1.28 - 1.42$ GHz. The amplifier's transmitance deviations during the RF-pulse are less than: 0.9° for phase and 0.2 dB for amplitude.

Wojciech Wojtasiak, Daniel Gryglewski, and Edward Sędek
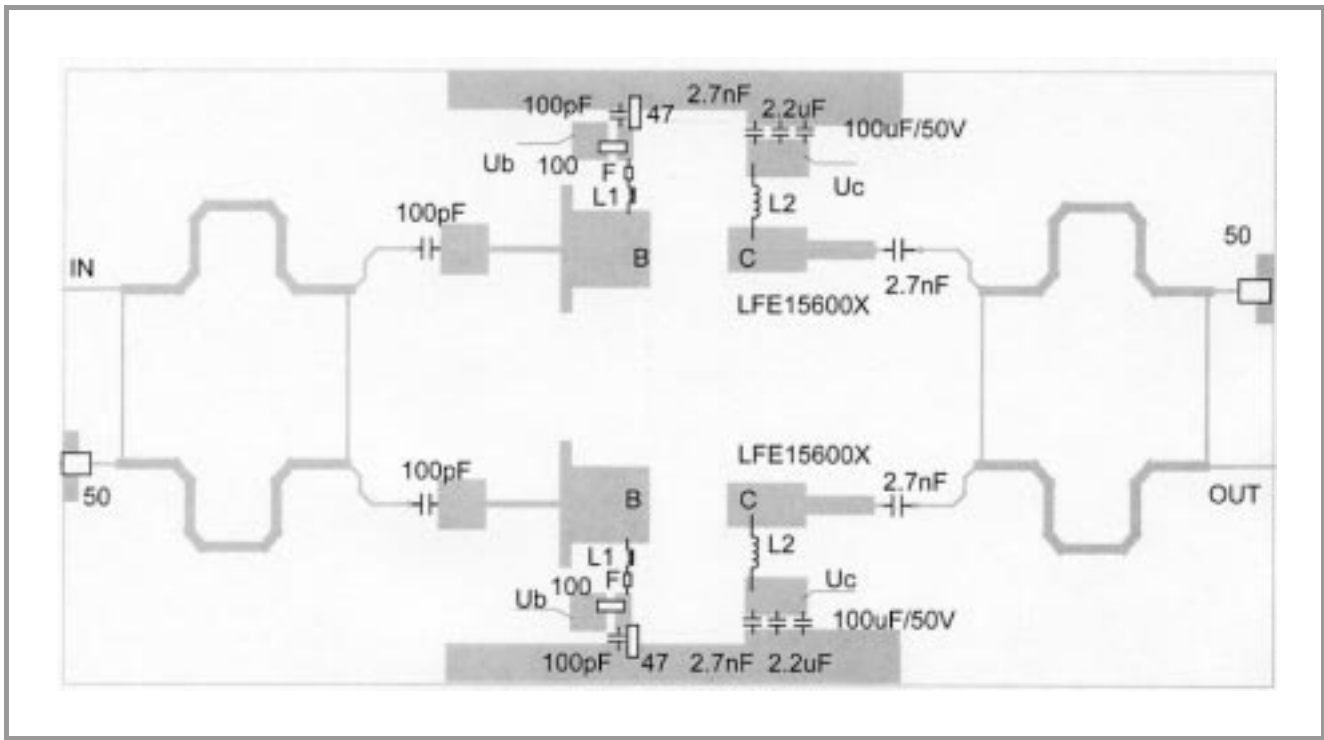


**Fig. 1.** The layout of the 100 W amplifier. Explanations: F – ferrite bead, L1 – 4 turns 0.5 mm copper wire, L2 – 3 turns 0.5 mm copper wire.
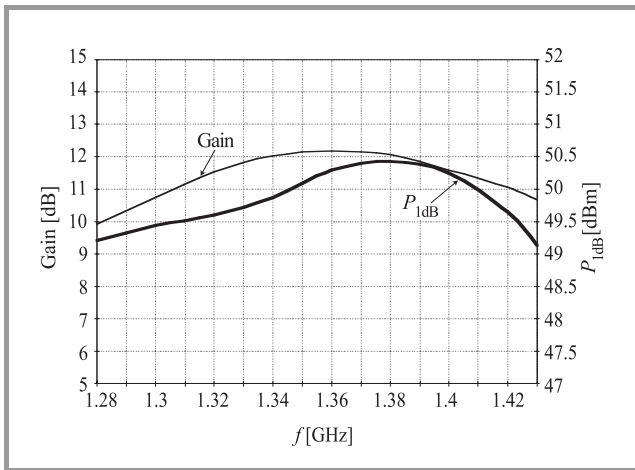


**Fig. 2.** The amplifier gain and output power at 1 dB compression point.



**Fig. 3.** The amplifier output power versus input power.

The amplifier worked in keyed class A mode. This kind of work permit to increase the supply conditions. The supply conditions were safe. It is possible to increase the $P_{1\,dB}$ above 50 dBm by changing supply: $U_{CE}$ up to 28 V and $I_C$ up to 8 A. The obtained results show that the amplifier can be applied in T/R module for active phased array radar.

## References

[1] J. L. B. Walker, Ed., *High- Power GaAs FET Amplifiers*. Artech House, Inc. 1993.

[2] W. Wojtasiak, T. Morawski, and E. Sędek, "A linear power amplifier for L-band T/R module", in *MIKON'96*, Warsaw, Poland, 1996, vol. 2, pp. 547–501.

[3] Final report for State Committee for Scientific Research, grant no. 8T11B03612, Warsaw, Sept. 1998.

**Wojciech Wojtasiak** received the M.Eng.Sc. degree and the Ph.D. degree in electronic engineering from the Warsaw University of Technology, Warsaw, Poland in 1984 and 1998, respectively. In 1984 he become a Lecture and

in 1998 an Assistant Professor at WUT. His primary research interests were characterization and application of nonuniform transmission lines. Now, his research interest concerns with design of high power microwave amplifiers. Since 1998 he has been a member of MTT.
e-mail: wwojtas@ire.pw.edu.pl
Institute of Radioelectronics
Warsaw University of Technology
Nowowiejska st 15/19
00-665 Warsaw, Poland

**Daniel Gryglewski** received the M.Eng.Sc. degree and the Ph.D. degree in electronic engineering from the Warsaw University of Technology, Warsaw, Poland in 1996 and 2001, respectively. In 2001 he become an Assistant Professor at WUT. His primary research interest was frequency synthesis. Now, his research interest concerns with design of high power microwave amplifiers.
e-mail: dgrygle@ire.pw.edu.pl
Institute of Radioelectronics
Warsaw University of Technology
Nowowiejska st 15/19
00-665 Warsaw, Poland

**Edward Sędek** received the M.Eng.Sc. degree and the Ph.D. degree in electronic engineering from the Warsaw University of Technology, Warsaw, Poland in 1968 and 1980, respectively. In 1968 he joined the Telecommunications Research Institute, Warsaw, and become an Assistant Professor in 1980. His primary research interests are microwave ferrite devices, CAD method of waveguide, strip-line, microstrip circulators and isolators and ferrite phase shifters. His other research interests include planar antenna techniques and optoelectronics method for scanning radar beam. In recognition of his contributions in the area of design, modeling and testing of microwave ferrite devices he received the Doctor of Engineering Degree (higher doctorate) from Warsaw University of Technology in 1990. In March 1991 he was appointed scientific director for Telecommunications Research Institute where he holds Professor of electronic engineering post. In the years 1994–1998 Dr Sędek was Chapter Chairman of Poland Section of MTT.
e-mail: sedek@pit.edu.pl
Telecommunications Research Institute
Poligonowa st 30
04-051 Warsaw, Poland

# Photovaractor performance
# for optically controlled microwave circuits

Sergey A. Malyshev, Vatslav F. Andrievski, Tamara O. Budko, Chen Chao, Alexander L. Chizh,
Elena V. Gushchinskaya, Liu Baolin, Ludmila I. Romanova, and Emilia V. Zaporozhets

**Abstract** — The photovaractor for optically controlled microwave circuits was designed and studied. The photovaractor module was fabricated as a planar *p-i-n* photodiode chip placed in a fibre optic matching receptacles. Study of *C-V* characteristics in the light illumination mode has shown that capacitance characteristics are strongly dependent on the light illumination power. These variations of the photovaractor diode capacitance are large enough to be used in optically controlled circuits such as oscillators, mixers and switchers.

**Keywords** — *circuits, photovaractor, optically controlled.*

## 1. Introduction

Various varactor diodes are extensively used in microwave applications, which include phase shifter, frequency multiplier, mixer and nonlinear transmission-line [1 – 4]. In recent years the application of photonic devices for such optically controlled microwave circuits are discussed widely in literature [5 – 9]. The advantages of optical control are high tuning speed and good isolation between controlling and microwave signals.

One of optical control means is the use of junction capacitance variation due to optical illumination. We propose to call such a device as the photovaractor. In this paper we report measurements of photovaractor fabricated as a planar *p-i-n* InP/InGaAs photodiode placed in a fibre optic matching receptacle. Variation of the photovaractor characteristics due to optical illumination with different light power are studied.

## 2. Photovaractor diode

The photovaractor described in this paper is a planar *p-i-n* photodiode with front illuminated $p^+$-region and back ohmic contact to $n^+$-InP substrate. The *p-i-n* photodiode has been fabricated in $n$-InP/$n$-InGaAs/$n^+$-InP heterostructure which was grown on a substrate by low pressure metal-organic vapour-phase epitaxy (LP-MOVPE). The heterostructure has been studied using electrochemical *C-V* profiling method before making the photodetector chip. Figure 1 shows the cross-section of the planar InP/InGaAs *p-i-n* photodiode. The epitaxial layer is composed of 0.6 $\mu$m, $1.2 \cdot 10^{15}$ cm$^{-3}$ undoped $n$-InP top layer, 1.5 $\mu$m, $1.2 \cdot 10^{15}$ cm$^{-3}$ undoped $n$-InGaAs absorption layer, 0.5 $\mu$m undoped $n$-InP buffer layer on 400 $\mu$m, $3 \cdot 10^{18}$ cm$^{-3}$ Te doped $n^+$-InP substrate. The Hall method

measurement has given following majority carrier mobility values in InGaAs absorption layer: 7735 cm$^2$/V·s at 300 K, and 64084 cm$^2$/V·s at 78 K.
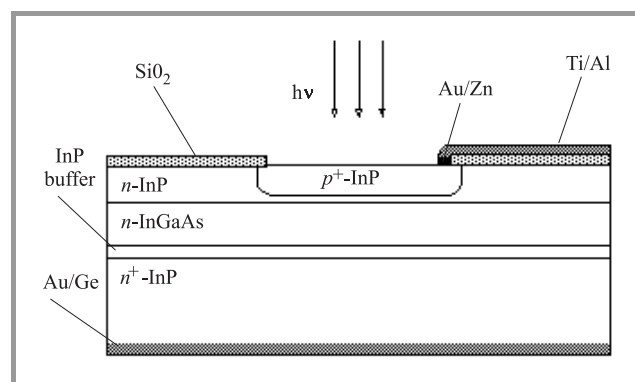


***Fig. 1.*** Cross-section of the planar InP/InGaAs *p-i-n* photovaractor.

The $p^+$-region was formed by local diffusion of Zn into the wide band gap $n$-InP top layer. The Zn diffusion was performed in an open gas flow system into unpassivated InP surface at 470°C [10]. The results of electrochemical *C-V* measurements indicated that the average doping level in the $p^+$-InP layer for this diffusion conditions was $7.5 \cdot 10^{18}$ cm$^{-3}$, and the layer thickness was 0.5 $\mu$m. SiO$_2$ films of $0.25 \pm 0.01$ $\mu$m thickness were used as diffusion mask and passivative layer for the planar diode structure. These films have been made by pyrolysis of tetraethoxysilane at $330 - 350$°C in O$_2$/N$_2$ flow. Ohmic contacts to $p^+$- and $n^+$-regions were formed using AuZn and AuGe binary alloys, respectively. Contact annealing was performed at 350°C in H$_2$ flow. Contact resistance for both $p^+$- and $n^+$-regions was $1 - 3 \cdot 10^{-6}$ $\Omega \cdot$ cm$^2$. The diameter of the photosensitive area was 100 $\mu$m.

The photovaractor module has been fabricated as a planar *p-i-n* photodiode chip placed in a fibre optic matching receptacle. To reduce reflection from the fibre-air, air-optics and air-chip boundaries, a special matching medium having a refractive index close to that of quartz fibre was used [11].

## 3. Results and discussion

Measurements of *I-V* characteristics of the photovaractor have shown that the breakdown voltage was 50 V. The values of dark current were $3.5 - 3.7 \cdot 10^{-9}$ A under 1.0 V reverse bias, and $4.0 - 4.1 \cdot 10^{-9}$ A under 15 V bias. Ca-

pacitance variation with bias voltage in dark condition is shown in Fig. 2. The measurements were carried out with LCG-meter at 1 MHz. One can see that with the bias voltage variation the capacitance change is small and the ratio $C_{max}/C_{min}$ is equal to 2.35. Frequency measurements were carried out using 1300 nm semiconductor laser with 2.5 mW power as a source. Spectral analyser with the bandwidth from 0.4 GHz up to 3.0 GHz was used as a receiver in the source-detector system. The receptacled *p-i-n* photodiode module with 50 Ω matching resistors has the bandwidth over 1.5 GHz.
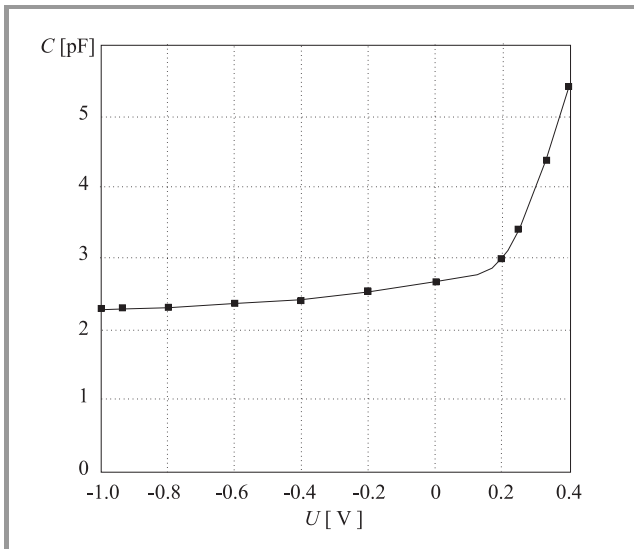


**Fig. 2.** *C-V* characteristic of the photovaractor in dark condition.

Figure 3 presents the response of the photovaractor module measured in the $700 - 1800$ nm range in bias free conditions. The photovaractor module response is $0.75 \pm 0.05$ A/W at wavelength 1300 nm. It is necessary to note that the response is not changed under reverse bias voltage variation. This fact gives us the possibility to conclude that the depleted region of *p-i-n* junction penetrates through the absorption InGaAs layer down to the buffer layer and photocarriers are collected completely even in the bias free conditions.

Figure 4 shows *I-V* characteristics of the photovaractor under different optical power illumination. It can be seen that the photovaractor has linear response up to 750 $\mu$W optical power in the bias free conditions.

Photovaractor's capacitance can be strongly modified by optical illumination. Figure 5 shows the capacitance variation versus optical illumination power under different bias voltages. In the dark condition we have usual a decrease of the diode capacitance with the reverse bias voltage because the diode's depleted region width slightly increases. The depleted region width decreases significantly with the optical power increase and this results in the increasing capacitance. The ratio $C_{max}/C_{min}$ depends on the variation range of the optical power and bias voltage (Fig. 5). For example, at the bias voltage $+0.1$ V the capacitance changes from
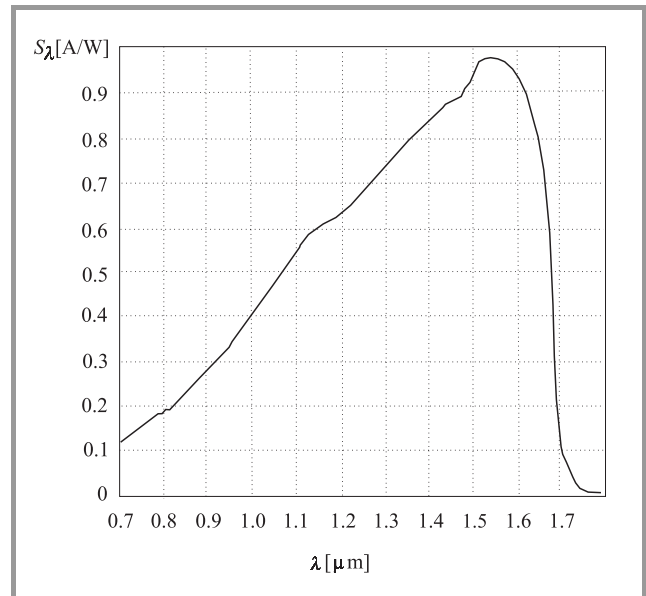


**Fig. 3.** Spectral response of the photovaractor.
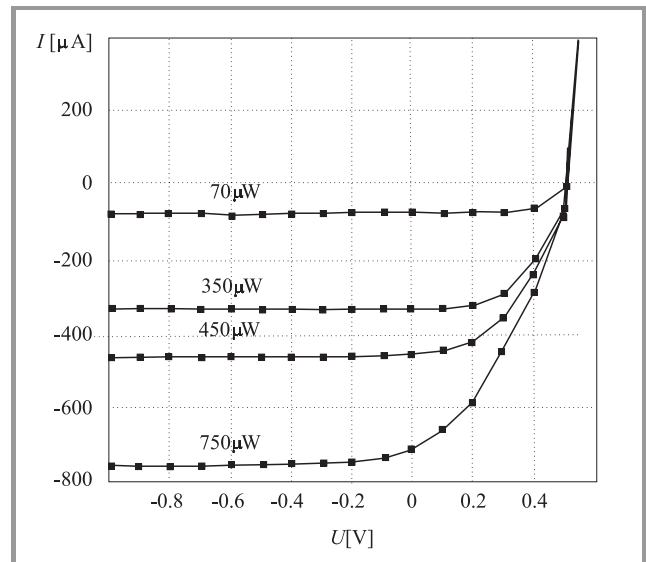


**Fig. 4.** *I-V* characteristics of the photovaractor under different optical power.

$C_{min}$ = 2.75 pF up to $C_{max}$ = 69 pF under the optical power variation from zero to 400 $\mu$W, i.e. the ratio $C_{max}/C_{min}$ is equal to 25. At the bias voltage $-0.4$ V and optical power variation from zero up to 750 $\mu$W the ratio $C_{max}/C_{min}$ decreases to 15. It is necessary to note that the capacitance nonlinearity increases when the optical power is increased. For example, under the bias $-0.4$ V and optical power variation from zero up to 400 $\mu$W the ratio $C_{max}/C_{min}$ is equal to 2, and it increases to 15 under the extension of optical power variation range up to 750 $\mu$W.

Analysis of capacitance change under different conditions gives the possibility to choose the optimum operation regime of the photovaractor. It seems that the best one is

S. A. Malyshev, V. F. Andrievski, T. O. Budko, C. Chao, A. L. Chizh, E. V. Gushchinskaya, L. Baolin, L. I. Romanova, and E. V. Zaporozhets

**Fig. 5.** The capacitance versus optical illumination power variation under different bias voltages.

near bias free region because the photovaractor has wide junction capacitance variation range due to illumination, as well as good sensitivity, frequency bandwidth and low dark current.

## 4. Conclusions

The receptacled *p-i-n* photovaractor module incorporating the matching medium are presented. The study of *C-V* characteristics in the light illumination mode has shown that the capacitance characteristics are strongly dependent on the light illumination power. These junction capacitance variations of the photovaractor diode are large enough to be used in optically controlled microwave circuits such as oscillators, mixers and switchers.

## Acknowledgements

## References

[1] D. M. Krafcsik, S. A. Imhoff, D. E. Dawson, and A. L. Conti, "A dual-varactor analog phase shifter operating at 6–18 GHz", *IEEE Trans. Microw. Theory Techn.*, vol. 36, no. 12, pp. 1938–1941, 1988.

[2] W. C. B. Peatman, T. W. Crowe, and M. Shur, "A novel Schottky/2-DEG diode for millimeter- and submillimeter-wave multiplier applications", *IEEE Electron. Dev. Lett.*, vol. 13, no. 1, pp. 11–13, 1992.

[3] J. N. Poelker and R. S. Robertson, "A comparison of planar doped barrier diode performance versus Schottky diode performance in a single balanced, MIC mixer with low LO drive", *IEEE Trans. Microw. Theory Techn.*, vol. 43, no. 6, pp. 1241–1246, 1995.

[4] M. J. W. Rodwell, M. Kamegawa, R. Yu, M. Case, E. Carman, and K. S. Giboney, "GaAs nonlinear transmission lines for picosecond pulse generation and millimeter-wave sampling", *IEEE Trans. Microw. Theory Techn.*, vol. 39, no. 7, pp. 1194–1204, 1991.

[5] Z. Szczepaniak and B. Galwas, "Optically-controlled microwave phase-shifter", in *Proc. Symp. High Perfor. Electron Dev. Microw. & Optoelectron. Appl. (EDMO'99)*, London, U.K., Nov. 1999, pp. 290–292.

[6] B. Galwas, "Photonic technology for microwave engineering", in *Proc. 12th Int. Conf. Microw. & Radar (MIKON)*, Krakow, Poland, May 1998, vol. 4, pp. 117–135.

[7] Z. Varga, G. Jaro, and B. Erdos, "Optical control of microwave filters using photodiodes", in *Proc. 10th MICROCOLL Conf.*, Budapest, Hungary, March 1999, pp. 299–302.

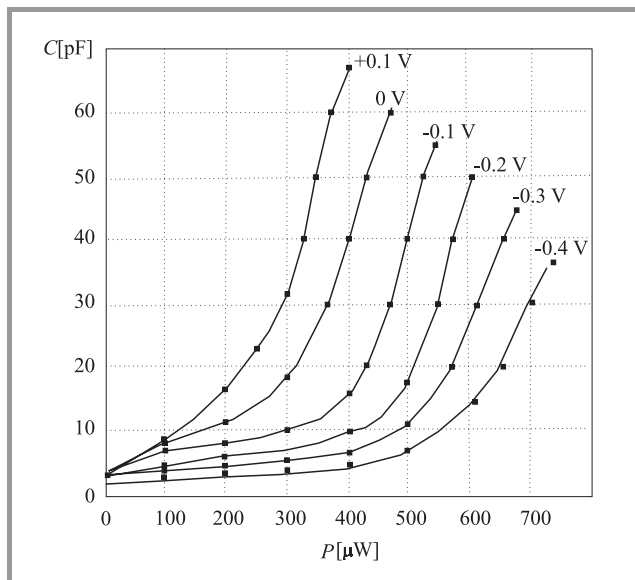[8] Dong-Wook Kim, Jae-Jin Lee, Young-Se Kwon, and Song-Cheol Hong, "Characteristics of an area-variable varactor diode", *IEEE Trans. Microw. Theory Techn.*, vol. 44, no. 11, pp. 2053–2057, 1996.

[9] C. K. Sun, C. T. Chang, R. Nguyen, and D. J. Albares, "Photovoltaic *p-i-n* diodes for RF control – switching applications", *IEEE Trans. Microw. Theory Techn.*, vol. 47, no. 10, pp. 2034–2036, 1999.

[10] T. O. Budko, E. V. Gushchinskaya, Yu. S. Emelyanenko, and S. A. Malyshev, "Diffusion of zinc into an unpassivated surface of indium phosphide", *Phys. Stat. Sol. (a)*, vol. 111, pp. 451–456, 1989.

[11] V. F. Andrievski and S. A. Malyshev, "High speed InGaAs photodetector modules for fibre optic communications", in *Proc. Workshop High Perfor. Electron Dev. Microw. & Optoelectron. Appl. (EDMO'97)*, London, U.K., Nov., 1997, pp. 335–339.

**Sergey A. Malyshev** graduated from the Minsk Radio-Engineering Institute in 1970. He received the Ph.D. degree in electronic engineering from the Institute of Electronics, National Academy of Sciences of Belarus, in 1979. Since 1985 he has been a head of the Laboratory of Semiconductor Optoelectronics. He has authored and co-authored over 70 papers. Research work conducted by Dr. Malyshev is devoted to experimental and theoretical investigation of physical processes in optoelectronic devices based on $A^{III}$-$B^{V}$ compounds, photodetectors for fiber-optic communication, and their applications.
e-mail: malyshev@inel.bas-net.by
Institute of Electronics
National Academy of Sciences of Belarus
22 Lagoiski Trakt
220090 Minsk, Belarus

**Vatslav F. Andrievski** graduated from the St. Petersburg Electroengineering Institute in 1983. His speciality is optoelectronic devices. From 1983 to 1991 he worked at the Institute of Radiomaterials and was involved in the project for studies of GaAs switches. He also investigated the electrophysical and optical properties of GaAs, InP and InGaAs. He joined the Institute of Electronics, National Academy of Sciences of Belarus, in 1991. His main research interest is

16

the study of electrophysical properties of bulk $A^{III}$-$B^V$ materials with use of photoelectrochemical method, optoelectronic component design and packaging. He has authored and co-authored more than 30 papers.
Institute of Electronics
National Academy of Sciences of Belarus
22 Lagoiski Trakt
220090 Minsk, Belarus

**Tamara O. Budko** worked at the Institute of Electronics, National Academy of Sciences of Belarus, from 1978, after graduation from Belarussian State University. Since 1998 she has worked at the Institute of Radiomaterials (Minsk). Her research interests include the chemical etching and treatment of the $A^{III}$-$B^V$ semiconductors. She has authored and co-authored more than 20 papers.
Institute of Electronics
National Academy of Sciences of Belarus
22 Lagoiski Trakt
220090 Minsk, Belarus

**Chen Chao** graduated in 1965 from the Department of Physics, Xiamen University, majoring in semiconductor physics and physics of semiconductor devices with B.S. degree. In 1992–1993 he was researching the photoelectronic properties and photoelectronic devices of III-V materials at the Department of Materials and Metallurgy, Toronto University, Canada, and the Department of Physics, Belarussian State University, Belarus. Chen Chao is a Professor at the Department of Physics, Xiamen University in China. He is engaged in scientific research on semiconductor photoelectronic properties, photoelectronic devices, OEIC and its application in optical fiber communication and CATV.
Department of Physics
Xiamen University
Xiamen 361005, China

**Alexander L. Chizh** graduated with honors from the Belarussian State University (Minsk) in June 1999 and received the degree of Bachelor of Science. Since 1999 he has worked towards the Ph.D. thesis at the Laboratory of Semiconductor Optoelectronics, Institute of Electronics (Minsk). His research interests are in the area of microwave photonics, theoretical and experimental studies of photoelectrical processes in multilayers heterostructures based on $A^{III}$-$B^V$ compounds, photodetectors for fiber-optic communication, and their applications. He is the author and co-author of 10 papers.
Institute of Electronics
National Academy of Sciences of Belarus
22 Lagoiski Trakt
220090 Minsk, Belarus

**Elena V. Gushchinskaya** has worked at the Laboratory of Semiconductor Optoelectronics, Institute of Electronics, National Academy of Sciences of Belarus, since 1977, after graduation from Minsk Radioengineering Institute. Her research interests include investigation of the Zn diffusion in the $A^{III}$-$B^V$ semiconductor materials.
Institute of Electronics
National Academy of Sciences of Belarus
22 Lagoiski Trakt
220090 Minsk, Belarus

**Liu Baolin** received his B.S. degree from the Department of Physics, Zhongshan University in 1984, the M.S. degree from 13th Institute of Electronic Department in 1987, and the Ph.D. degree from Electronical Engineering Department, Jilin University in 1993. From Oct. 1999 to Sept. 2001 he worked at Venture Business Lab. of Chiba University in Japan as a Research Scientist. He has been engaging in the research of MOCVD growth and optoelectronic device for optical fiber communication and wide gap material. Liu Baolin is an Associate Professor at the Department of Physics, Xiamen University in China.
Department of Physics
Xiamen University
Xiamen 361005, China

**Ludmila I. Romanova** has worked at the Institute of Electronics, National Academy of Sciences of Belarus, since 1974, after graduation from Moscow Institute of Electronic Techniques. Since 1991 she works at the Laboratory of Semiconductor Optoelectronics. Her research interest include the forming of ohmic contacts in the optoelectronic devices.
Institute of Electronics
National Academy of Sciences of Belarus
22 Lagoiski Trakt
220090 Minsk, Belarus

**Emilia V. Zaporozhets** graduated from the Department of Chemistry, Moscow Chemistry and Technology Institute, in 1966. She received the Ph.D. degree in chemistry in 1972. She has worked at the Institute of Electronics, National Academy of Sciences of Belarus, since 1979. Her research interests include investigations of processes in $A^{III}$-$B^V$ semiconductor surfaces and forming the ohmic contacts to the $A^{III}$-$B^V$ compounds.
Institute of Electronics
National Academy of Sciences of Belarus
22 Lagoiski Trakt
220090 Minsk, Belarus

# Optical-microwave transmission system with subcarrier multiplexing for industrial measurement systems

Jarosław Dawidczyk, Bogdan A. Galwas, Jerzy Skulski, Zenon Szczepaniak, Henryk Gruchała, and Sergey Malyshev

**Abstract — We describe short-distance three-channel optical-microwave link with subcarrier multiplexing for transmission digital and/or analog data between different points of industrial measurement systems. The optical fiber link operates with Fabry-Perot laser at 1300 nm, multimode fiber and PIN photodiode receiver. From microwave point of view three carriers with frequencies 600 MHz, 800 MHz and 1000 MHz were chosen. The structure and main parameters of a link are reported and discussed.**

*Keywords — optical-microwave link, subcarrier multiplexing.*

## 1. Introduction

The contemporary optical communication systems base on multichannel digital high-speed fiber transmission [1]. The driving force motivating the use of multichannel optical systems is the enormous bandwidth of optical fiber. To exploit of the fiber's terahertz bandwidth the wavelength-division multiplexing WDM is used typically. However, analog optical communications has some very appealing characteristics that make it a possible solution for some near – term general communications problems. These include CATV, video distribution, local area networks etc. In such case subcarrier multiplexing SCM seems to be the best solution of multichannel transmission problems [2, 3]. Many industrial measurements systems operate at extremely difficult conditions, with high level of industrial noise, disturbances and distortions. If a distance between sensors and a central controlling unit is long, than the transmission of measurement data arises to the great problem [4, 5]. Application of fiber transmission line could be very helpful and useful because of its natural immunity to electromagnetic interference. The properties of the fibre optic link can be measured with the use of the special photonic techniques [6].

## 2. Basic structure of optical-microwave transmission system with SCM

The essence of subcarrier multiplexing system is to take all the modulating, demodulating, multiplexing and demultiplexing functions and perform them electrically. The only

optical functions that remain are: optical generation with semiconductor laser, optical transmission over an optical fiber and optical detection using a photodiode. Sometimes some passive optical elements could be used (splitters, couplers, etc.).

The schematic representation of a link is shown in Fig. 1. At the transmitter side of the link three streams of data are directed to the three microwave transmitters. The carrier frequencies of these transmitters are equal to 600 MHz, 800 MHz and 1000 MHz, respectively. The signals of carriers are modulated in different manner. The output signals are combined by multiplexer, next amplified and directed by driver to laser diode. The basic characteristics of multiplexer are shown in Fig. 2.

The transmitted optical signal is at first detected by photodiode at the receiver side of the link. Next, after amplification, demultiplexer directs the signal to three arms. Three different microwave receivers recover the transmitted data.

## 3. Optical link

Three main elements create an optical link: optical transmitter with laser semiconductor diode, multimode fiber and optical receiver with PIN photodiode.

The main device of transmitter is a laser package. The most fundamental component of a laser package is, of course, laser diode. An important auxiliary component is the photodiode sensing the laser power. The special optical power loop is used for stabilization a mean optical power of the laser.

More sophisticated laser packages include the thermoelectric cooler needed to keep the laser temperature constant and the thermistor used as a temperature sensor (Fig. 3). The developed cheep model of optical link uses Fabry-Perot 1300 nm laser diode HP-LST2825-T-FP with output optical power about 1.2 mW, but for more difficult industrial conditions of exploitation a laser package with thermoelectric cooler may be used.

On the basis of results published earlier [3] simple three-transistor driving circuit was developed. The bandwidth of the driving circuit is greater than 1200 MHz. The circuit includes power loop for stabilization an output optical power.
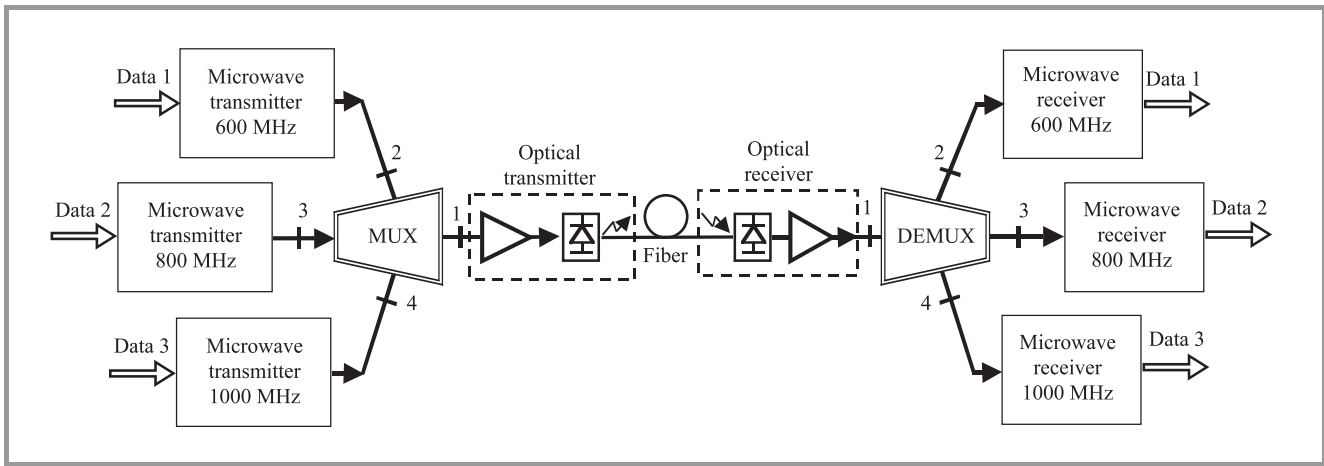
**Fig. 1.** Block diagram of optical-microwave transmission system.
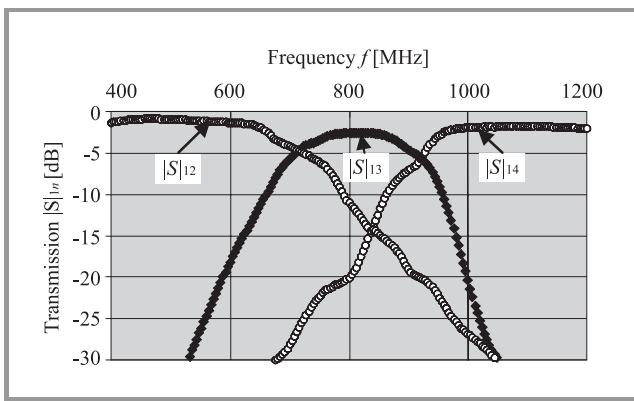


**Fig. 2.** Measured transmission between different arms of microwave multiplexer.
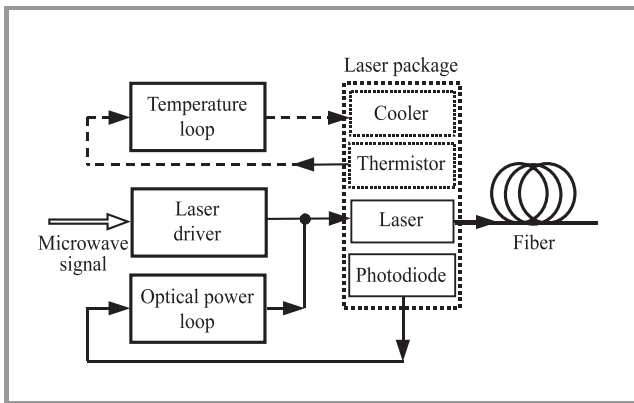


**Fig. 3.** Diagram of the laser driving circuit of optical transmitter.

Because the distance of transmission is expected to be below 1000 meters, a cheap multimode fiber has been used. For optical receiver a InP/InGaAs PIN FDD1003FC1[1] pho-

---

[1]This type of photodiode has been developed by Institute of Electronics, National Academy of Sciences of Belarus, 22 Lagoiski Trakt, 220090, Minsk, Belarus.
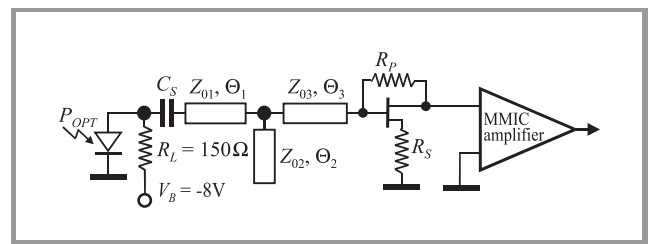
**Fig. 4.** Diagram of optical receiver with input matching circuit of the wideband low-noise transistor amplifier.

todiode was used with a bandwidth better than 3.5 GHz and a responsivity of 1 A/W [7]. Low-noise wideband amplifier, design with special input matching circuit, first amplifies output signal from photodiode. The signal is next amplified by monolithic integrated amplifier (Fig. 4). The capacitance $C_S$ effectively protects the preamplifier from the high DC component of the photocurrent. The 3 dB bandwidth of optical receiver is about 1.5 GHz.

## 4. Microwave signal processing

The optical-microwave transmission system is able to transmit three different streams of data: one analog signal and two signals in digital form.

The microwave processing of the one of the digital signals is shown in diagram in Fig. 5. The frequency of carrier is equal to 800 MHz. The amplitude modulation has been used at the transmitter side. At the receiver side the input signal is exactly filtered, next amplified and mixed with local oscillator frequency, then amplified and detected.

Two other microwave links use process of a frequency modulation (Fig. 6). The link with frequency carrier equal to 600 MHz is able to transmit an analog signal. The input analog signal between $+2$ V $\ldots -2$ V gives the changes of VCO frequency 600 MHz $\pm30$ MHz. Maximum of frequency deviation is equal to 30 MHz.

Jarosław Dawidczyk, Bogdan A. Galwas, Jerzy Skulski, Zenon Szczepaniak, Henryk Gruchała, and Sergey Malyshev
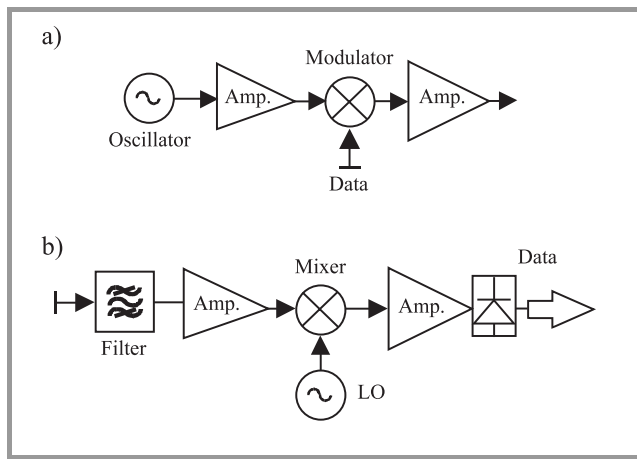
**Fig. 5.** Block diagram of microwave transmitter (a) and microwave receiver (b) for 800 MHz link with amplitude modulation.
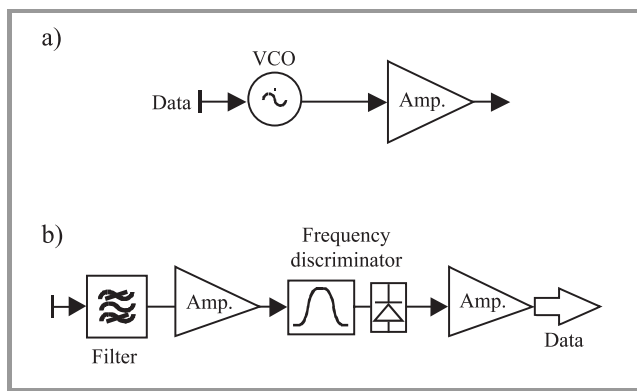


**Fig. 6.** Block diagram of microwave transmitter (a) and microwave receiver (b) for 600 MHz and 1000 MHz links with frequency modulation.

At the receiver side an input signal is filtered and next amplified. The frequency discriminator changes the frequency modulation to amplitude one. The detection and amplification complete the processing. The receiver filters together with demultiplexer selectivity give very good isolation between channels. The frequency responses of the channels are determined by the characteristics of receiver filters.

The second digital links uses 1000 MHz carrier frequency. This frequency is keying with deviation of 30 MHz. The block diagram of receiver is the same like in the case of analog one.

## 5. Conclusions

Multi-channels optical-microwave link with subcarrier multiplexing provides a unique set of advantages for telemetry industrial installations. The measured signals can be carry directly at RF and microwave frequencies over wide bands, with high dynamic range and without influence of industrial noise and disturbances. These capabilities allow telemetry electronics to be placed together with their operators, even when the sensors are hundred meters away.

In the nearest future full-duplex transmission system will be design. It will make possible to transmit data and orders in two directions, from operators to sensors also.

## References

[1] L. Kazovsky, S. Benedetto, and A. Willner, *Optical Fiber Communication Systems*. Boston, London: Artech House, 1996, Chapt. 7.

[2] R. Olshansky, V. A. Lanziesera, and P. M. Hill, "Subcarrier multiplexed lightwave systems for broad band distribution", *IEEE J. Lightw. Technol.*, vol. 7, pp. 1329–1342, 1989.

[3] T. Berceli *et al.*, "Improvements in fiber-optic transmission of multi-carrier TV signals", *IEEE Trans. MTT*, vol. 40, no. 8, pp. 910–914, 1992.

[4] J. Skulski, R. Perkowski, J. Piotrowski, and B. Galwas, "Mikrofalowy rezonatorowy czujnik do przemysłowych pomiarów stratnych materiałów dielektrycznych", in *Proc. Conf. COE'96*, Szczyrk, Poland, May 1996.

[5] B. Galwas, J. K. Piotrowski, and J. Skulski, "New type of microwave resonator sensors with waveguide below cut-off", in *Proc. Conf. Precis. Electromagn. Measur.*, Braunschweig, Germany, June 1996.

[6] J. Jasenek, O. Čermák, "Optical reflectometry with synthesized coherence function, in photonics, devices, and systems", *Proc. SPIE*, no. 4016, pp. 204–210, 2000.

[7] K. Piotrowski, B. A. Galwas, S. A. Malyshev, and V. F. Andrievski, "Investigation of InGaAs PIN photodiode for optical microwave mixing process", in *Proc. 12th Int. Microw. Conf. MIKON'98*, Cracow, Poland, May 1998.

**Jarosław Dawidczyk** received the M.Sc. degree in microelectronics from Warsaw University of Technology (Poland) in 1998. Since 1998 he is a Ph.D. student at the Institute of Microelectronics and Optoelectronics, Warsaw University of Technology. His research interests include modelling of optical-microwave mixing processes and modelling of optical-microwave devices.
e-mail: j.dawidczyk@elka.pw.edu.pl
Institute of Microelectronics and Optoelectronics
Warsaw University of Technology
Nowowiejska st 15/19
00-665 Warsaw, Poland
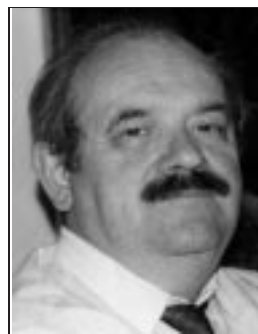
**Bogdan A. Galwas** was born in Poland, on October 31, 1938. In 1962, he joined the Faculty of Electronics, Warsaw University as Lecturer. He received the M.Sc. degree in 1962, the Ph.D. degree in 1969, and the D.Sc. degree in 1976, all in electronic engineering from Warsaw University of Technology, Poland. In 1986 he was promoted to Full Professor. His current research interests are microwave electronics and photonics. He is the author of more than

120 scientific papers and 2 books in these areas. His main field of academic interest is connected with technology of education, continuing engineering education and open distance learning. He is a Chairman of the International Management Committee of the International Travelling Summer Schools '91, Member of IACEE '97 and Member of SEFI '97.
e-mail: galwas@imio.pw.edu.pl
Institute of Microelectronics and Optoelectronics
Warsaw University of Technology
Koszykowa st 75
00-662 Warsaw, Poland

**Jerzy Skulski** received the M.Sc. degree in microelectronics from Warsaw University of Technology (Poland) in 1970. Actually he is a Lecturer at the Institute of Microelectronics and Optoelectronics, Warsaw University of Technology. His research interests include microwave sensors, generators, amplifiers and microwave measurement systems.
e-mail: jskulski@imio.pw.edu.pl
Institute of Microelectronics and Optoelectronics
Warsaw University of Technology
Nowowiejska st 15/19
00-665 Warsaw, Poland

**Zenon R. Szczepaniak** received the M.Sc. degree in optoelectronics from Warsaw University of Technology (WUT), Poland in 1998. Since 1998 he is a Ph.D. student at the Microwave Devices Division at the Warsaw University of Technology. His research interests include optically-controlled microwave circuits, modelling of optical-microwave devices and systems for telecommunication.
e-mail: zenon.szczepaniak@elka.pw.edu.pl
Institute of Microelectronics and Optoelectronics
Warsaw University of Technology
Koszykowa st 75
00-662 Warsaw, Poland

**Henryk Gruchała**
Military Academy of Technology
Kaliskiego st 2
01-476 Warsaw, Poland

**Sergey Malyshev** – for biography, see this issue, p. 16.

# Microwave harmonic generation in fiber-optical links

Attila Hilt

**Abstract** — **Optical transmission of microwave (MW) and millimeter-wave (MMW) signals has become an intensive research area in the last decade. There is a growing interest in optical processing of MW signals [1, 2], phased array applications [3] and wireless distribution of broadband data in fiber-fed MMW subscriber access systems [4 – 10]. This paper extends the existing models of MW/MMW optical links that are based on optical intensity [10, 11]. The model is suitable for estimating harmonic levels of the MW modulation signal generated in the optical path. Considering a MW fiber-optic link both the optical transmitter and the receiver are responsible for harmonic generation. Furthermore, the optical fiber itself inserted between the transmitter and receiver induces harmonics due to dispersion. Exact modelling of harmonic generation requires a calculation based on the optical field instead of on a purely intensity basis [12 – 14].**

*Keywords* — *optical transmission, fiber dispersion, microwaves, harmonics, IM/DD, coherent model, fiber length-bandwidth product.*

## 1. High-speed modulation of light

In interferometric modulators the light of the optical source is splitted into two beams and then interference is created between these beams (Fig. 1). Interferometric optical modulators are usually called Mach-Zehnder modulators (MZM).
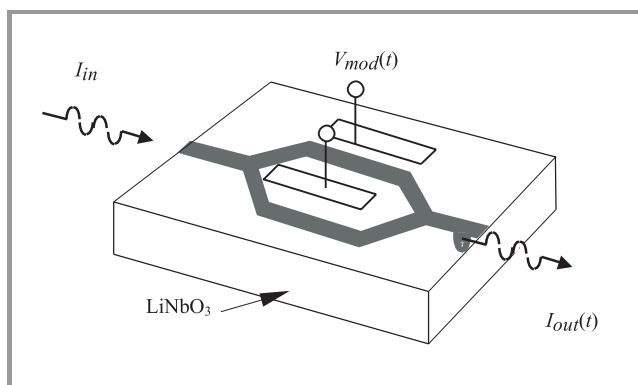


**Fig. 1.** MZM integrated on LiNbO$_3$ (one arm modulated).

A phase modulator is inserted into one branch inducing phase difference between the beams. If the phase difference is $\pi$ a rejection of the input optical signal occurs. When the beams interfere constructively, the output intensity is equal to the input intensity assuming lossless modulator ($A = 1$).

If the power dividers split and recombine the optical power equally, the output intensity is written as:

$$I_{out}(t) = A\frac{I_{in}}{2}\left(1 + \cos\varphi(t)\right) = AI_{in}\cos^2\frac{\varphi(t)}{2}, \qquad (1)$$

where $A$ is the optical loss in the modulator and $\varphi(t)$ is the phase difference between the propagating waves,

$$\varphi(t) = \pi\frac{V_{mod}(t)}{V_\pi} = \pi\frac{V_{DC} + V_{RF}(t)}{V_\pi}. \qquad (2)$$

Figure 2 shows the modulator transmittance as a function of the modulation voltage. $V_{DC}$ is the bias voltage of the modulator. The half-wave voltage $V_\pi$ introduces $\pi$ phase difference between the modulator arms. This voltage is required to drive the modulator between adjacent minima and maxima. Applying periodic modulation as:

$$V_{mod}(t) = V_{DC} + V_{RF}\cos(\omega_{RF}t) \qquad (3)$$

the intensity becomes

$$I_{out}(t) = \frac{I_{in}}{2}\left[1 + \cos\left(\pi\gamma + \pi\alpha\cos\omega_{RF}t\right)\right], \qquad (4)$$

where $\gamma = V_{DC}/V_\pi$ and $\alpha = V_{RF}/V_\pi$ are the normalized bias and $RF$ signal amplitudes driving the MZM, respectively. The optimal DC bias for linear operation is: $V_{DC} = V_\pi/2 + iV_\pi$ where $i \in Z$. The case of $i = 0$ is called the quadrature.
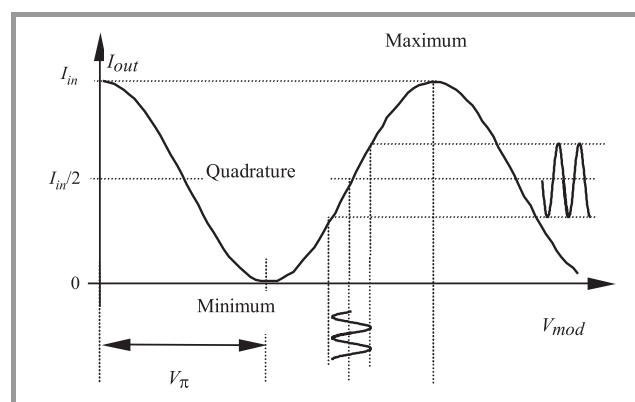


**Fig. 2.** Calculated double sided optical intensity spectrum at linear operation ($\gamma = 0.5$ or 1.5) for $\alpha = 0.25$.

The output optical intensity can be expressed from Eq. (4) by Bessel-function expansion:

$$I_{out}(t) = \frac{I_{in}}{2} + \frac{I_{in}}{2}\cos(\gamma\pi) \times$$

$$\times \left\{ J_0(\alpha\pi) + 2\sum_{k=1}^{+\infty}(-1)^k J_{2k}(\alpha\pi)\cos\left[2k\omega_{RF}t\right] \right\} +$$

$$-\frac{I_{in}}{2}\sin(\gamma\pi) \times$$

$$\times \left\{ 2\sum_{k=1}^{+\infty}(-1)^k J_{2k+1}(\alpha\pi)\cos\left[(2k+1)\omega_{RF}t\right] \right\}. \quad (5)$$

Equation 5 indicates that due to nonlinearity of the modulation function the output intensity contains harmonics of the modulation frequency $\omega_{RF}$ in spite of that the modulation voltage is an ideal sinusoid. The double sided intensity spectrum has been calculated at the MZM output by fast Fourier transform (FFT) as a function of the harmonic number $k$. From the general expression of Eq. (5) the special cases are the quadrature (or linear) operation, the minimum and the maximum transmission modes. If the MZM is biased for linear operation the intensity contains only odd harmonics and a DC component (Fig. 3).
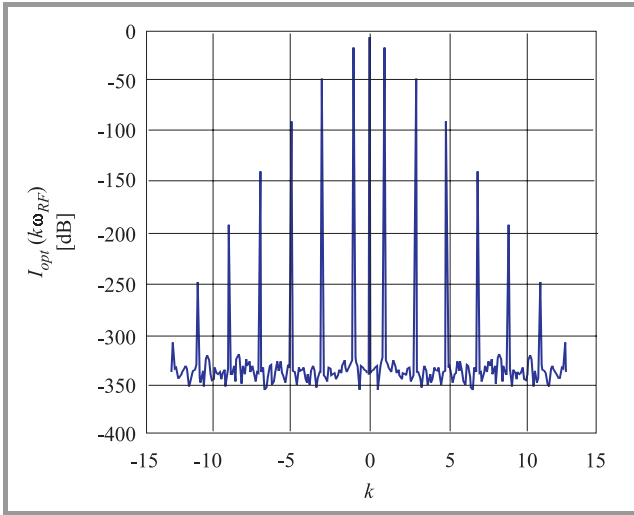


***Fig. 3.*** Calculated double sided optical intensity spectrum at maximum transmission ($\gamma = 2$), for $\alpha = 0.25$.

In Fig. 4 the MZM is biased for maximum transmission. Compared to Fig. 3, odd harmonics disappeared and only even harmonics of the modulation signal are present in the intensity spectrum. The DC term has larger amplitude but the modulation signal and all its odd harmonics are strongly suppressed. In other words, at this special bias point the MZM generates second harmonic of the modulation signal (Fig. 4). Such special operation modes find interesting applications in transmission of MMW signals over dispersive fiber as well as in optical generation of MMW signals. Considering small modulation indices

(of $V_{RF}(t) << V_\pi$ so $\alpha << 1$) and a DC bias for linear operation with $\gamma = 1.5$, Eqs. (4) and (5) simplify to:

$$I_{out}(t) = \frac{I_{in}}{2}\left[1 + \cos\left(\frac{3}{2}\pi + \pi\alpha\cos\omega_{RF}t\right)\right] =$$

$$= \frac{I_{in}}{2}\left[1 + \sin\left(\pi\alpha\cos\omega_{RF}t\right)\right] \approx \frac{I_{in}}{2}\left[1 + m\cos\omega_{RF}t\right], \quad (6)$$

where $m = \alpha\pi$ denotes the optical modulation depth (OMD). Small-signal modulation allows linear approximation of the sinusoidal modulator transmittance function. Let us suppose now that the MZM is biased at quadrature for linear operation. Power level of the detected fundamental signal and any odd harmonic can be calculated as a function of MZM driving voltage:

$$P_{DET}(n, V_{RF}) = \frac{R_{50}}{8}\left(R_{PD}J_{out}\right)^2 =$$

$$= \frac{R_{50}}{8}R_{PD}^2 I_{in}^2 A^2 J_n^2\left(\pi\frac{V_{RF}}{V_\pi}\right), \quad (7)$$

where $n = 2k + 1$; $R_{50}$ stands for the resistive load and $n = 1$ means the detected fundamental signal. Optical intensities at the modulator input and output are denoted by $I_{in}$ and $I_{out}$, respectively. In Eq. (7) a resistive matching to the 50 $\Omega$ load is supposed. Figures 5 and 6 show harmonic levels as a function of MW power and DC bias driving the modulator, respectively.

The optical field at the MZM output is:

$$E(t) = E_0\cos\omega_0 t\cos\left[\gamma\frac{\pi}{2} + \alpha\frac{\pi}{2}\cos\omega_{RF}t\right]. \quad (8)$$
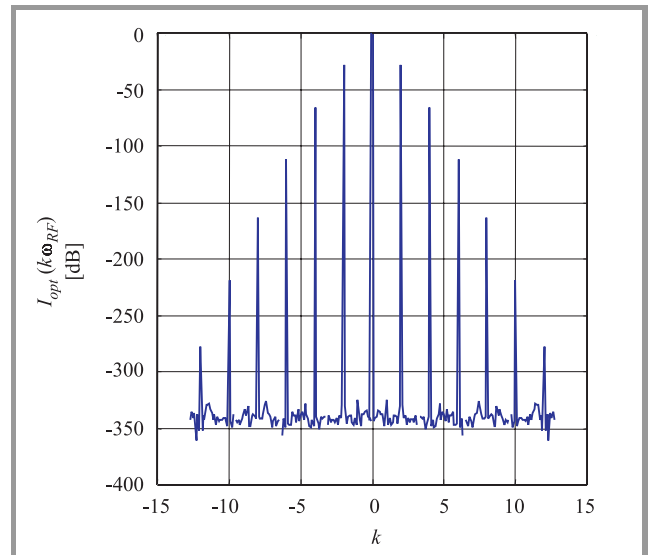


***Fig. 4.*** Fundamental and odd harmonics of the detected optical intensity versus MW driving power; $I_{in} = 1.2$ mW, $A = 3$ dB, $V_\pi = 5$ V, $R_{PD} = 0.8$ A/W .
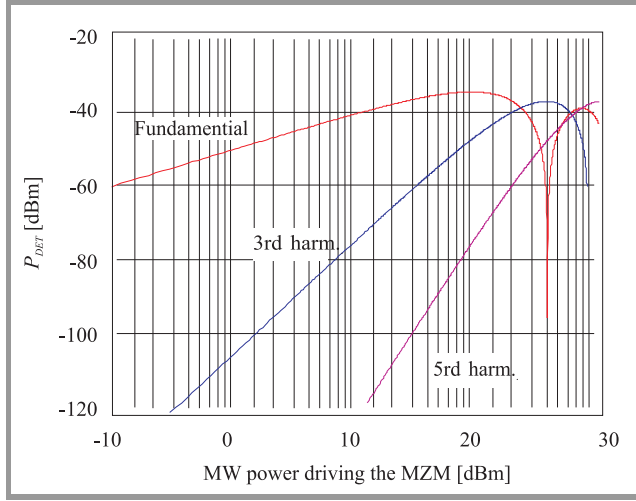
**Fig. 5.** Detected DC and harmonic contents versus $\gamma$ (calculated with $I_{opt} = 400\ \mu$W, $R_{PD} = 0.356$ A/W, $m = 0.586$).
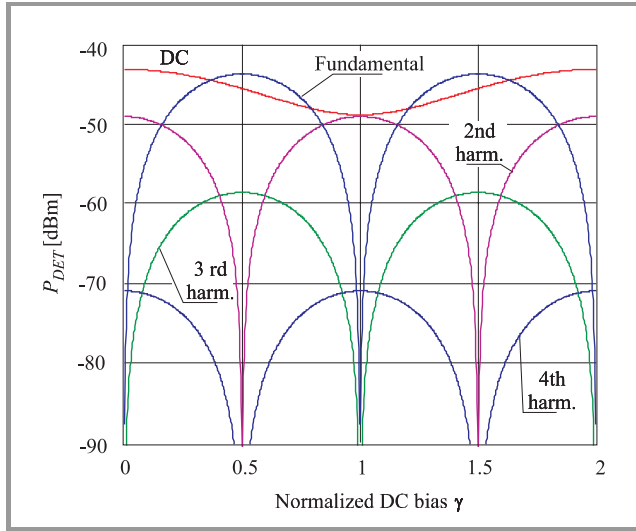


**Fig. 6.** Maximum SMF length $L$ resulting 3 dB $C/N$ degradation versus dispersion parameter $D$.

In Eq. (8) $E_0 \cos \omega_0 t$ is the optical carrier. The optical field expressed from Eq. (8) by Bessel-function expansion is:

$$
\begin{aligned}
E(t) = {} & E_0 J_0\left(\alpha\frac{\pi}{2}\right) \cos\left(\gamma\frac{\pi}{2}\right) \cos\omega_0 t + \\
& -E_0 J_1\left(\alpha\frac{\pi}{2}\right) \sin\left(\gamma\frac{\pi}{2}\right) \cos\left(\omega_0 \pm \omega_{RF}\right)t + \\
& -E_0 J_2\left(\alpha\frac{\pi}{2}\right) \cos\left(\gamma\frac{\pi}{2}\right) \cos\left(\omega_0 \pm 2\omega_{RF}\right)t + \\
& +E_0 J_3\left(\alpha\frac{\pi}{2}\right) \sin\left(\gamma\frac{\pi}{2}\right) \cos\left(\omega_0 \pm 3\omega_{RF}\right)t + \dots \quad (9)
\end{aligned}
$$

# 2. Quadratic photodetection

Usually the photocurrent calculated by Eq. (10) and said to be proportional to the modulated optical intensity [15]:

$$
i_{PD}(t) = R_{PD} P_{opt}(t). \quad (10)
$$

In Eq. (10) the phase information of the optical wave is lost. Since in a coherent model the phase cannot be neglected, let us consider now the general case when instead of the intensity the optical field is given:

$$
i_{PD}(t) \propto R_{PD} 2\left\langle E^2(t) \right\rangle = R_{PD} \left\langle E(t) E^*(t) \right\rangle. \quad (11)
$$

Here, $\langle\ \rangle$ means time averaging taken over a few optical periods, $E(t)$ represents a real valued function and factor 2 is chosen for later convenience [16]. Time averaging means the physical fact, that the PD cannot response to rapid changes at optical frequencies, only the MW/MMW modulation envelope of the optical carrier is detected. Supposing an incident optical field as a combination of two spectral components having the same polarization:

$$
\begin{aligned}
i_{PD}(t) \propto {} & R_{PD} 2\Big\langle \big[ E_1 \cos(\omega_1 t + \varphi_1) + \\
& + E_2 \cos(\omega_2 t + \varphi_2) \big]^2 \Big\rangle = \\
= {} & R_{PD} \Big\langle E_1^2 + E_2^2 + E_1^2 \cos 2(\omega_1 t + \varphi_1) + \\
& + E_2^2 \cos 2(\omega_2 t + \varphi_2) + \\
& + 2E_1 E_2 \cos\left[(\omega_1 - \omega_2)t + \varphi_1 - \varphi_2\right] + \\
& + 2E_1 E_2 \cos\left[(\omega_1 + \omega_2)t + \varphi_1 + \varphi_2\right] \Big\rangle = \quad (12) \\
= {} & R_{PD} \Big\{ E_1^2 + E_2^2 + 2E_1 E_2 \cos\left[(\omega_1 - \omega_2)t + \varphi_1 - \varphi_2\right] \Big\}.
\end{aligned}
$$

The above calculation is referred to a coherent beating of the input optical signals. Terms $2\omega_1$, $2\omega_2$ and $\omega_1 + \omega_2$ disappeared due to averaging. Remaining terms represent a DC component and a current having a MW frequency equal to the difference of the input optical frequencies. As seen from Eq. (12) coherent beating can be used to generate MW and MMW signals optically. Let us consider now the optical field present at a MZM output in the case of small OMD. This optical field is approximated now by three spectral lines only. Using the complex form of Eq. (11) we can calculate the photocurrent as:

$$
\begin{aligned}
i_{PD}(t) \propto {} & R_{PD} 2\Big\langle \Big\{ E_{RF} \cos\left[(\omega_0 - \omega_{RF})t - \varphi_1\right] + \\
& + E_0 \cos(\omega_0 t) + E_{RF} \cos\left[(\omega_0 + \omega_{RF})t + \varphi_2\right] \Big\}^2 \Big\rangle = \\
= {} & R_{PD} \Big\{ E_{RF} e^{j\left[(\omega_0 - \omega_{RF})t - \varphi_1\right]} + E_0 e^{j\omega_0 t} + \\
& + E_{RF} e^{j\left[(\omega_0 + \omega_{RF})t + \varphi_2\right]} \Big\} * \Big\{ E_{RF} e^{-j\left[(\omega_0 - \omega_{RF})t - \varphi_1\right]} + \\
& + E_0 e^{-j\omega_0 t} + E_{RF} e^{-j\left[(\omega_0 + \omega_{RF})t + \varphi_2\right]} \Big\} = R_{PD} \Big[ E_0^2 + 2E_{RF}^2 + \\
& + 4E_0 E_{RF} \cos\left(\frac{\varphi_2 - \varphi_1}{2}\right) \cos\left(\omega_{RF} t + \frac{\varphi_1 + \varphi_2}{2}\right) + \\
& + 2E_{RF}^2 \cos 2\left(\omega_{RF} t + \frac{\varphi_1 + \varphi_2}{2}\right) \Big]. \quad (13)
\end{aligned}
$$

It is seen from Eq. (13) that second harmonic of the modulation signal $\omega_{RF}$ is generated, however small OMD and ideal photodetector have been supposed. The modulation signal cannot be recovered if the phase difference $\varphi_2 - \varphi_1$ is equal to $(2n+1)\pi$. Generally the optical field $E(t)$ is composed of several spectral lines (see Eq. (9)). In this case the exact calculation is difficult, since $\omega_{RF}$ components arise from the mutual beating of each pair of spectral lines that are separated by $\omega_{RF}$. Similarly, the harmonic $n\omega_{RF}$ is generated from the beating of any two lines being separated $n$ times $\omega_{RF}$ apart. Finally, the photocurrent has a discrete spectrum of:

$$i_{PD}(\omega) \propto R_{PD}(\omega) \sum_{k=0}^{N-1} i(k\omega_{RF}), \qquad (14)$$

where $N$ is the number of the optical field spectral components taken into account. The DC term is given by $k=0$ and $k=N-1$ gives the higher order harmonic. Calculation by Eqs. (13)–(14) is rather tedious. An easier solution starts with the optical field $E(t)$ given in time domain and uses the complex form of Eq. (11). Then the spectrum of the photocurrent at the PD output can be simply determined by Fourier transform. For calculation simplicity, this method using FFT has been used in our computer simulations:

$$i_{PD}(\omega) \propto R_{PD}(\omega) \mathbf{F}\left\{ E(t)E^*(t) \right\}. \qquad (15)$$

# 3. Effect of chromatic dispersion on MW transmission

Considering small modulation index ($\alpha << 1$) and optimal modulator bias for linear operation, the optical field at the MZM output can be approximated by three main spectral components at $\omega_0$ and $\omega_0 \pm \omega_{RF}$ (Eqs. (8)–(9)). This field suffers from dispersion during propagation in a standard single mode fiber (SMF) exhibiting a chromatic dispersion factor of $D = 17$ ps/km/nm. The optical field at the SMF output is calculated with the fiber transfer function $H(\omega)$ approximated by its Taylor series up to the second order:

$$E_{out}(\omega) = E_{in}(\omega)H(\omega) \approx$$
$$\approx E_{in}(\omega)e^{-j\left(\beta_0 + \beta_0'\Delta\omega + \beta_0''\frac{\Delta\omega^2}{2}\right)L}. \qquad (16)$$

For simplicity we omitted the linear fiber attenuation. In the exponent of Eq. (16) the first term results in a phase delay, meanwhile the second term represents the group delay. These terms are out of interest here. However, the third term introduces additional phase change due to chromatic dispersion. Inserting the dispersion parameter $D$ into Eq. (16) from $\beta_0'' = -\lambda^2 D / 2\pi c$, supposing an input optical field of Eq. (9) and applying Eq. (16), the photocurrent after quadratic photodetection is written as:

$$i_{PD}(t) = R_{PD}\Big\{ E_0^2 + 2E_{RF}^2 + 4E_0E_{RF}\cos\left(\frac{LD}{4\pi c}\lambda^2\omega_{RF}^2\right) \cdot$$
$$\cdot \cos\left[\omega_{RF}(t-\tau)\right] + 2E_{RF}^2\cos\left[2\omega_{RF}(t-\tau)\right] \Big\}, \quad (17)$$

where $\tau = \beta_0'L$ is the group delay. As seen in Eq. (17) the detected signal is composed of a DC photocurrent, the fundamental signal delayed by $\tau$ and its second harmonic. Neglecting DC and harmonic terms, omitting the delay and inserting $E_{RF} = mE_0/4$ into Eq. (17) the photocurrent at the fundamental of the modulation frequency $f_{RF}$ is:

$$i_{PD,\omega_{RF}}(t) =$$
$$= R_{PD}mE_0^2\cos\left(cD\pi L\left(f_{RF}/f_{opt}\right)^2\right)\cos\left(\omega_{RF}t\right). \quad (18)$$

Based on Eq. (18) the electrical power delivered from the matched photodiode to the load is proportional to:

$$P_{RF}^{[dB]}(f_{RF},L,D) \propto$$
$$\propto 10\log\left\{ \left(R_{PD}mE_0^2\right)^2\cos^2\left[cD\pi L\left(f_{RF}/f_{opt}\right)^2\right] \right\} \propto$$
$$\propto 20\log\left| \cos\left[cD\pi L\left(f_{RF}/f_{opt}\right)^2\right] \right|. \qquad (19)$$
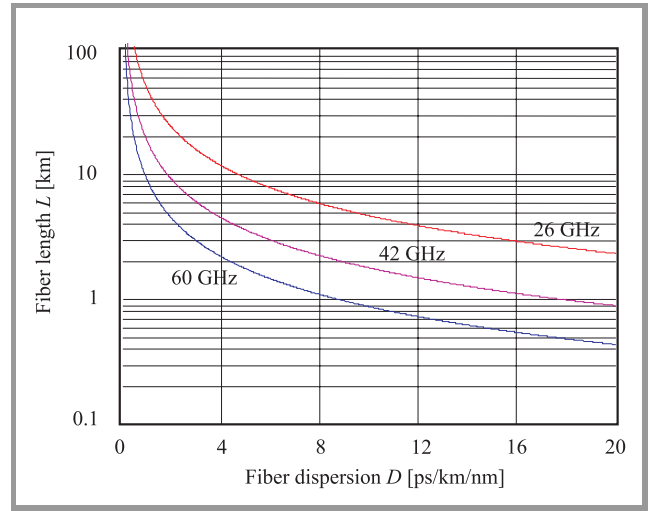


**Fig. 7.** Measured rejection at $f_{RF} = 14.2$ GHz for a fiber length of $L = 19.2$ km.
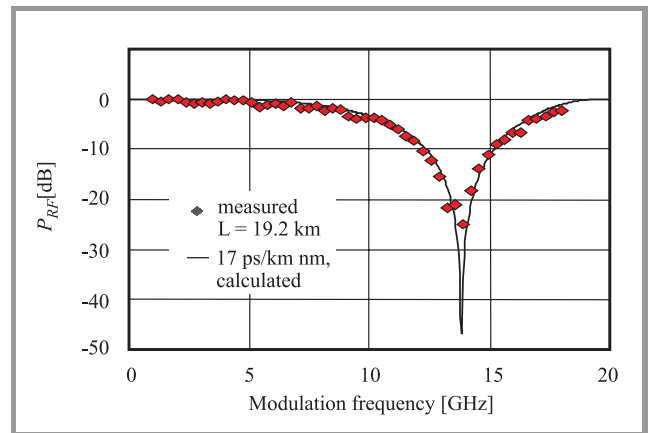


**Fig. 8.** Measured rejection at $f_{RF} = 14.2$ GHz for a fiber length of $L = 19.2$ km.

As it is shown in Figs. 7 and 8, the phase difference between the spectral components propagating in the fiber can result in a complete rejection of the transmitted MW or MMW signals. In Fig. 8 results obtained by scalar measurements on the $L = 19.2$ km long FDDI ring of our University are compared to the theoretical curve [10].

## 4. Harmonics in dispersive transmission

In Section 3 the optical field $E(\omega)$ present at the SMF input has been approximated by three spectral lines only. This simplification reduced the calculation difficulties significantly and we were able to derive analytical results. In the general case however, several optical field spectral lines are present at the fiber input. Detected amplitude and phase of these optical field spectral components are determined by the LD, by the MZM as well as by parameters of propagation in the dispersive fiber. Only coherent models can explain properly detected levels of different harmonics of the modulation signal. Based on the coherent model of the MW optical link we simulated the effect of chromatic dispersion in the general case of several spectral lines. In this coherent model the calculation is based on the optical field and not on the optical intensity. Here we present simulation results for harmonic generation. Harmonics are generated due to propagation in dispersive fiber. When the MZM is biased for linear operation, only odd components are present in the optical intensity (Fig. 3). In the optical field both even and odd spectral components are present (Fig. 9). When this optical field is launched into a SMF, due to dispersion even intensity components will appear after propagation. Calculated levels of harmonics are shown in Fig. 10. Since phase of harmonics are rotated faster in the fiber than
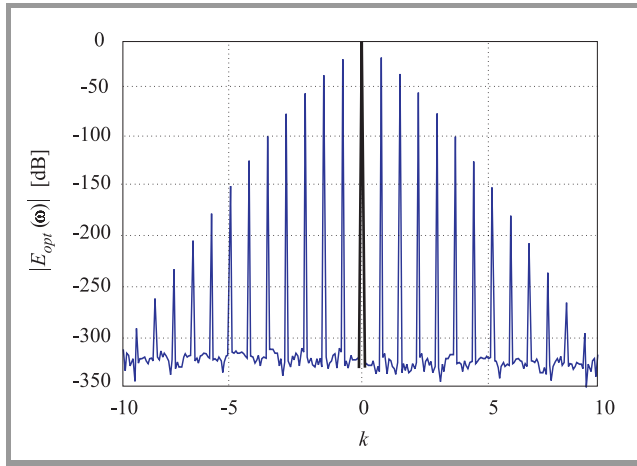


**Fig. 9.** MZM output field at bias for linear operation, $\alpha = 0.4$; $\gamma = 0.5$; $\omega = \omega_0 \pm k\omega_{RF}$.
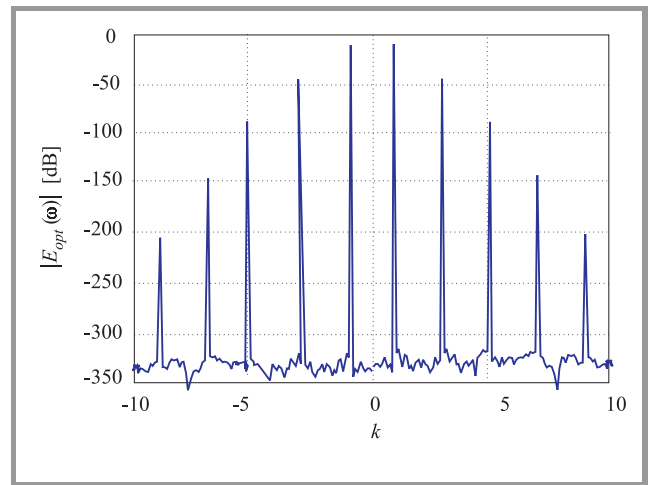


**Fig. 11.** MZM output field at bias for minimum transmission, $\alpha = 0.4; \gamma = 1; \omega = \omega_0 \pm k\omega_{RF}$.
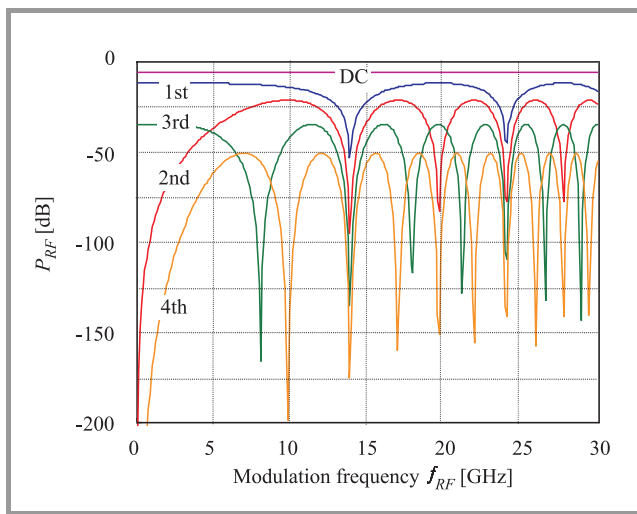


**Fig. 10.** Detected signals after propagation in dispersive fiber of $L = 19.2$ km, input field as in Fig. 9.
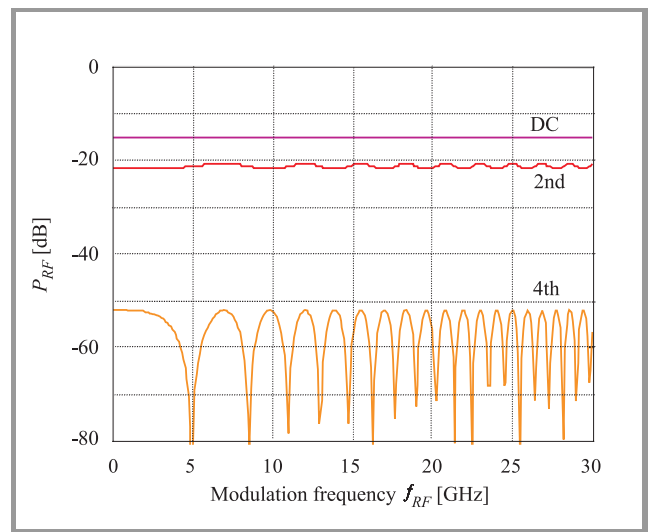


**Fig. 12.** Detected signals after propagation in dispersive fiber of $L = 19.2$ km, input field as in Fig. 11.

phase of the fundamental, second harmonic has two times, third harmonic has three times more rejections between two rejections of the fundamental. We note that this phenomena cannot be explained by the incoherent model of the MW optical link.

On the other hand, if the MZM is biased for minimum transmission (Fig. 11), the second harmonic of the modulation signal is not rejected, even after propagation in a nearly 20 km dispersive fiber (Fig. 12). In this case the phase difference cannot create complete rejection, since the optical carrier is suppressed. The advantage of the method is that only the subharmonic of the desired MMW signal is desired to drive the optical modulator. The developed method is rather general, it is suitable for calculating the effect of fiber dispersion simultaneously with effect of modulator bias in external modulation and chirp of direct modulated laser diodes as well [13 –15].

# 5. Conclusions

Effect of chromatic dispersion on optical transmission of digital baseband signals is well described in the literature. However, for analogue MW/MMW IM/DD optical links chromatic dispersion has not been fully analyzed yet. In this paper MW harmonic generation in IM/DD fiber-optical links is discussed. The influence of chromatic dispersion on the optical transmission of MW/MMW signals in standard single mode fibers has been also examined. It was pointed out that standard SMF links operating at $\lambda = 1550$ nm cannot be used for transmission of MW/MMW signals without encountering the effect of chromatic dispersion. It was shown that dispersion penalty significantly limits the transmission distance in IM/DD optical links operating above 10 GHz. A several km long fiber-optical link filters the transmitted MW or MMW signal. As a function of fiber length $L$ rejections are periodic and these periods are shorter and shorter as the modulation frequency $f_{RF}$ is increased. First analytic explanation of the problem was given. Chromatic dispersion results in a difference between phase states of optical IM field sidebands. These sidebands are beaten coherently on the photodetector. As introduced in Eq. (13) as soon as the phase difference approaches $\pi$ the modulation signal is lost. Then we presented a general model to calculate the harmonic levels and the effect of chromatic dispersion numerically. By the presented coherent model detected harmonics are estimated. To avoid chromatic dispersion problems, one might propose tailoring the fiber length exactly at the maxima of the penalty function shown in Fig. 8. As we demonstrated in Fig. 10 the locations of these maxima do not depend only on the fiber span but also on the IM frequency. Furthermore, temperature dependence, aging and polarization mode dispersion should be considered too.

# References

[1] R. Helkey, "Advances in frequency conversion optical links", in *Proc. 10th Microw. Coll. MICROCOLL'99*, Budapest, Hungary, March 1999, pp. 365–369.

[2] A. Hilt, "Transmission et traitement optiques des signaux dans les systemes de télécommunications hertziens". Ph.D. thesis, Institut National Polytechnique de Grenoble, Grenoble, France, May 1999.

[3] I. Frigyes and A. J. Seeds, "Optically generated true-time delay in phased-array antennas", *MTT (Special Issue)*, vol. 43, no. 9, part II, pp. 2378–2386, 1995.

[4] T. Berceli, A. Hilt, G. Járó, and G. Maury, "Optical processing and transmission of subcarrier multiplexed microwave signals", in *Proc. Opt. Technol. Microw. Syst. Workshop 29th EuMC*, München, Germany, Oct. 1999.

[5] T. Berceli, G. Járó, T. Marozsák, A. Hilt *et al.*, "Generation of millimeter waves for mobile radio systems", in *Proc. 10th Microw. Coll., MICROCOLL'99*, Budapest, Hungary, March 1999, pp. 375–378.

[6] A. Hilt, A. Vilcot, T. Berceli, T. Marozsák, and B. Cabon. "New carrier generation approach for fiber-radio systems to overcome chromatic dispersion problems", in *Proc. IEEE MTT Symp.*, Baltimore, USA, June 1998, part TH3C-5, pp. 1525–1528.

[7] T. Marozsák, T. Berceli, G. Járó, A. Zólomy, A. Hilt, S. Mihály, E. Udvary, and Z. Varga, "A new optical distribution approach for millimeter wave radio", in *Proc. IEEE MTT Top. Meet. Microw. Phot., MWP'98*, Princeton, New Jersey, USA, Oct. 1998, pp. 63–66.

[8] A. Hilt, T. Marozsák, G. Maury, T. Berceli, B. Cabon, and A. Vilcot, "Radio-node upconversion in millimeter-wave fiber-radio distribution systems", in *Proc. Int. Conf. Microw. Radar, MIKON'98*, Kraków, Poland, May 1998, vol. 1, pp. 176–180.

[9] A. Hilt, A. Zólomy, T. Berceli, G. Járó, and E. Udvary, "Millimeter wave synthesizer locked to an optically transmitted reference using harmonic mixing", in *Techn. Dig. IEEE Top. Meet. Microw. Phot., MWP'97*, Duisburg, Germany, Sept. 1997, pp. 91–94.

[10] I. Frigyes, I. Habermajer, B. Molnár, A. J. Seeds, and F. Som, "Noise and loss characteristics of microwave direct modulated optical links", in *Proc. 27th EuMC*, Jerusalem, Israel, 1997.

[11] C. H. Cox III., G. E. Betts, and L. M. Johnson, "An analytic and experimental comparison of direct and external modulation in analog fiber-optic links", *MTT*, vol. 38, no. 5, pp. 501–509, 1990.

[12] A. Hilt, G. Maury, A. Vilcot, and B. Cabon, "Numerical model of chromatic dispersion effects in analogue IM/DD optical links", in *Proc. 2nd Int. Summer School Interact. Microw. Opt., OMW'99*, Autrans, France, July 1999, pp. 141–142.

[13] A. Hilt, G. Maury, B. Cabon, A. Vilcot, and L. Giacotto, "General approach to chromatic dispersion analysis of microwave optical link architectures", in *Proc. 10th Conf. Microw. Techn., COMITE'99*, Pardubice, Czech Republic, Oct. 1999, pp. 177–180.

[14] G. Maury, A. Hilt, B. Cabon, V. Girod, and L. Degoud, "Remote upconversion in microwave fiber-optic links employing an unbalanced Mach-Zehnder interferometer", in *Proc. SPIE's 44th Ann. Meet., THz & GHz Phot. Conf.*, Denver, Colorado, USA, July 1999, part 3795–71.

[15] A. Hilt, G. Járó, A. Zólomy *et al.*, "Microwave characterization of high-speed pin photodiodes", in *Proc. 9th Conf. Microw. Techn. COMITE'97*, Pardubice, Czech Republic, Oct. 1997, pp. 21–24.

[16] B. E. A. Saleh and M. C. Teich, *Fundamentals of Photonics*. John Wiley & Sons Inc., 1991.

---

**Attila Hilt** graduated in electrical engineering at the Technical University of Budapest, Hungary in 1990. In 1989 he joined the Research Institute for Telecommunications (TKI Rt., presently called the Innovation Company for Telecommunications), Hungary. He worked on the design and development of microwave, millimeter-wave and optical circuits and systems. His research interests include various communication systems, MW and MMW photonics, combined optical-wireless and GSM systems. He received his Ph.D. degree in optics, optoelectronics and microwaves from the Institut National Polytechnique de Grenoble (INPG), France in May 1999 and from the Budapest University of Technology and Economics in September 2000. Until 1999 he headed the Communications Test Laboratory of TKI. In 2000 he joined NOKIA Hungary as Sr. transmission network planner. He is involved in the design of Vodafone's nationwide GSM access network in Hungary. He is currently leading a research contract on high speed optical receivers at the Microwave Telecommunications Department of the Budapest University of Technology and Economics. He is an author/co-author of more than 50 papers presented in conferences or published in scientific journals. He is a member of the IEEE MTT and Communications societies.
e-mail: attila.hilt@nokia.com
Nokia Hungary Kft.
H-2040 Budaörs, Szabadság út 117./B.
Atronyx House, 5th floor.
BMGE-MHT, Budapest University
of Technology and Economics
Dept. of Microwave Telecommunications
H-1111 Budapest
Goldmann György tér 3. V2 épület, Hungary

# Lowering the uncertainty
# in fast noise measurement procedures

Gianluca Acciari, Franko Giannini, Ernesto Limiti, and Giovanni Saggio

**Abstract** — **To completely characterise the noise behaviour of a two port device, four noise parameters $F_{min}$, $R_n$, $G_{opt}$ and $B_{opt}$ must be determined. This paper reports improvements in the uncertainty related to the above parameters, taking into account measurement errors due both to the limited instrument precision and connection repeatability. Results are reported for noise characterisation of 0.3 $\mu$m $\delta$-doped HEMT devices by Alenia, demonstrating as the common hot-cold measurement procedure can result with an error confidence as low as 0.2% for all the noise parameters.**

*Keywords* — *noise, device characterisation, measurement errors, lowering uncertainty.*

## 1. Introduction

The F50 method [1] is recognised as a well established procedure to determine the four noise parameters of a noisy two port. It allows simple and fast measurement procedures with respect to standard method characterisation, where a tuner is needed. Nevertheless, the F50 method has an important drawback since an equivalent circuit model of the DUT is necessary. It is therefore important an exhaustive investigation of the standard procedure also to establish the final obtainable measurement accuracy it can provide.

To overcome the overall measurement uncertainty problem it is necessary to maximise the measure repeatability and to compensate for systematic errors. In order to solve the Friis formula for the determination of the noise parameters, more than four measurements (corresponding to four different values of the source reflection coefficient $\Gamma_s$), are required for redundancy. The evaluation of the optimum number of measurements which are convenient to carry out is not an easy task, and many efforts have been spent to determine its minimum value, since the measurement procedure is quite time consuming.

Assuming the DUT as a two port device, its noise behaviour as a function of the source admittance $Y_s = G_s + jB_s$, can be expressed as:

$$F = F_{min} + \frac{R_n}{Re\{Y_s\}} \left| Y_{opt} - Y_s \right|^2, \qquad (1)$$

where $Y_{opt} = G_{opt} + jB_{opt}$ is the optimum source admittance which gives the minimum noise figure $F_{min}$ for the DUT and $R_n$ is the equivalent noise resistance.

Since the noise figure $F$ value depends on the source admittance $Y_s$, its determination is consequently subordinated to random and/or systematic measurement errors. In order to evaluate the four unknown values $F_{min}$, $R_n$, $G_{opt}$ and $B_{opt}$,

in principle the $Y_s$ value can be experimentally varied until a minimum in the $F_{min}$ value is obtained. From a practical point of view, four different values of source admittance could be enough in order to solve, a linearised system [2] of four equations. Nevertheless, to minimise the errors due to measurement inaccuracy, is commonplace to consider more than four $Y_s$ values for redundancy.

It has been previously reported how the accuracy increases with the redundancy of experimental data [3], but at the same time, different criteria may help in the reduction of the needed experimental data to the order of tens [4]. These criteria come from the necessity of a simple algebric manipulation for a few measurement points but exhibit the drawback of the time consuming search for particular $\Gamma_s$ values varying the position of the tuner's probe. Thanks to modern computer-controlled mechanical tuners and to efficient and adequate equipment, heavy procedures in terms of calculus can be implemented with no particular computing overhead. So it appears common sense to increase the number of redundant measurements since the effort established in reducing it can be generally paid just in terms of accuracy.

Taking advantage of the fact that all the measurement set-up is computer-controlled via GP-IB, the measurement procedure here adopted is fully automated and completely optimised so that, to collect a data set in the order of hundreds, both the $S$ parameter characterisation and the noise measurements need only few minutes per frequency.

## 2. Experimental set-up

The proposed experimental set-up is optimised for on-wafer measurement. To characterise each block of the measurement chain a preliminary standard SOLT calibration has been performed, while a TRL procedure has been adopted to de-embed the contribution of the probes by a home-made software algorithm. The source admittance is varied by a slide screw computer controlled mechanical tuner. The set-up is fully controlled via a GP-IB bus.

Before noise measurements, a S parameter characterisation has been performed for all parts of the measurement chain, by a HP8510C vector network analyser.

## 3. Experimental results

The overall measurement accuracy can be affected by many potential errors, generally classified into a first group eval-

uated by statistical methods and a second group evaluated by manufacturer specifications [5]. Statistical methods can be applied to evaluate the error amounts which can be due, for instance, to mismatch problems, to EM susceptance of the set-up or to connection repeatability. Manufacturer specification accuracies can be adopted for the standards when the calibration procedure is performed, for the factory tabled ENR values of the noise source, for the tuner position repeatability, and in general for the instrumentation uncertainty.
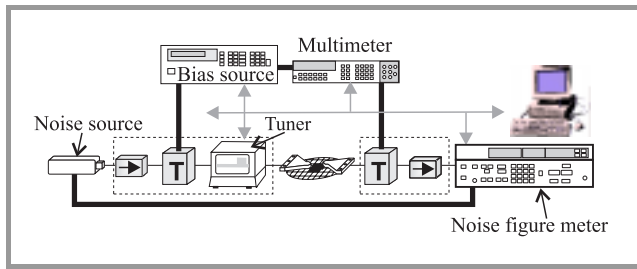


**Fig. 1.** Measuring system scheme. It is based on the HP346C noise source, home-designed wafer probe station, HP8970B noise figure test set and on the Focus 1808 mechanical tuner. The input block (isolator, bias tee, tuner) and the output block (bias tee, isolator) are highlighted.

Given their large number, it is practically impossible to account for all the possible error sources but, in our experience, the influence of all of them on the final results can be summarised in a percentage variation both on the measured $S$ parameters (for each block in the measurement chain), and on the overall insertion gain $G_{ins}$ and noise figure $F_{tot}$. In particular for the measured $S$ parameters a $\pm4\%$ error has been assumed for the DUT and for the block before DUT it in the measurement chain (first **isolator, bias tee** and **tuner** in Fig. 1), and an error of $\pm0.3$ dB has been assumed for the insertion gain $G_{ins}$ measured by the noise figure meter and for the measured noise figure $F_{tot}$ of the entire chain. With such error adoptions, a Monte Carlo analysis has been performed based on 3000 iterations, adopting a gaussian parameter variation. Several investigations for different devices and for different bias conditions have been carried on, in the aim of determining how the resulting noise parameters can be affected in the sense of percentage errors. For comparison purpose, different data analysis have been adopted, such as the Mitama-Katoh evaluating method [5] (for which an integrated microstrip tuner was adopted), and the Boudiaf-Laporte recursive fitting procedure [6]. However the most suitable method has been demonstrated to be a least-squares fitting procedure proposed by Lane [2] who reduced the noise figure expression (1) to the following linearised expression:

$$F = A + BG_S + \frac{C + BB_S^2 + DB_S}{G_S}, \quad (2)$$

where the coefficients $A$, $B$, $C$ and $D$ are functions of the four noise parameters and are evaluated minimising the estimated error $\varepsilon$:

$$\varepsilon = \frac{1}{2} w_i \sum_{i=1}^{N_{TOT}} \left[ A + B\left(G_{s,i} + \frac{B_{s,i}^2}{G_{s,i}}\right) + \frac{C}{G_{s,i}} + D\frac{B_{s,i}}{G_{s,i}} - F_i \right]^2, \quad (3)$$

where $w_i$ is a weighting factor that we selected, after some optimisation, to be equal to $1/F^{1.5}$.

Figure 2 shows the $F_{min}$ behaviour with frequency for the H300 device as an example, and in Fig. 3 is reported the experimental results and the evaluated corresponding errors for the same device, 50% $I_{dss}$. It is worth noting a meaningful improvement in accuracy with redundancy increasing.
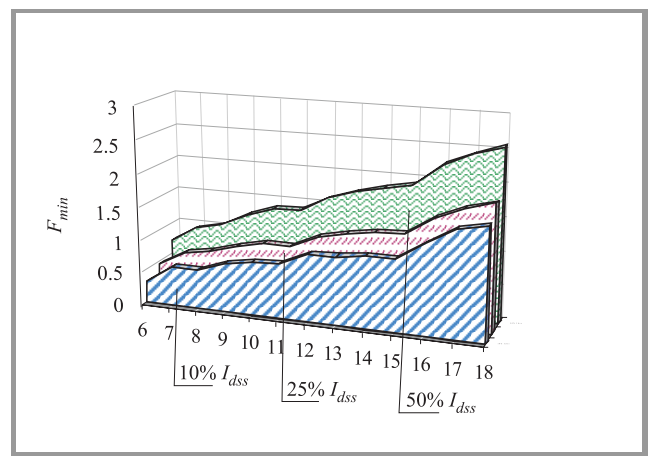


**Fig. 2.** The minimum noise figure $F_{min}$ versus frequency for different biasing conditions for the H300 device.
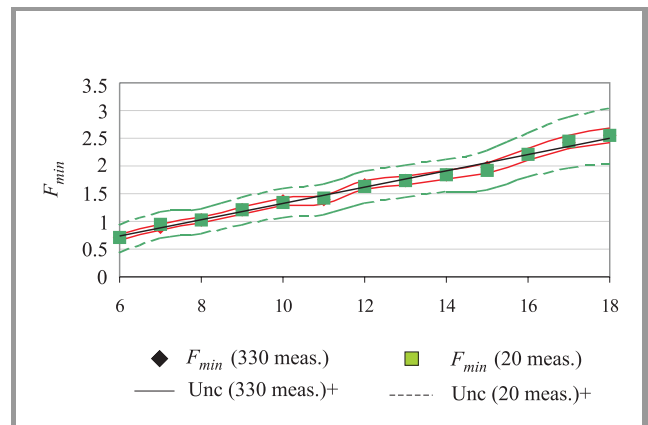


**Fig. 3.** $F_{min}$ at the 50% $I_{dss}$ versus frequency. Uncertainty range is reported for high redundancy (330) and low redundancy (20) measures.

For all the DUTs at all the bias conditions the equivalent noise resistance $R_n$ decreases as frequency increases (e.g. Fig. 4), while its uncertainty can be considered neg-
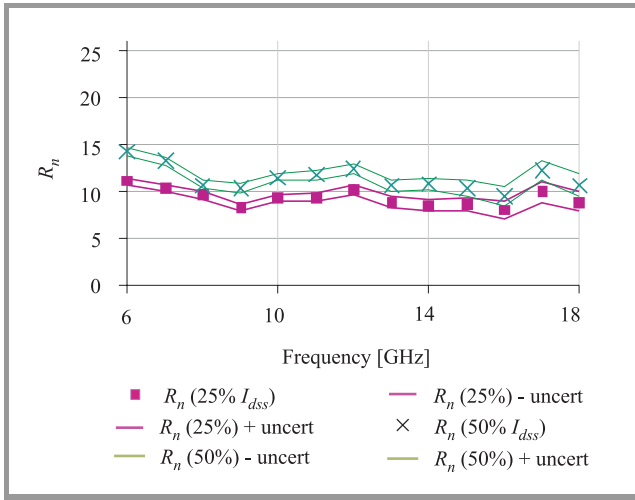
**Fig. 4.** Equivalent noise resistance $R_n$ versus frequency for the H300 device at two bias condition: 25% and 50% $I_{dss}$.
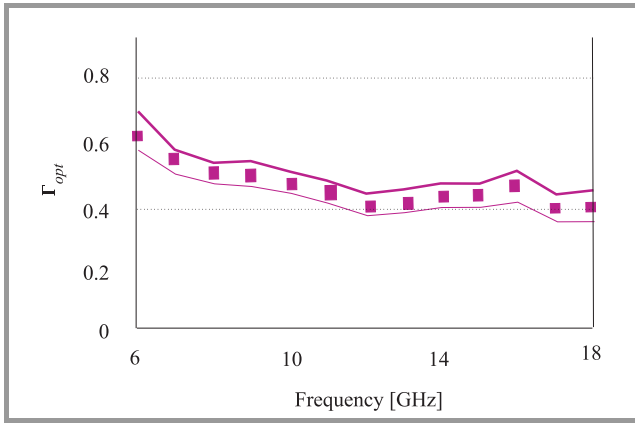


**Fig. 5.** $|\Gamma_{opt}|$ versus frequency for the H300 device at the 25% $I_{dss}$ bias condition.
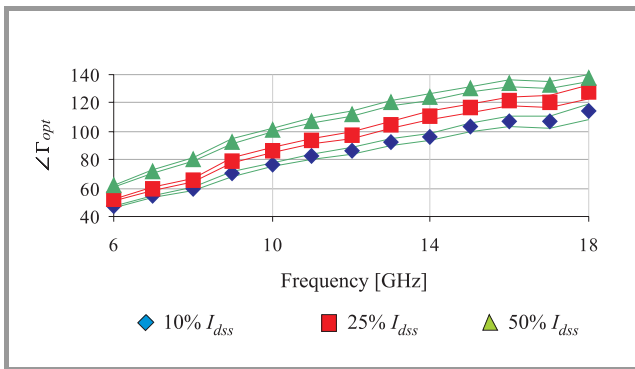


**Fig. 6.** $\angle\Gamma_{opt}$ versus frequency for the H300 device at three bias conditions.



| | 18 | 17 | 16 | 15 | 14 | 13 | 12 | 11 | 10 | 9 | 8 | 7 | 6 |
|---|---|---|---|---|---|---|---|---|---|---|---|---|---|
| ■ 330 meas. | 0.25 | 0.21 | 0.19 | 0.13 | 0.12 | 0.11 | 0.1 | 0.1 | 0.09 | 0.09 | 0.09 | 0.07 | 0.12 |
| ■ 165 meas | 0.38 | 0.28 | 0.26 | 0.18 | 0.16 | 0.15 | 0.15 | 0.14 | 0.12 | 0.13 | 0.13 | 0.11 | 0.18 |
| ■ 110 meas | 0.41 | 0.36 | 0.31 | 0.22 | 0.19 | 0.19 | 0.18 | 0.17 | 0.15 | 0.17 | 0.16 | 0.12 | 0.2 |
| ■ 82 meas | 0.47 | 0.43 | 0.36 | 0.25 | 0.22 | 0.21 | 0.2 | 0.19 | 0.18 | 0.2 | 0.2 | 0.15 | 0.24 |
| □ 41 meas | 0.64 | 0.57 | 0.51 | 0.34 | 0.3 | 0.29 | 0.28 | 0.27 | 0.26 | 0.28 | 0.25 | 0.2 | 0.28 |
| ■ 20 meas | 0.99 | 0.75 | 0.76 | 0.49 | 0.44 | 0.4 | 0.44 | 0.36 | 0.34 | 0.4 | 0.34 | 0.29 | 0.34 |



| | 18 | 17 | 16 | 15 | 14 | 13 | 12 | 11 | 10 | 9 | 8 | 7 | 6 |
|---|---|---|---|---|---|---|---|---|---|---|---|---|---|
| ■ 330 meas. | 0.19 | 0.17 | 0.15 | 0.12 | 0.1 | 0.09 | 0.08 | 0.08 | 0.07 | 0.08 | 0.07 | 0.06 | 0.13 |
| ■ 165 meas | 0.26 | 0.22 | 0.2 | 0.15 | 0.13 | 0.12 | 0.11 | 0.11 | 0.1 | 0.11 | 0.1 | 0.09 | 0.18 |
| ■ 110 meas | 0.32 | 0.27 | 0.24 | 0.19 | 0.16 | 0.15 | 0.13 | 0.12 | 0.12 | 0.14 | 0.13 | 0.11 | 0.2 |
| ■ 82 meas | 0.33 | 0.31 | 0.29 | 0.23 | 0.19 | 0.16 | 0.16 | 0.14 | 0.15 | 0.16 | 0.15 | 0.13 | 0.22 |
| □ 41 meas | 0.51 | 0.43 | 0.39 | 0.3 | 0.26 | 0.23 | 0.21 | 0.21 | 0.21 | 0.23 | 0.22 | 0.18 | 0.27 |
| ■ 20 meas | 0.64 | 0.6 | 0.57 | 0.4 | 0.37 | 0.36 | 0.3 | 0.29 | 0.29 | 0.32 | 0.28 | 0.26 | 0.32 |

**Fig. 7.** Error percentage for $F_{min}$ versus frequency and measurement number with (a) $\alpha = 0$ and (b) $\alpha = 1.5$.

ligible since it is in the $0.5 - 1.5 \ \Omega$ range in the worst case of 10% $I_{dss}$. Being the $R_n$ value a weighting factor for the mismatch of the measured source reflection coeffi-

cient $\Gamma_s$ from its optimum value $\Gamma_{opt}$, its behaviour justifies that the device mismatch assumes less importance with frequency. In spite of that, the $|\Gamma_{opt} - \Gamma_s|$ value increases quite rapidly with frequency, reducing the positive smoothing effect that can be due to $R_n$ with frequency.

The uncertainty for $|\Gamma_{opt}|$ values results to be higher when its value is near unity (Fig. 5 as an example). In any

Gianluca Acciari, Franko Giannini, Ernesto Limiti, and Giovanni Saggio

case, at all the biasing conditions and for all the devices under test, the same $\angle\Gamma_{opt}$ behaviour can be observed (Fig. 6 as an example). At low frequency it increases rapidly while tends to saturate for higher frequencies. Its uncertainty increases with frequency, remaining however almost negligible.

Figure 7 shows how the accuracy increases with redundancy, both for the least-squares fitting procedure (Fig. 7a) and for the same fitting considering the $1/F^{\alpha}$, with $\alpha = 1.5$, weighting factor (Fig. 7b). In addition it can be noticed as an error confidence as low as 0.2% can be obtained for all the determined noise parameters.

# 4. Conclusions

This work demonstrates how the accuracy in measuring the four noise parameters can be drastically improved collecting a data set with a certain redundancy. This consideration is to be associated with the reported criteria of choice the experimental points in certain regions of the Smith Chart [3, 4]. A method is also proposed to estimate the overall measurement accuracy taking into account measurement errors due to both the limited instrument precision and to connection repeatability.

# References

[1] M. W. Pospieszalski, "Modeling of noise parameters of MESFET's and MODFET's and their frequency and temperature dependence", *IEEE Trans. Microw. Theory Techn.*, vol. 37, pp. 1340–1350, 1989.

[2] R. Q. Lane, "The determination of device noise parameters", *Proc. IEEE*, vol. 57, pp. 1461–1462, 1969.

[3] G. Caruso and M. Sannino, "Computer-aided determination of microwave two-port noise parameters", *IEEE Trans. Microw. Theory Techn.*, vol. MTT-26, no. 9, pp. 639–642, 1978.

[4] J. M. O'Callaghan and J. P. Mondal, "A vector approach for noise parameter fitting and selection of source admittances", *IEEE Trans. Microw. Theory Techn.*, vol. MTT-39, no. 8, pp. 1376–1381, 1991.

[5] M. Lahdes, "Uncertainty analysis of V-band on-wafer noise parameter measurement system", in *28th Eur. Microw. Conf. Proc.*, Amsterdam, Netherlands, 1998, pp. 445–450.

[6] M. Mitama and H. Katoh, "An improved computational method for noise parameter measurement", *IEEE Trans. Microw. Theory Techn.*, vol. MTT-27, no. 6, pp. 612–615, 1979.

[7] A. Boudiaf and M. Laporte, "An accurate and repeatable technique for noise parameter measurements", *IEEE Trans. Instrum. Measur.*, vol. 42, no. 2, 1993.

**Gianluca Acciari** was born in Marino, Italy, in 1966. He received the Laurea degree (cum laude) in electronic engineering from the University of Roma "Tor Vergata", Italy, in 1995. He received the Ph.D. degree in telecommunications and microelectronic engineering from the same University in 1999. In 1999 he joined the Department of Electronic Engineering of the University of Roma "Tor Vergata" as Research Assistant. His main research interests concern high frequency electronics and, in particular, the linearisation of power amplifiers and physics based simulation of active devices. Since 1995 he has been involved in several microwave circuits design.
e-mail: acciari@uniroma2.it
Department of Electronic Engineering
University of Rome "Tor Vergata"
Via del Politecnico 1
00133 Rome, Italy

**Franco Giannini** was born in Galatina (LE) Italy, on November 9, 1944. Since 1980 he has been Full Professor of Applied Electronics, presently at the University of Roma "Tor Vergata", and Honorary Professor of the Warsaw University of Technology since 2001. He has been working on problems concerning modelling, characterisation and design methodologies of passive and active high frequency components, circuits and subsystems, including microwave and millimeter wave MIC's. He is a consultant for various national and international organizations, including the International Telecommunication Union and the European Union. Prof. Giannini authored or co-authored more than two hundred and seventy scientific papers.
e-mail: giannini@ing.uniroma2.it
Department of Electronic Engineering
University of Roma "Tor Vergata"
Via del Politecnico 1
00133 Roma, Italy

**Ernesto Limiti** was born in Roma, Italy, on March 26, 1965. In 1989 he was a consultant for MICREL S.p.A., contributing to the design and fabrication of millimeter-wave hybrid frequency doublers. Since 1991 he has been with the Department of Electronic Engineering of the University of Roma "Tor Vergata", where he is actually Professor of Electronic Measurements and Instrumentation at microwave frequencies. His research interests include modelling of active and passive microwave devices and design methodologies for microwave and millimeter-wave nonlinear circuits. He has been active in several European and National research projects.
e-mail: limiti@ing.uniroma2.it
Department of Electronic Engineering
University of Roma "Tor Vergata"
Via del Politecnico 1
00133 Roma, Italy

**Giovanni Saggio** was born in Roma, Italy, on March 14, 1964. He received the Laurea degree in electronic engineering in 1991 and the Ph.D. degree in telecommunications and microelectronic engineering in 1997 from the University of Roma "Tor Vergata", Italy. Since 1997 he has been with the Department of Electronic Engineering of the Uni-

versity of Roma "Tor Vergata", where he is actually as Research Assistant. His research interests include noise measurement and modelling of active microwave devices.
e-mail: saggio@uniroma2.it
Department of Electronic Engineering
University of Roma "Tor Vergata"
Via del Politecnico 1
00133 Roma, Italy

# A method for evaluation
# of uncertainties of noise parameter
# measurement

Marek Schmidt-Szałowski and Wojciech Wiatr

**Abstract** — **The assessment of uncertainties of a two-port noise parameters measurement, presented in the paper, relies on modeling of sources of errors and an investigation of propagation of the errors through a measurement system. This approach is based on a simplified additive error model and small-change sensitivity analysis. The evaluated uncertainties agrees with those observed in experiments. This method may be implemented in automatic noise measurement systems for on-line uncertainty assessment and for optimization of the design of an experiment.**

**Keywords** — *microwaves, noise metrology, measurement system, four noise parameters, sensitivity analysis, error propagation, uncertainty.*

## 1. Introduction

The trade-off between the measurement through-put and the measurement accuracy is a well-known dilemma encountered in the practice of industrial measurements. This problem becomes critical in case of very sensitive instrumentation like radiometers and noise figure meters, whose accuracy can be essentially improved by extending measurement time. In general, two complementary approaches can be useful in such cases: uncertainty analysis, which enables to predict the accuracy of a measurement, and design of experiment, which tells how to conduct a measurement to obtain the highest accuracy. Although both approaches are well established and commonly used in many fields of engineering they are barely exploited in noise parameter measurements [1 − 5]. As a result, even state-of-the-art noise-measurement systems does not provide on-line evaluation of accuracy.

The uncertainty of the two-port noise parameters can be estimated either numerically or analytically. In the first approach, called also perturbation method, the two-port parameters are repeatedly calculated from artificially randomly perturbed values of the system parameters and the observed values. This approach allows for various probability distributions of errors and accounts for non-linearities of the model but is very time-consuming. The latter approach based on small-change sensitivities relies on the investigation of the error propagation through the system. This approach is much faster and sufficiently accurate for typical noise measurement systems [6].

This paper concerns the analytical method of an uncertainty analysis. First, a method for determining of the noise pa-

rameters of a microwave receiver is described. Secondly, measurement errors are analyzed and a simple error model is introduced. Then, the error propagation is analyzed and the confidence intervals are calculated for all noise parameters. Finally, the results of total-power radiometer calibrations are presented as exemplary applications of this approach.

## 2. The model of the measurement system

In this paper an identification of the noise parameters is discussed for the case of a microwave receiver calibration. The receiver is characterized in terms the noise correlation matrix $C_r$, and the small-signal parameters: the input reflection coefficient $\Gamma_r$ and the power gain $g_r$. A multi-state noise generator attached to the input of the receiver consist of a bi-state noise source and a multi-state mechanical tuner. The measurement set-up shown in Fig. 1 allows one to observe the output noise temperature $T_r$ as a function of generator parameters: the reflection coefficient $\Gamma_g$ and the noise temperature $T_g$.

According to [7] the receiver parameters may be determined from a seven-term model

$$\boldsymbol{\beta}^T \boldsymbol{A} \boldsymbol{\beta} + \boldsymbol{a}^T \boldsymbol{\beta} + a = 0, \qquad (1)$$

where seven-element real vector $\boldsymbol{\beta}$ contains unknown receiver parameters, while matrix $\boldsymbol{A}$, vector $\boldsymbol{a}$, and coefficient $a$ depend on the generator state

$$\boldsymbol{\beta} = \begin{bmatrix} \Re\Gamma_r \\ \Im\Gamma_r \\ g_r \\ g_r c_{r11} \\ g_r c_{r22} \\ g_r \Re c_{r21} \\ g_r \Im c_{r21} \end{bmatrix}, \boldsymbol{A} = T_r \begin{bmatrix} |\Gamma_g|^2 & 0 & \dots & 0 \\ 0 & |\Gamma_g|^2 & \dots & 0 \\ \vdots & \vdots & \ddots & \vdots \\ 0 & 0 & \dots & 0 \end{bmatrix},$$

$$\boldsymbol{a} = \begin{bmatrix} -2T_r\Re\Gamma_g \\ 2T_r\Im\Gamma_g \\ -T_g(1-|\Gamma_g^2|) \\ -|\Gamma_g^2| \\ -1 \\ 2\Re\Gamma_g \\ 2\Im\Gamma_g \end{bmatrix}, \quad a = T_r. \qquad (2)$$

Equation (1) is real, quadratic with respect to $\beta_1$ and $\beta_2$ but linear with respect to the other unknowns. It is worth noting that a separate measurement of $\Gamma_r$ is not required since its value is to be determined simultaneously with the other receiver parameters [7].
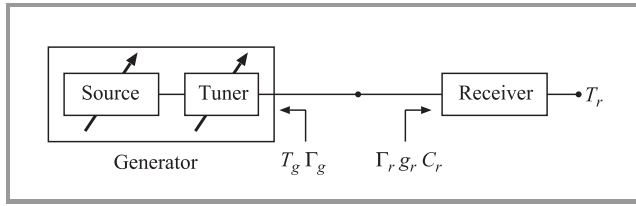


**Fig. 1.** The measurement set-up.

The deterministic model (1) does not fit reality because $A$, $a$, and $a$ are affected by various errors. Typically for small and moderate errors an additive error model may be used

$$\beta^T A \beta + 2a^T \beta + a = \varepsilon, \qquad (3)$$

where $\varepsilon$ is a random variable representing errors of $\Gamma_g$, $T_g$, and $T_r$. It should be emphasised that error $\varepsilon$ does not account for all types of errors emerging in the system but only those that produce random dispersion of $\beta$, i.e. related to type-A uncertainty [8]. Usually, it is assumed that $\varepsilon$ is distributed according to a normal distribution with null mean and variance $\sigma^2$. Evaluation of $\sigma$ is the most difficult part of the the uncertainty analysis. To simplify this task, it is assumed that error $\varepsilon$ results from two independent sources:

- Errors related to tuner calibration errors and tuner nonrepeatability, which are modeled as uncorrelated random errors of $\Gamma_g$ with constant variance var $\Gamma_g$ and random errors of $T_g$ with variance var $T_g$ proportional to $T_{g\text{exc}}^2$, where $T_{g\text{exc}} = T_g - T_0$.

- Errors caused by finite time of integration of noise power $T_r$, which are modeled as random errors of $T_r$ with variance var $T_r$ proportional to $T_r^2$.

The values of var $\Gamma_g$, var $T_g$, and var $T_r$ can be estimated for each frequency of interest on the basis of long term monitoring and general knowledge of the measurement system.

Owing to the assumed independence of errors the variance $\sigma^2$ can be expressed in an additive form

$$\sigma^2 = \left|\frac{\partial \varepsilon}{\partial \Gamma_g}\right|^2 \text{var } \Gamma_g + \left(\frac{\partial \varepsilon}{\partial T_g}\right)^2 \text{var } T_g +$$

$$+ \left(\frac{\partial \varepsilon}{\partial T_r}\right)^2 \text{var } T_r, \qquad (4)$$

where sensitivities $\partial \varepsilon / \partial \cdot$ are calculated from Eqs. (1) and (2)

$$\frac{\partial \varepsilon}{\partial \Gamma_g} = 2\left(c_{r21} + \Gamma_g \left(g_r T_g - c_{r11}\right) - T_r \Gamma_r^* \zeta\right),$$

$$\frac{\partial \varepsilon}{\partial T_g} = -g_r \left(1 - |\Gamma_g|^2\right),$$

$$\frac{\partial \varepsilon}{\partial T_r} = |\zeta|^2, \quad \zeta = 1 - \Gamma_r \Gamma_g.$$

## 3. Identification method

The value of $\beta$ can be determined on the basis of a series of measurements of $T_r$ made for several states of the generator through solving a system of equations

$$\beta^T A \beta + a^T \beta + a = \varepsilon \quad \text{for} \quad i = 1, \ldots, M. \qquad (5)$$

Since these equations are nonlinear (quadratic) the deterministic case $M = 7$ usually leads to more than one solution $\beta$ [7] and additional knowledge is needed to choosing the proper one. For this reason the system (5) should be overdetermined which also benefits in better immunity to random errors.

According to the Gauss-Markov theorem a generalized least squares estimator $b$ is the best linear unbiased estimator of $\beta$ defined as in model (3) [9]. If errors $\varepsilon$, related to different states of the generator, are statistically independent $b$ can be obtained by minimizing the sum of squared residuals

$$\phi(\beta) = \sum_{i=1}^{M} \sigma_i^{-2} e_i^2(\beta)$$

$$\text{with} \quad e_i(\beta) = \beta^T A_i \beta + a_i^T \beta + a_i. \qquad (6)$$

Since the normal equation $\partial / \partial \beta \, \phi(\beta) = 0$ is nonlinear (as the model (3) is) and it can be solved using the Gauss-Newton method. Once the estimator $b$ is known the covariance matrix cov $b$ can be calculated [9]

$$\text{cov } b = s^2 M^{-1} \quad \text{with} \quad M = \sum_{i=1}^{M} \sigma_i^{-2} \frac{\partial e_i(b)}{\partial \beta} \left(\frac{\partial e_i(b)}{\partial \beta}\right)^T,$$

$$s^2 = \frac{1}{M-7} \sum_{i=1}^{M} \sigma_i^{-2} e_i^2(b). \qquad (7)$$

Factor $s^2$ can be treated as a measure of goodness of the error model and should equals 1 for the the best model. The receiver noise parameters $T_{\min}$, $T_N$, and $\Gamma_{\text{opt}}$ can be calculated from $\beta$. To properly account for their correlations an auxiliary vector $t$ may be introduced

$$t = \begin{bmatrix} T_{\min} \\ T_N \\ \Re\Gamma_{\text{opt}} \\ \Im\Gamma_{\text{opt}} \end{bmatrix} = \frac{1}{2\beta_3} \begin{bmatrix} \beta_5 - \beta_4 + \beta_3 T_N \\ \sqrt{(\beta_4 + \beta_5)^2 - 4\beta_6^2 - 4\beta_7^2} \\ \vartheta \beta_3 \beta_6 \\ \vartheta \beta_3 \beta_7 \end{bmatrix}$$

$$\text{with} \quad \vartheta = \frac{2}{\beta_4 + \beta_5 + \beta_3 t_2}. \qquad (8)$$

Hence

$$\mathrm{cov}\,\boldsymbol{t} = \partial \boldsymbol{t}/\partial \boldsymbol{\beta} \;\; \mathrm{cov}\,\boldsymbol{\beta} \;\; (\partial \boldsymbol{t}/\partial \boldsymbol{\beta})^T \,, \qquad (9)$$

where

$$\frac{\partial \boldsymbol{t}}{\partial \boldsymbol{\beta}} = \frac{1}{\beta_3} \times$$

$$\times \begin{bmatrix} 0 \; 0 \; -t_1 & \frac{v-1}{2} & \frac{v+1}{2} & -2\frac{\beta_6}{t_2} & -2\frac{\beta_7}{t_2} \\ 0 \; 0 \; -t_2 & v & v & -4\frac{\beta_6}{t_2} & -4\frac{\beta_7}{t_2} \\ 0 \; 0 \; -t_3 & -\vartheta\, t_3 \frac{v+1}{2} & -\vartheta\, t_3 \frac{v+1}{2} & 2\frac{t_3^2}{t_2}+\vartheta & 2\frac{t_3 t_4}{t_2} \\ 0 \; 0 \; -t_4 & -\vartheta\, t_4 \frac{v+1}{2} & -\vartheta\, t_4 \frac{v+1}{2} & 2\frac{t_4 t_3}{t_2} & 2\frac{t_4^2}{t_2}+\vartheta \end{bmatrix}$$

$$\text{with}\;\; v = \frac{\beta_4 + \beta_5}{t_2} \,. \qquad (10)$$

Finally the uncertainties of the noise parameters can be determined as

$$\mathrm{unc}\,T_{\min} = 2\sqrt{\mathrm{var}\,T_{\min}}, \quad \mathrm{unc}\,T_N = 2\sqrt{\mathrm{var}\,T_N},$$

$$\mathrm{unc}\,\Gamma_{\mathrm{opt}} = 2\sqrt{\mathrm{var}\,\Re\,\Gamma_{\mathrm{opt}} + \mathrm{var}\,\Im\,\Gamma_{\mathrm{opt}}}. \qquad (11)$$

The correlation coefficient, needed in some applications, can be also determined from cov $\boldsymbol{b}$.

## 4. Experimental results

The described method for identification of the noise parameters was used to calibrate a total-power radiometer (TPR) with various two-ports attached to its input. In the first case the TPR with the noise injection circuit (NIC, a part of the multi-state radiometer [7]) was tested in several states of the circuit (Table 1). For each state the output noise temperature $T_r$ was measured for twelve values of $\Gamma_g$ and two values of $T_g$ thus $M = 24$. It was assumed that the standard deviation of $T_{gexc}$ was equal to 0.002 dB, the standard deviation of $\Gamma_g$ was equal to 0.001, and the standard deviation of $T_r$ was equal to 0.01 dB. For each state the mean square error (MSE) was calculated as the rms value of differences between the observed values of $T_r$ and those predicted by the model. MSE may be treated as a measure of the quality of the fit. The values of $s$ show whether the assumed levels of errors were underestimated ($s > 1$) or overestimated ($s < 1$). Since the values of $s$ approach to one the error model may be considered accurate.

The obtained uncertainties of $T_{\min}$ and $T_N$ significantly depend on the state of the NIC, from 0.5% for the states ln and ma up to 9% for the state Bs. This effect results from the distribution of $\Gamma_g$ on the Smith chart. For the first two states the value of $\Gamma_{\mathrm{opt}}$ approximately lay in the center of the $\Gamma_g$ constellation so the system of Eqs. (5) was well-conditioned. Since the same constellation was used for all states of NIC, for some of them the value of $\Gamma_{\mathrm{opt}}$ departed far from the center of the $\Gamma_g$ constellation which may have deteriorated the conditioning.

In the next example two independent calibrations of TPR with NIC are compared (Fig. 2). The confidence intervals of both sets of parameters are in a good agreement. Similar results were obtained for other frequencies.

Moreover, the uncertainties obtained using this method agreed with ones calculated using perturbation method.
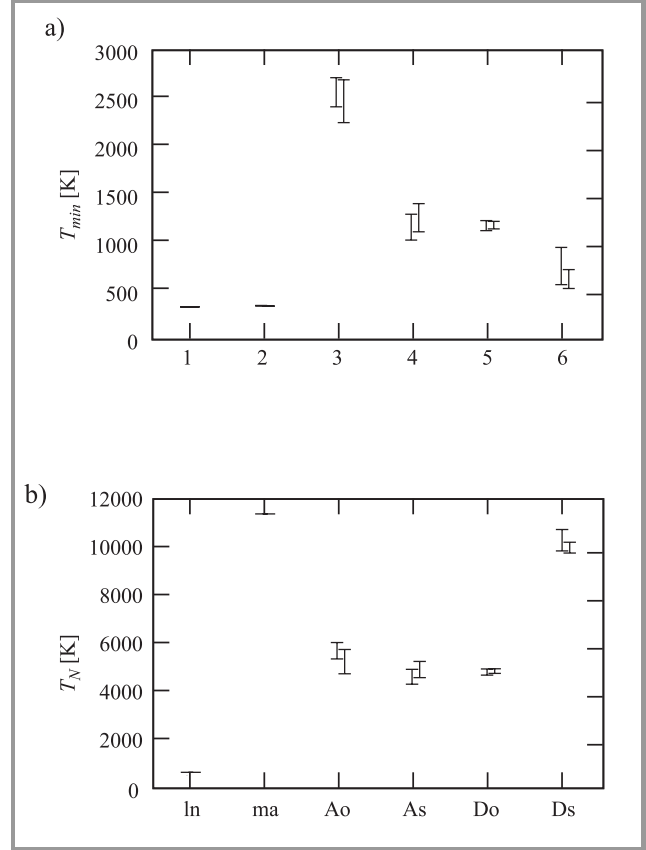


***Fig. 2.*** Comparison of two calibrations of the TPR with NIC: (a) $T_{\min}$ and (b) $T_N$, $f = 1$ GHz.

As the final case the TPR with an FET at the input was measured at several operating points (Table 2). For each bias point the output noise temperature $T_r$ was measured for twelve cold states of the generator with $\Gamma_g < 0.85$ and two hot ones with $\Gamma_g \sim 0$. The values of var $T_{gexc}$, var $\Gamma_g$, and var $T_r$ were like those in the first case but they seem to be underestimated ($s$ is up to 1.7). It is also worth noting that unc $T_{\min}$ and unc $T_N$ get smaller when $I_D$ increases. This can be explained as an improvement of conditioning for $\Gamma_{\mathrm{opt}}$ approaching the center of the $\Gamma_g$ constellation.

## 5. Conclusions

The presented method for two-port noise parameter identification allows one to estimate the uncertainties of the parameters and their correlations. A simplified additive error model, which the method is based on, very well agrees with errors observed in experiments. The procedures for

Table 1

The results of calibration of a TPR with a noise injection circuit, $f = 2$ GHz

| State | $T_{\min}$ [K] | unc $T_{\min}$ [K] | $T_N$ [K] | unc $T_N$ [K] | $|\Gamma_{opt}|$ [mag] | $\angle\Gamma_{opt}$ [deg] | unc $\Gamma_{opt}$ [mag] | $|\Gamma_r|$ [mag] | $\angle\Gamma_r$ [deg] | $g_r$ [dB] | MSE [dB] | $s$ |
|---|---|---|---|---|---|---|---|---|---|---|---|---|
| ln | 482.5 | 2.0 | 731.6 | 4.0 | 0.1068 | -139.0 | 0.0039 | 0.0895 | 163.7 | -19.631 | 0.010 | 0.9 |
| ma | 488.0 | 5.2 | 8895.5 | 44.3 | 0.1112 | -113.7 | 0.0021 | 0.0845 | 161.6 | -19.687 | 0.015 | 1.1 |
| Ao | 2463.1 | 68.4 | 6044.8 | 131.1 | 0.7223 | 40.6 | 0.0044 | 0.0792 | 152.9 | -19.719 | 0.008 | 0.7 |
| As | 1281.1 | 76.9 | 3760.8 | 150.2 | 0.7133 | -150.2 | 0.0081 | 0.0850 | 160.7 | -19.647 | 0.012 | 1.0 |
| Bo | 1404.0 | 55.4 | 4025.8 | 104.1 | 0.6543 | 142.4 | 0.0069 | 0.0881 | 160.3 | -19.646 | 0.014 | 1.3 |
| Bs | 1502.9 | 137.9 | 7505.2 | 323.6 | 0.6692 | -64.7 | 0.0095 | 0.0820 | 161.0 | -19.721 | 0.015 | 1.3 |
| Co | 1308.9 | 58.2 | 5148.7 | 114.9 | 0.6000 | 97.9 | 0.0065 | 0.0921 | 157.6 | -19.665 | 0.014 | 1.3 |
| Cs | 927.1 | 21.1 | 5965.8 | 96.8 | 0.6166 | -108.5 | 0.0039 | 0.0844 | 161.2 | -19.676 | 0.013 | 1.0 |
| Do | 870.6 | 26.1 | 5765.6 | 95.4 | 0.6037 | -117.6 | 0.0044 | 0.0850 | 160.9 | -19.671 | 0.013 | 1.1 |
| Ds | 997.7 | 34.6 | 7702. 7 | 66.4 | 0.5290 | 38.2 | 0.0031 | 0.0863 | 156.4 | -19.707 | 0.011 | 0.8 |

Table 2

The results of calibration of TPR with a FET (MGF1412), $f = 2$ GHz, $V_{DS} = 3$ V

| $I_D$ [mA] | $T_{\min}$ [K] | unc $T_{\min}$ [K] | $T_N$ [K] | unc $T_N$ [K] | $|\Gamma_{opt}|$ [mag] | $\angle\Gamma_{opt}$ [deg] | unc $\Gamma_{opt}$ [mag] | $|\Gamma_r|$ [mag] | $\angle\Gamma_r$ [deg] | $g_r$ [dB] | MSE [dB] | $s$ |
|---|---|---|---|---|---|---|---|---|---|---|---|---|
| 2 | 79.6 | 19.4 | 143.5 | 34.2 | 0.8746 | -163.3 | 0.0223 | 0.9692 | 157.8 | -15.068 | 0.007 | 1.1 |
| 5 | 50.9 | 15.2 | 95.3 | 31.0 | 0.8458 | -162.0 | 0.0357 | 0.9622 | 153.2 | -11.258 | 0.012 | 1.6 |
| 10 | 45.9 | 11.8 | 83.1 | 25.5 | 0.8181 | -161.1 | 0.0392 | 0.9499 | 149.5 | -9.070 | 0.012 | 1.7 |
| 20 | 45.4 | 8.2 | 83.3 | 18.3 | 0.7967 | -158.8 | 0.0314 | 0.9424 | 146.0 | -7.520 | 0.010 | 1.4 |
| 50 | 65.8 | 7.0 | 121.5 | 16.0 | 0.7655 | -152.8 | 0.0223 | 0.9311 | 141.4 | -6.207 | 0.007 | 1.0 |

calculating the uncertainties are tightly connected with the general least squares algorithm of noise parameters estimation. The numerical overheads related to the presented method are much smaller than in the perturbation method. The uncertainties of the two-port noise parameters calculated using the presented method may be used as a quick validation of the quality of a chosen $\Gamma_g$ constellation. If implemented in the automatic measurement systems it may be utilised as a criterion for on-line optimization of the design of experiment, which may be extended or shrunk as needed for a given measurement accuracy. It may also facilitate finding out the most critical elements to be improved in order to minimise the sensitivity of the system to errors.

# Acknowledgment

# References

[1] J. W. Archer and R. A. Batchelor, "Fully automated on-wafer noise characterization of GaAs MESFET's and HEMT's", *IEEE Trans. Microw. Theory Techn.*, vol. 40, no. 2, pp. 209–216, 1992.

[2] R. Benelbar, B. Huyart, and R. G. Bosisio, "Microwave noise characterization of two-port devices using an uncalibrated tuner", *IEEE Trans. Microw. Theory Techn.*, vol. 44, no. 10, pp. 1725–1728, 1996.

[3] S. Van den Bosch and L. Martens, "Improved impedance-pattern generation for automatic noise-parameter determination", *IEEE Trans. Microw. Theory Techn.*, vol. 46, no. 11, pp. 1673–1678, 1998.

[4] A. C. Davidson, B. W. Leake, and E. W. Strid, "Accuracy improvements in microwave measurement of noise parameterss", *IEEE Trans. Microw. Theory Techn.*, vol. MTT-37, pp. 1973–1977, 1989.

[5] G. Mamola and M. Sannino, "Errors in measurement of microwave transistor noise parameters", *Alta Freq.*, vol. XLII, no. 10, pp. 551–556, 1973.

[6] M. Schmidt-Szałowski, "Experimental verification of measurement uncertainties of multi-state radiometer system", in *Conf. MIKON'96*, Warsaw, Poland, 1996, pp. 331–335.

[7] M. Schmidt-Szałowski and W. Wiatr, "An improved method for simultaneous small-signal and noise characterization of two-ports using multi-state radiometer", in *Conf. EuMC'99*, Muenchen, Germany, 1999, pp. 61–64.

[8] B. N. Taylor and C. E. Kuyatt, "Guidelines for evaluating and expressing the uncertainties of NIST measurement results", *NIST Techn. Note*, no. 1297, 1994.

[9] E. F. Vonesh and V. M. Chinchilli, *Linear and Nonlinear Models for the Analysis of Repeated Measurements*. New York, Basel, Hong Kong: Marcel Dekker, Inc. 1997.

**Marek Schmidt-Szałowski** received the M.Sc. and Ph.D. degrees in electronic engineering from Warsaw University of Technology (Poland) in 1995 and 2000, respectively. His theses concerned novel measurement techniques for small-signal and noise characterization of microwave devices. He is a co-inventor of the multistate radiometer. In 2000, he joined Philips' Business Line RF Modules (Nijmegen, The Netherlands). His responsibilities include characterization and modeling of RF semiconductor devices. He is presently engaged in characterization of high-frequency low-noise SiGe BJT's.
Institute of Electronic Systems
Warsaw University of Technology
Nowowiejska st 15/19
00-665 Warsaw, Poland

**Wojciech Wiatr** received the M.Sc., and the Ph.D. degrees in electronic engineering from Warsaw University of Technology, Warsaw, Poland in 1970 and 1980, respectively. In 1971, he joined the Institute of Electron Technology CEMI in Warsaw, affiliated to national semiconductor industry. Since 1972, he has been with the Institute of Electronic Systems at the Warsaw University of Technology, presently as an Assistant Professor. His main scientific interests are in the field of precision microwave measurements. He developed new techniques and instrumentation for broadband scattering and noise parameter measurements of microwave transistors and MMICs. Recently, he invented the RF multistate total power radiometer realizing simultaneous noise and vector analysis of microwave networks with natural noise excitation. He was engaged in realization of many research projects. In noise metrology, he collaborated with the National Radio Astronomy Observatory in Charlottesville, VA, USA and the Ferdinand-Braun-Institut für Höchstfrequenztechnik in Berlin. For five years, he has been an Affiliate Researcher of the National Institute of Standards and Technology in Boulder, CO, USA. Dr. Wojciech Wiatr published 1 book, over 70 papers and holds two patents.
e-mail: Wiatr@ise.pw.edu.pl
Institute of Electronic Systems
Warsaw University of Technology
Nowowiejska st 15/19
00-665 Warsaw, Poland

# Estimation of internal distribution of temperature inside biological tissues by means of multifrequency microwave thermograph

Bronisław Stec and Andrzej Dobrowolski

**Abstract** — **The paper presents problems connected with thermal radiation of human bodies in microwave range in aspect of diagnosis breast carcinoma. A mathematical model of transmission thermal radiation through tissues is introduced and methods of measurement of temperature, depth and size of heat source, by means of multifrequency microwave thermograph [1 − 7], are described. Theoretical considerations are supplemented with presentation of result experiments.**

*Keywords — microwave thermograph, radiometer, thermal radiation, breast carcinoma.*

## 1. Introduction

A monofrequency passive microwave radiometry enables measurements of average temperature of an object on certain depth. From a practical point of view, the problem of estimation of the temperature spatial distribution inside investigated object is extremely interesting. The presented solution uses power thermography on different frequencies. The method is based on the decreasing power penetration distance into biological tissues and simultaneous increasing intensity of thermal radiation versus frequency.

Because of a build of tissue and specificity of breast carcinoma one can conclude, that focus has spherical shape and a distribution of temperature resulted from it exponentially disappears to zero in layer of gland. Thus, the Gauss curve describing deep-seated distribution of temperature, has been assumed.

As presented in [7] in a three-layer model of tissue [4, 6] the real increase of temperature $T$ of the internal heat source leads to increasing brightness of the effective temperature $T_f$ on the surface of tissue, measured by a radiometer working on frequencies $f$. This relationship can be written as follows:

$$T_f = T \exp\left(-\frac{d_g}{\delta_g}\right) t_{gf} \exp\left(-\frac{d_f}{\delta_f}\right) t_{fs} \exp\left(-\frac{d_s}{\delta_s}\right) (1-|\Gamma_f|^2),$$

(1)

where: $d_g$, $d_f$, $d_s$ – lengths of ways in layers of gland, fat and skin, $\delta_g$, $\delta_f$, $\delta_s$ – power penetration distance in each layer, $t_{gf}$, $t_{fs}$ – coefficients of power transmission on the interfaces contact, $\Gamma_f$ – reflection coefficient on antenna and skin interface.

## 2. Three – band microwave radiometer system

Since the temperature distribution is given by:

$$T(z) = T_S \exp\left[-\left(\frac{z-d_g}{\sigma}\right)^2\right],$$

(2)

the temperature brightness (1) in surface model of tissue, shown in Fig. 1, can be written as

$$T_f = T_g t_{gf} \exp\left(-\frac{d_f}{\delta_f}\right) t_{fs} \exp\left(-\frac{d_s}{\delta_s}\right) \left(1-|\Gamma_f|^2\right),$$

(3)

where temperature $T_g$ on the gland and fat interface is defined with an integral of temperature distribution $T(z)$ in range $<0, \infty>$, with regard of transfer coefficient

$$\xi(z) = \exp\left(-\frac{z}{\delta_g}\right).$$

(4)
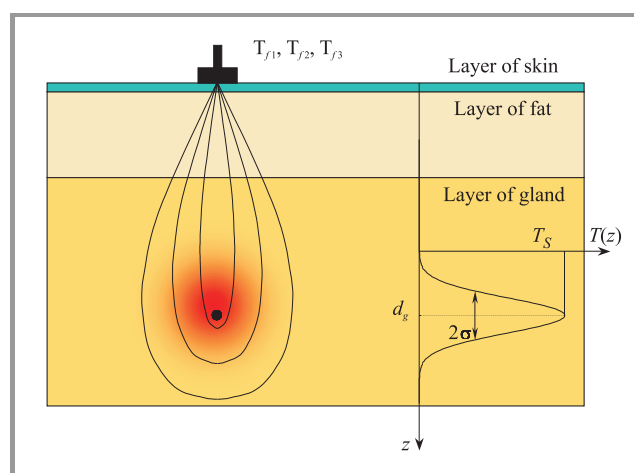


**Fig. 1.** Distribution of temperature inside biological tissue.

From Eqs. (2) and (4), $T(\xi)$ can be found to be:

$$T(\xi) = T_S \, e^{-\left(\frac{d_g}{\sigma}\right)^2} \xi^{-\frac{\delta_g}{\sigma^2}(\delta_g \ln \xi + 2d_g)}.$$

(5)
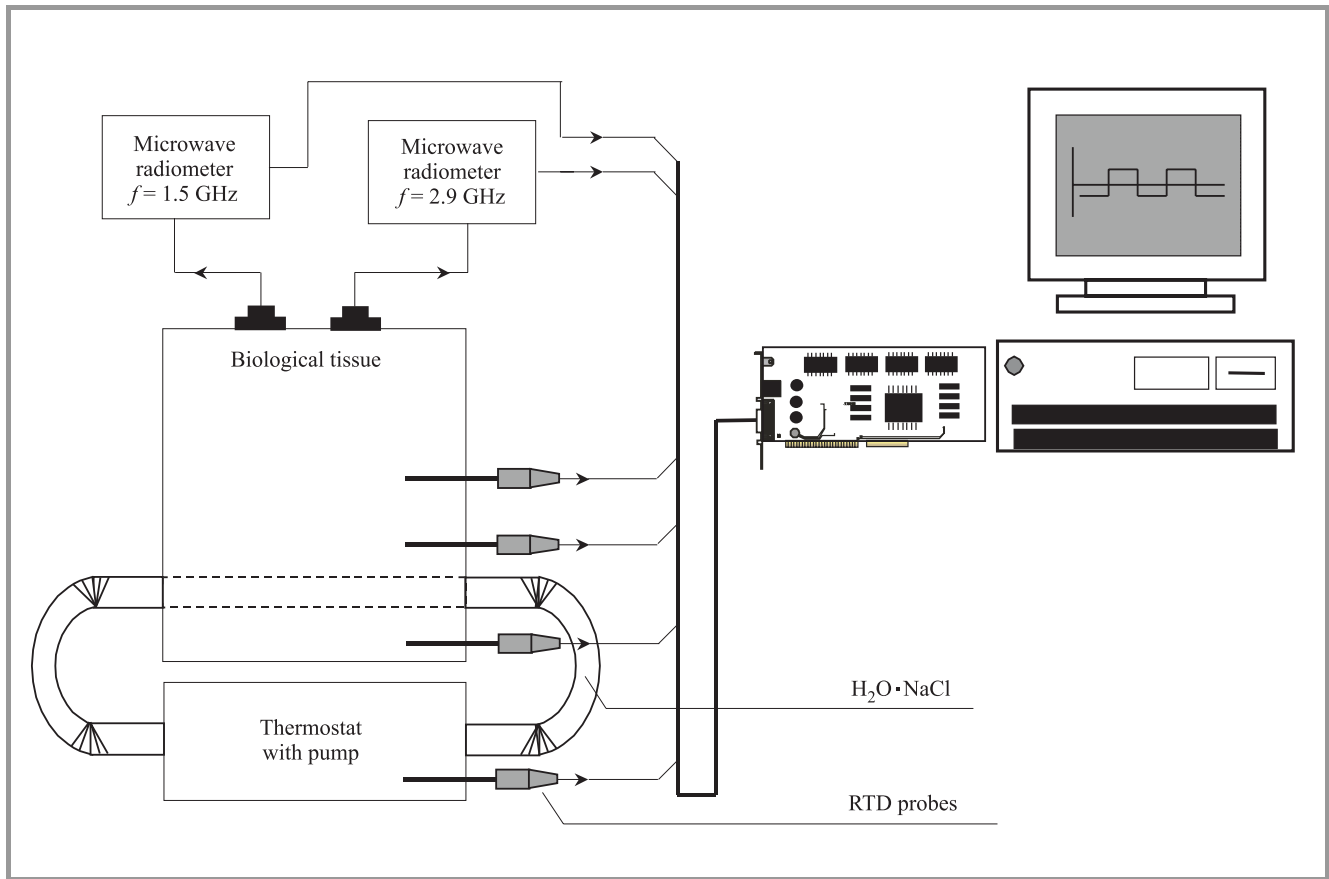
**Fig. 2.** Scheme of the measurement.

Integration of the relation with respect to $z$ from 0 to $\infty$ is equivalent to the integration of the relation with respect to $\xi$ in a range $<0, 1>$ and consequently, for

$$d_g \le d_{g\ min} = 2\sigma + \frac{\sigma^2}{2\delta_g}, \qquad (6)$$

the effective temperature of noise on border of gland and fat is defined as:

$$T_g = \frac{T_S \sigma \sqrt{\pi}}{\delta_g} \exp\left(\frac{\sigma^2 - 4\delta_g d_g}{4\delta_g^2}\right). \qquad (7)$$

Because of the slender thickness of the skin layer in tested place, one can treat it as a thin layer. Thus, in radiometers constructed in Military University of Technology in Warsaw $\Gamma_f = 0$ [8], the dependence (3) takes the following form

$$T_f = \frac{T_S \sigma \sqrt{\pi}}{\delta_g} \exp\left(\frac{\sigma^2 - 4\delta_g d_g}{4\delta_g^2}\right) K, \qquad (8)$$

where

$$K = t_{gf} \exp\left(-\frac{d_f}{\delta_f}\right). \qquad (9)$$

Knowing the coefficient $K$ (appointed in a calibration process for three radiometers working on different frequencies

and their respective power penetration distances) one can estimate the real distribution of temperature realising multi-frequency measurement. Solving the set of Eq. (8) for three frequencies $f_1$, $f_2$, $f_3$ we obtain expressions describing the real distribution of temperature in investigated tissue:

$$d_g = \frac{\alpha\,\delta_{g1}^2(\delta_{g2}^2 - \delta_{g3}^2) - \beta\,\delta_{g3}^2(\delta_{g1}^2 - \delta_{g2}^2)}{\delta_{g1}^2(\delta_{g2} - \delta_{g3}) - \delta_{g2}^2(\delta_{g1} - \delta_{g3}) + \delta_{g3}^2(\delta_{g1} - \delta_{g2})},$$

$$\sigma = 2\delta_{g1}\delta_{g2}\sqrt{\frac{d_g(\delta_{g2}^{-1} - \delta_{g1}^{-1}) - \alpha}{\delta_{g1}^2 - \delta_{g2}^2}}, \qquad (10)$$

$$T_S = \frac{T_{f1}\delta_{g1}}{\sigma K_1 \sqrt{\pi}} \exp\left(\frac{4\delta_{g1}d_g - \sigma^2}{4\delta_{g1}^2}\right), \qquad (11)$$

where:

$$\alpha = \ln\left(\frac{T_{f1} K_2\,\delta_{g1}}{T_{f2} K_1\,\delta_{g2}}\right), \quad \beta = \ln\left(\frac{T_{f2} K_3\,\delta_{g2}}{T_{f3} K_2\,\delta_{g3}}\right). \qquad (12)$$

Entire depth of heat source definite is sum

$$d = d_g + d_f + d_s. \qquad (13)$$

## 3. Temperature measurement experiments

In measurements, beef meet has been used as a tissue. The polypropylene tube of diameter 5 mm, with 1.5% saline solution NaCl has been used as the heat source. A thermostat has regulated the temperature of the liquid. In the range of temperatures ($30°C - 45°C$) the conductivity of the solution is about 2 S/m, and relative permittivity falls into a range ($70 - 75$). Such parameters assure very good coefficient of power transmission on the solution and tissue interface. In measuring range of frequency it is equal to 0.99. Side of tube can be omitted in analysis because its thickness is equal to 0.1 mm.

Measuring position is presented schematically in Fig. 2. To inspection of distribution of temperature inside the tissue mini hypodermic probes with platinum RTD element have
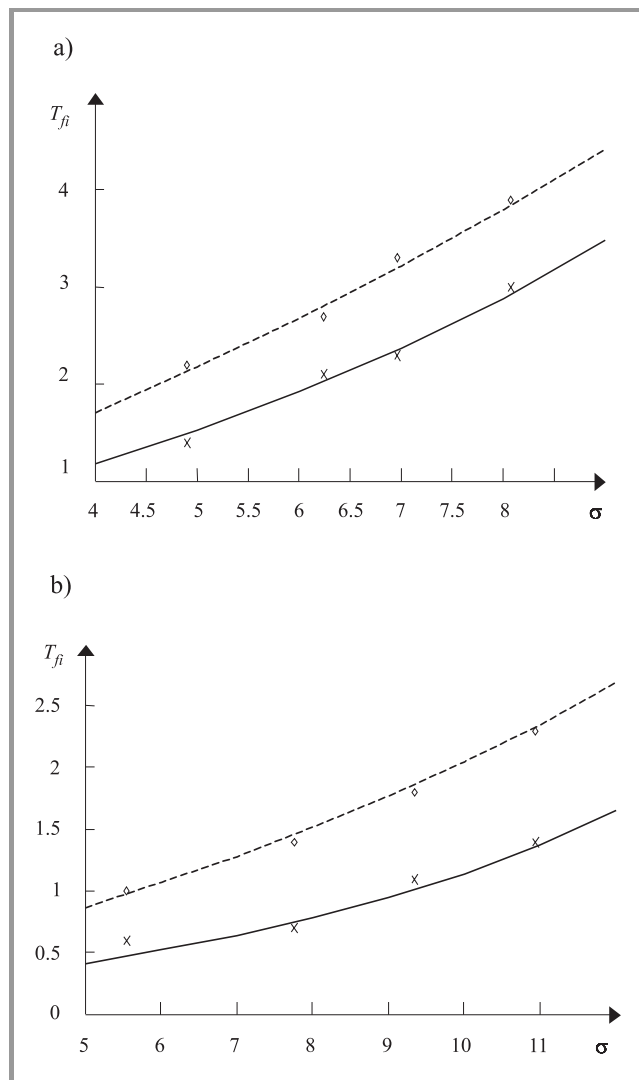
been used. To test the noninvasive thermometry based on the principles described in this paper, we have developed an experimental two – band radiometer system that measures the brightness temperature at 1.5 and 2.9 GHz. Measurements have been made automatically and results have been displayed on the computer CRT in real time.

Experiment has been realised for two widths of layer the muscle with use of wide distribution of temperature. Distribution should be sufficiently wide in relation to dimensions of tube, so that its influence on results was prevailing, and simultaneously not too wide because of an error of integrating [condition (6)].

In Fig. 3 the results of the measurements and theoretical characterisations – Eq. (8) – describing behaviour of the effective temperatures illustrated by radiometers versus width distribution of the temperature for two distances antennas – heat source are shown.

## 4. Conclusion

The aim of this work is elaboration of a measurement method permitting the construction of a spatial microwave thermograph. The paper presents problems related to thermal radiation of human bodies in microwave range and description of transmission properties of living tissues. The correctness of the presented analysis is confirmed by the experiment described in the paper. The results of the work point at a possibility of detecting and measurement of temperature, depth and size of heat sources inside human body, by means of multifrequency microwave thermograph [7].

The idea of spatial microwave thermography, resulting from theoretical analysis and results of experiments, is described in the paper. The theoretical analysis and experiments confirmed initial expectations, which has formed a base to an attempt of estimation of spatial temperature distribution inside biological tissues. At present, most promising is a construction of a thermograph as a multichannel receiver, with each channel being separate radio receiver. Also, a delivery of signal simultaneously to all channels by one wide-band antenna would be advisable. In practice, however, the above postulate is difficult to realise.



***Fig. 3.*** Results of measurements and calculations for radiometers working on frequencies 1.5 GHz (dashed line) and 2.9 GHz (continuous line) for $d_g = 24.5$ mm (a) and $d_g = 34.5$ mm (b).

## References

[1] L. Dubois, J. Pribetich, J. Falbre, M. Chive, and Y. Moschetto, "Noninvasive microwave multifrequency radiometry used in microwave hyperthermia for bidimensional reconstruction of temperature patterns", *Int. J. Hyperther.*, vol. 9, pp. 415–431, 1993.

[2] S. Mizushina, T. Shimizu, K. Suzuki, M. Kinomura, H. Ohba, and T. Sugiura, "Retrieval of temperature-depth profiles in biological objects from multifrequency microwave radiometric data", *J. Electromagnet. Wav. Appl.*, vol. 7, pp. 1515–1548, 1993.

[3] H. Ohba, M. Kinomura, M. Ito, T. Sugiura, and S. Mizushina, "Multifrequency microwave radiometry for non-invasive thermometry using a new temperature profile model function", in *Asia Pacific Microw. Conf.*, Tokyo, Japan, 1994, vol. 17-1, pp. 401–404.

[4] B. Stec and A. Dobrowolski, "Analiza własności transmisyjnych tkanek biologicznych w zastosowaniu do przestrzennej termografii mikrofalowej", in *VIII Symp. URSI'96*, Wroclaw, Poland, 1996, pp. 277–280.

[5] B. Stec and A. Dobrowolski, "Przestrzenna termografia mikrofalowa", in *Symp. KST'97*, Bydgoszcz, Poland, 1997, pp. 442–448.

[6] B. Stec and A. Dobrowolski, "Analiza własności transmisyjnych tkanek biologicznych w zastosowaniu do przestrzennej termografii mikrofalowej", *Biul. WAT*, no. 11, pp. 31–40, 1997.

[7] B. Stec and A. Dobrowolski, "Wieloczęstotliwościowa termografia mikrofalowa", *Kwart. Elektron. Telekomun. PAN*, vol. 45, no. 2, pp. 225–233, 1999.

[8] B. Stec and M. Żurawski, "Compensated microwave thermometer for medical applications", in *Asia Pacific Microw. Conf.*, Tokyo, Japan, 1994, vol. 17-2, pp. 405–408.

itary warning device and a recognise receiver of satellite telecommunications were created under his leadership. From 1980 to 1994 he was a Deputy Director and Director of the Institute of Electronic Circuits. In 1991 he became an Associate Professor at the Military University of Technology.

Faculty of Electronics
Military University of Technology
Kaliskiego st 2
00-908 Warsaw, Poland

**Bronisław Stec** has worked at the Military University of Technology since 1962. He participates in works of Scientific Council of the Faculty of Electronics and the Senate of the Military University of Technology, Warsaw, Poland. He implemented a microwave frequency detector, a monopulse finding direction system and a microwave thermograph for non-invasive measurement of temperature distribution inside biological objects. A military warning device...

**Andrzej Dobrowolski** was born in 1966. He received the M.Sc. degree in the field of radiolocations and the Ph.D. degree in the field of telecommunications, both from the Military University of Technology, Warsaw, Poland, in 1990 and 2001, respectively. Currently, he works at the Institute of Fundamentals of Electronics, Military University of Technology. His current scientific interests focus on applications of digital signal processors in a microwave thermograph.

e-mail: ADobrowolski@wel.wat.waw.pl
Faculty of Electronics
Military University of Technology
Kaliskiego st 2
00-908 Warsaw, Poland

# Whispering gallery resonator method for permittivity measurements

Krzysztof Derzakowski, Adam Abramowicz, and Jerzy Krupka

**Abstract — The new method of measuring permittivity is described. The measurements are performed using whispering gallery mode open dielectric resonators. The accuracy is assured by applications of the mode matching method. Three resonant modes (HE$_{511}$, HE$_{611}$ and HE$_{711}$) are used in measurement procedure. Accuracy of the method is much better than 0.3% for the relative permittivity having values from 20 to 50.**

*Keywords — dielectric resonator, permittivity, loss tangent, measurement method, whispering gallery modes.*

## 1. Introduction

In the whispering gallery (WG) modes the electromagnetic field distribution is such that the most of the modal energy is confined in the dielectric cylinder (or ring) close to its edge. Thus due to small radiation losses the WG resonators can be used without shielding. At millimeter wave frequency range the low permittivity dielectrics are usually used due to dimensions of elements and possibility of fabrication. High permittivity resonators are interesting at lower frequencies. At microwave frequencies typical dielectric resonators are shielded and suffer from conductor losses. The WG resonators offer a most effective way to decrease conductor losses and as a result to increase the unloaded quality factor of the resonators. That is why the high permittivity whispering gallery mode resonators have been used in measurements of ultra-low loss dielectric materials [1]. Precise computations of the complex permittivities require the knowledge of the mode type and well defined structure what means dimensions of the resonator and a shield over resonator. Typically the resonant mode used in measurements of the material properties is TE$_{011}$.

In the case of open dielectric resonators operating in the whispering gallery modes one can resign from shielding. The other problem in using WG modes is their recognition which in general is not easy. Fortunately the distribution of the WG modes in open resonator structures is very convenient and at least three first modes can be recognised accurately. In our method an open dielectric resonator is measured. From the full spectrum of modes three resonant frequencies having consecutive mode subscripts are used to calculate the permittivity of the resonator. WG modes are easy to recognise because they have high quality factors, much higher than lower order modes. The resonant frequencies of the consecutive modes have almost linear dependence on the mode subscripts. Having resonant frequencies and resonator dimensions a permittivity can be calculated in the process of adjusting its value to the resonant frequencies of WG modes.

Moreover, an investigation of the WG modes behaviour brought us to the conclusion that the HE$_{511}$, HE$_{611}$, HE$_{711}$ and HE$_{811}$ WG modes are always first WG modes that can be observed. The difference between resonant frequencies of the HE$_{511}$ and HE$_{711}$ modes depends nearly linearly on the permittivity and can provide a simple and accurate method of the measurements.

## 2. Mode matching method computations

To calculate the resonant frequencies of the WG resonators a variety of methods can be used [2]. Our idea is to apply the radial mode matching method [3, 4] to the open structures. In the case of high permittivity dielectrics this concept works very well. In the computations we have considered shielded structure but the metal shield was located at the distance sufficiently large to have no influence on the resonant frequencies and field distribution of the WG modes.

The radial mode matching method is used in its classical form as described in [4]. As usual the multilayered cylindrical dielectric resonator structure is divided into separate regions in which the permittivities are independent of coordinate $r$, and are piecewise constant functions of $z$. In each region the electromagnetic field is represented as a superposition of the TE and TM multilayered radial waveguide modes. The $E_z$ and $H_z$ field components in each layer are given below:

$$E_z^{(\alpha)}(r,\varphi,z) = \sum_{m=0}^{\infty}\sum_{i=0}^{\infty}\left[a_i^{(\alpha)}J_m\left(\sqrt{t_i^{(\alpha)}}r\right) + \right.$$
$$\left. + b_i^{(\alpha)}N_m\left(\sqrt{t_i^{(\alpha)}}r\right)\right]\Psi_i^{(\alpha)}(z)\cos\left(m\varphi+\psi_i^{(\alpha)}\right), \quad (1)$$

$$H_z^{(\alpha)}(r,\varphi,z) = \sum_{m=0}^{\infty}\sum_{i=1}^{\infty}\left[c_i^{(\alpha)}J_m\left(\sqrt{\lambda_i^{(\alpha)}}r\right) + \right.$$
$$\left. + d_i^{(\alpha)}N_m\left(\sqrt{\lambda_i^{(\alpha)}}r\right)\right]\Phi_i^{(\alpha)}(z)\sin\left(m\varphi+\varphi_i^{(\alpha)}\right), \quad (2)$$

where $a_i$, $b_i$, $c_i$ and $d_i$ are the unknown expansion coefficients, $\lambda_i$ and $t_i$ are the eigenvalues of the eigenfunctions $\Phi_i$ and $\Psi_i$ which form the complete and biorthogonal series,

$\alpha$ is the number of a region, $i$ and $m$ are the multilayered radial waveguide mode subscripts.

In the region I containing symmetry axis the Neumann function must be omitted from the field expressions. The eigenfunctions $\Phi_i$ and $\Psi_i$ describe the dependence of the fields along $z$ axis. Taking advantage of the axial symmetry the fields of resonant modes can be expressed as a linear combination of modes having the same mode subscript $m$. By applying the continuity relations at the discontinuity surfaces (for $\mathbf{r} = R^\alpha$), and by numerical matching the fields at the structure walls, for each $m$ a set of linear equations is found. This system of infinite equations can be numerically solved only for a finite number of terms, but then equations are met with an error depending on the number of used terms. By rewriting the equations into a form expressing mean-square errors, and using variational methods, a set of homogeneous linear equations with a finite number of unknown coefficients is obtained, which has a following general form:

$$\overline{W} \left[ a_i^I, ., c_i^I, ., a_i^{II}, ., b_i^{II}, ., c_i^{II}, ., d_i^{II}, ., a_i^{III}, .. \right]^T = [0], \quad (3)$$

where $\overline{W}$ is a square matrix with elements depending on structure parameters and a frequency, $T$ means a transposed matrix.

Table 1
Measured and computed resonant frequencies
(resonator dimensions $D = 63.43$ mm, $L = 6.36$ mm)

| Number | Measured frequency $f_m$ [MHz] | Computed frequency $f_c$ [MHz] | Error [%] $100(f_c - f_m)/f_m$ | Mode type |
|---|---|---|---|---|
| 1 | 1882.4 | 1896.9 | +0.767 | $m = 2$ |
| 2 | 2172.9 | 2178.1 | +0.239 | $m = 3$ |
| 3 | 2442.6 | 2446.1 | +0.143 | $m = 4$ |
| 4 | 2704.2 | 2704.7 | +0.0185 | $HE_{511}$ |
| 5 | 2909.1 | 2915.3 | +0.213 | $m = 3$ |
| 6 | 2956.4 | 2956.4 | 0 | $HE_{611}$ |
| 7 | 3196.2 | 3198.2 | +0.0626 | $m = 4$ |
| 8 | 3203.5 | 3203.1 | −0.0125 | $HE_{711}$ |
| 9 | 3446.8 | 3446.1 | −0.0203 | $HE_{811}$ |
| 10 | 3470.5 | 3471.1 | +0.0115 | $HE_{521}$ |
| 11 | 3687.4 | 3686.5 | −0.0244 | $HE_{911}$ |
| 12 | 3737.5 | 3737.6 | +0.0027 | $HE_{621}$ |

The nontrivial solution of the system exists if and only if the determinant of the matrix $\overline{W}$ is equal zero. All the resonant frequencies of the structure can found from the zeros of the determinant. After finding the resonant frequencies for each of them Eqs. (3) can be solved and all unknown expansion coefficients can be found. From the known field expressions, expansion coefficients and resonant frequencies we calculate the electromagnetic field distributions. The computer program written in Microsoft's FORTRAN PowerStation has the following limitations: up to 10 layers of dielectrics in up to 7 cylindrical regions

and up to 30 radial waveguide modes taken into account in each region. The user can choose the electromagnetic field mapping accuracy by selecting a desired number of grid points.

Another limitation in the program is that the structure must be fully surrounded by the PEC or PMC walls (the types of walls can be mixed). This is a certain limitation because the open structures basically are not considered. Fortunately due to the WG modes characteristics the open WG resonators can be analysed with high level of accuracy.

The resonant modes having first index 5 or higher reveal the typical WG mode behaviour i.e. the resonant frequencies of shielded structures and without shield are nearly the same what can be observed experimentally. A comparison of the computed resonant frequencies with the measured ones shows an excellent agreement – for the WG modes the average error was on the level of 0.015% as can be seen in Table 1.

## 3. Numerical and experimental results

The transmission characteristic has been measured in the structure shown in Fig. 1. The dielectric resonator has been excited by the microstrip lines in such a way that coupling coefficient was small enough to observe resonances without disturbing them. The characteristic has been measured
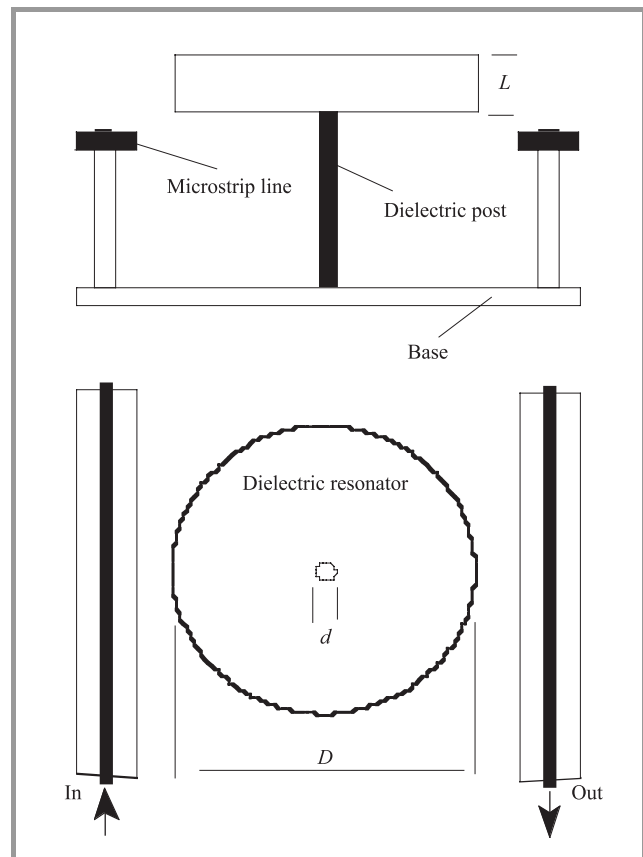


*Fig. 1.* Measured structure ($D = 63.43$ mm, $d = 6.15$ mm, $L = 6.35$ mm, $\varepsilon_r = 45$).

in the frequency range $1.7 - 3.8$ GHz which allowed us to observe several lowest WG resonances. The measured results are shown in Fig. 2 and in Table 1. For the quality factor measurements the excitation through the coupling loops has been performed. The WG modes have unloaded quality factor on the level of 14000. Lower order modes have unloaded quality factors in the range $100 - 4000$ thus the WG modes can be easily distinguished.
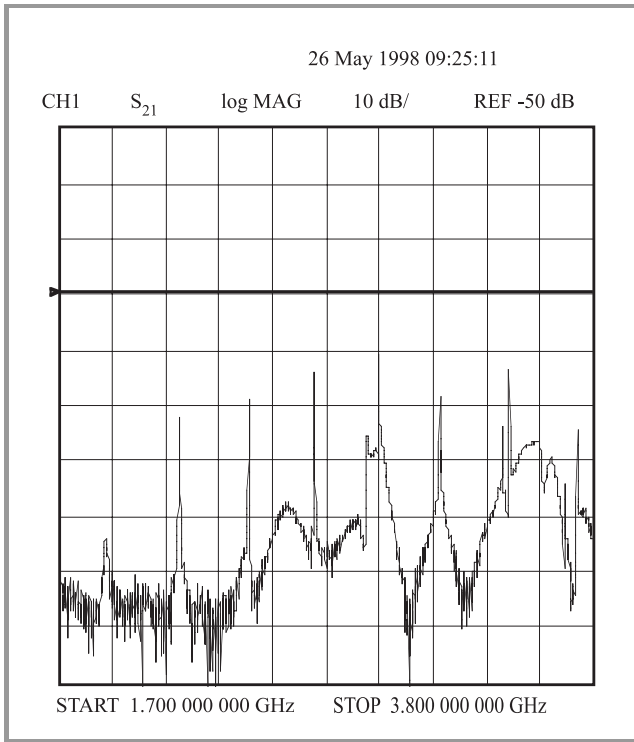


26 May 1998 09:25:11

CH1     $S_{21}$     log MAG     10 dB/     REF -50 dB

START  1.700 000 000 GHz     STOP  3.800 000 000 GHz

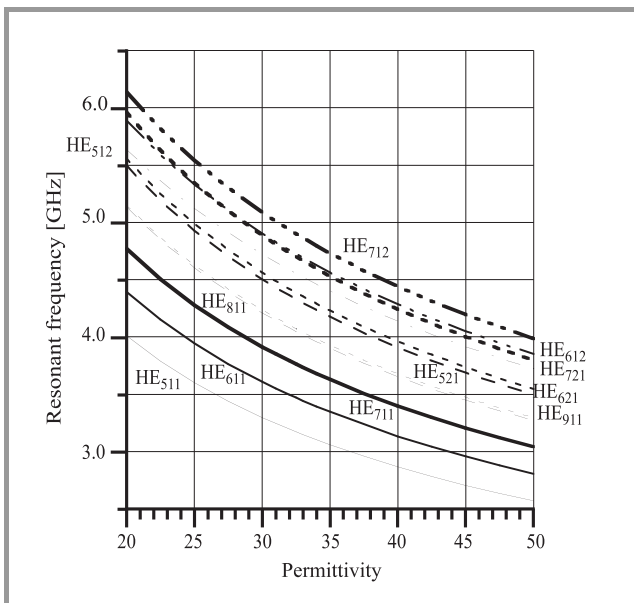**Fig. 2.** Measured frequency response.



**Fig. 3.** Mode chart of the lowest WG modes.

The resonant frequencies of the resonator have been computed by means of the radial mode matching method assuming the permittivity of 45 as given by the producer (Trans-Tech). For WG modes the field distributions have been computed and then the mode indices found. The computed resonant frequencies and the mode designation is presented in Table 1.

The agreement between measured and computed resonant frequencies of the WG modes is better than 0.025%. The lower order modes have measured resonant frequencies shifted down in comparison with computed ones. This is an effect of metal walls surrounding the structure present in a case of simulations. The lower mode number the bigger discrepancy can be noticed. Having such a good agreement of measured and computed resonant frequencies one can be sure that the radial mode matching method can provide reliable results when used in measurements.

The computer simulations have been used to investigate the WG modes behaviour. The resonant frequencies of the structure have been computed for different values of the relative permittivity as shown in Fig. 3. It is easy to notice that four first WG modes are always the same: $HE_{511}$, $HE_{611}$, $HE_{711}$ and $HE_{811}$. From the practical point of view the mode $HE_{811}$ is not very useful because it has resonant frequency close to the next WG mode $HE_{521}$ and their characteristics can interfere. Also the $HE_{611}$ mode is close to the lower order mode but this mode ($m = 3$) has very low quality factor ($Q_0 \approx 400$) and should has no significant influence on the $HE_{611}$ mode what we confirmed experimentally. The $HE_{511}$ mode is separated from any other modes. What is also interesting the difference between resonant frequencies of the $HE_{611}$ and $HE_{511}$ modes is nearly equal
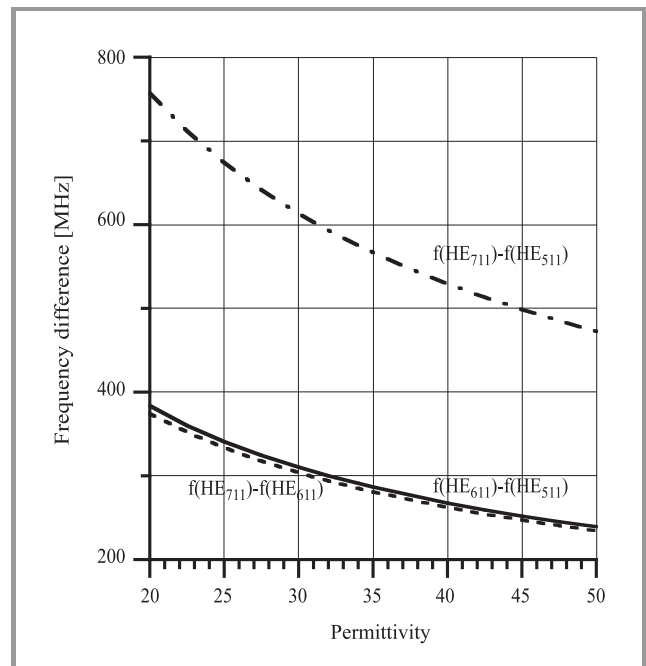


**Fig. 4.** Differences between resonant frequencies of the WG modes.

to the difference between resonant frequencies of the $HE_{711}$ and $HE_{611}$ modes as shown in Fig. 4. (In the Fig. 4 the difference between resonant frequencies $HE_{711}$ and $HE_{511}$ is also shown). In general three first WG modes can be always easily identified thus with the proper algorithm the resonant frequencies of this modes can be used to calculate the permittivity.

## 4. The measurement procedure

The measurements are done in a following way:

- first, the resonant frequencies and quality factors of the modes of open dielectric resonator are measured using network analyser;

- second, the WG modes are identified taking into account quality factors and distribution of modes;

- third, the real part of permittivity is found using distance between resonant frequencies $HE_{711}$ and $HE_{511}$.

In our test measurements (resonator $D = 63.43$ mm, $L = 6.36$, WG modes $HE_{511}$, $HE_{611}$, $HE_{711}$) the determined permittivity was $\varepsilon_r = 44.95$. The agreement with classical methods (the producer values) is considerably high.

Table 2
Computed coefficients used in Eq. (4)
(diameter of the resonator $D = 63.43$ mm)

| Resonator thickness $L$/mm | $A$ | $B$ |
|---|---|---|
| 2 | 15.614413 | 1.837472 |
| 3 | 15.815942 | 1.900219 |
| 4 | 15.889140 | 1.928469 |
| 5 | 15.928919 | 1.944443 |
| 6.36 | 15.964069 | 1.957261 |
| 7.72 | 15.994913 | 1.965745 |

If one can assume the accuracy of the resonant frequency measurement better then 0.2 MHz the permittivity of the resonator can be established with the accuracy better than 0.15%, which is sufficiently enough for industrial practice. Depending on the resonator dimensions similar to that presented in Fig. 4 characteristics can be computed and applied in measurements of dielectrics. However this characteristics are good for the real part of the permittivity measurements only. Depending on the diameter to height ($D/L$) ratio the computed characteristics of the difference between resonant frequencies $HE_{711}$ and $HE_{511}$ differ in values but reveal the same behaviour that can be described with a following equation:

$$\varepsilon_r = e^{[A - B \ln(\Delta f)]}, \qquad (4)$$

where $\Delta f$ is frequency difference, $A$ and $B$ coefficients. The coefficients $A$ and $B$ for several resonator dimensions are given in Table 2. To obtain the permittivity of the

resonator it is enough to measure the difference between resonant frequencies of the $HE_{711}$ and $HE_{511}$ modes and to use Eq. (4).

## 5. Conclusions

The new, simple and precise measurement method is presented. Open WG dielectric resonator structures used to determine the permittivity of the resonators offer high accuracy of the measurements. The real part of the permittivity is directly related to the difference between resonant frequencies of the $HE_{711}$ and $HE_{511}$ modes. The method is so simple that there is no need for numerical computations and results are obtained from the simple equation.

## References

[1] J. Krupka *et al.*, "Complex permittivity measurements of extremely low loss dielectric materials using whispering gallery modes", in *IEEE MTT-S Int. Microw. Symp. Dig.*, Denver, USA, 1997, pp. 1347–1350.

[2] Xiao Hu Jiao *et al.*, "Whispering-gallery modes of dielectric structures: applications to millimeter-wave bandstop filters", *IEEE Trans. Microw. Theory Techn.*, vol. 35, pp. 1169–1175, 1987.

[3] S. Maj and M. Pospieszalski, "A composite multilayered cylindrical dielectric resonator", in *IEEE MTT-S Int. Microw. Symp. Dig.*, San Francisco, USA, 1984, pp. 190–192.

[4] K. Derzakowski and A. Abramowicz, "Dielectric resonator figure of merit", *Bull. Polish Acad. Sci., Techn. Sci.*, vol. 44, no. 2, pp. 129–139, 1996.

**Krzysztof Derzakowski** was born in Mińsk Mazowiecki, in 1959. He received the M.Sc. and Ph.D. degrees (with honors) in electronic engineering from Warsaw University of Technology, Warsaw, in 1984 and 1991, respectively. Since 1985, he has been associated with the Institute of Radioelectronics, Warsaw University of Technology, where he is currently an Assistant Professor. His current research interests are concerned with measurements of dielectric and magnetic material properties at microwave frequencies, applications of dielectric resonators, and electromagnetic-field theory. He has authored numerous scientific papers.
e-mail: K.Derzakowski@ire.pw.edu.pl
Institute of Radioelectronics
Warsaw University of Technology
Nowowiejska st 15/19
00-665 Warsaw, Poland

**Adam Abramowicz** received the M.Sc. and Ph.D. degrees (with honors) from Warsaw University of Technology, Warsaw, in 1982 and 1993, respectively, both in electronic engineering. In June 1982 he joined the Institute of Electronics Fundamentals, Warsaw University of Technology, where he is currently an Assistant Professor. In 1996, he was a JSPS Post-Doctoral Fellow at Utsunomiya University, Japan. From September 1996 to August 1997, he worked on high-temperature superconductor (HTS) filters

at FIT-Messtechnik GmbH, Bad Salzdetfurth, Germany. He has authored numerous scientific papers and has co-authored a book on dielectric resonators. His research interests include microwave filters, dielectric resonators, HTS, electromagnetic-field theory, and computer-aided design (CAD) of microwave circuits
e-mail: aabr@ise.pw.edu.pl
Institute of Electronic Systems
Warsaw University of Technology
Nowowiejska st 15/19
00-665 Warsaw, Poland

**Jerzy Krupka** was born in Cracow, on April 7, 1949. He received the M.Sc., Ph.D. and D.Sc. (habilitation) degrees from Warsaw University of Technology, Warsaw, in 1973, 1977, and 1989, respectively. Since 1973, he has been with the Institute of Microelectronics and Optoelectronics, Warsaw University of Technology, where he is currently a Professor. His research deals mainly with methods of measurements of electromagnetic properties of dielectrics, ferrites and superconductors at microwave frequencies, construction of equipment for these measurements, and numerical methods for electromagnetic-field analyses, and has taken part in several projects on these subjects in Poland, France, Germany, the U.S., and Australia. He is an Editorial Board member of the IEEE Transactions on Microwave Theory and Techniques.
e-mail: J.Krupka@imio.pw.edu.pl
Institute of Microelectronics and Optoelectronics
Warsaw University of Technology
Nowowiejska st 15/19
00-665 Warsaw, Poland

# Low order autoregressive models for FDTD analysis of microwave filters

Piotr Kozakowski and Michał Mrozowski

**Abstract —** **The forward-backward autoregressive (AR) model is applied to extract time signatures generated by the FDTD algorithm. It is shown that using simple techniques of model parameters selection one is able to reduce the model complexity for low and medium Q circuits.**

*Keywords —* *FDTD, signal processing, AR, filters.*

## 1. Introduction

The finite-deference time-domain method is a versatile numerical technique that has been extensively used for solving electromagnetic problems. Due to its flexibility it has been applied to both simple problems and more complicated ones. However the main drawback of the FDTD method is a long computation time needed to analyze high Q circuits. In order to obtain the frequency domain characteristics of a circuit by means of the Fourier transform, a very long time-domain record of samples is needed. Premature termination of the simulation usually results in inaccurate extraction of narrow-band components in frequency-domain. In order to circumvent the aforementioned problem signal processing the system identification methods have recently been proposed to be used with the FDTD algorithm. Most of these techniques allow one to extract time signature features form a short segment of the original FDTD sequence. The number of methods such as autoregression, Prony's, general-pencil-of-function, to name but a few, have been employed to meet the challenge.

In this contribution we use a forward-backward autoregressive model for signal extrapolation. We show that using some simple techniques for model parameters determination it is possible to considerably reduce the numerical costs of signal extrapolation without the lost of accuracy of the method.

Applications of autoregressive method have been described in [3, 4, 6]. Nevertheless the model orders reported by the authors seem to be very large [3, 6]. This causes unnecessary numerical burden or even may lead to numerical instability of the algorithm used for extracting filter coefficients. Besides, most of the work has been confined to investigation of simple structures without considering the influence of Q-values on efficiency of the method.

Herein the application of AR method is illustrated by investigating the time signatures obtained from the FDTD simulation of three structures:

– a low Q pass-band microstrip filter [3],

– a three-section pass-band waveguide filter with medium Q [6],

– a high Q dual-mode waveguide filter.

All time signatures have been obtained using a commercial FDTD software QuickWave 3D [7].

## 2. Methodology

The autoregressive method is extensively described in signal processing literature [5]. For this reason we shall not describe the algorithm but rather concentrate on practical problems associated with its application to electromagnetics. Our purpose is to demonstrate that using the forward-backward autoregressive process [4, 5] with some simple techniques of model parameters selection it is possible to reduce model orders to the number of poles laying in the bound of interest.

If the sequence $x[1], x[2], \ldots, x[N]$ is to be modeled as an AR process of the $p$ order the following model is assumed

$$x[n] = -a_1 x[n-1] - a_2 x[n-2] + \\ - \ldots - a_p x[n-p] + v[n], \qquad (1)$$

where $v[n]$ is a white-noise process. The constants $a_1, a_2, \ldots, a_p$ are determined using the least square method minimizing forward and backward errors.

The frequency response of the model is calculated from the filter coefficients using the following formula

$$H(j\omega) = \qquad (2)$$
$$= \frac{b_0 + b_1 \exp(-j\omega n\Delta t) + \ldots + b_p \exp(-j(p-1)\omega n\Delta t)}{1 + a_1 \exp(-j\omega n\Delta t) + \ldots + a_{p-1} \exp(-jp\omega n\Delta t)},$$

where the coefficients $b_1, b_2, \ldots, b_p$ are defined by the equation

$$\underline{\mathbf{b}}_p = \begin{bmatrix} 1 & 0 & \ldots & 0 \\ a_1 & 1 & \ldots & 0 \\ a_2 & a_1 & \ldots & 0 \\ \vdots & \vdots & \ddots & \vdots \\ a_{p-1} & a_{p-2} & \ldots & 1 \end{bmatrix} \begin{bmatrix} x[0] \\ x[1] \\ \vdots \\ x[p-1] \end{bmatrix}. \qquad (3)$$

The successful application of the AR method requires the knowledge of model parameters, namely the number of initial samples of the original FDTD record to be discarded, the number of samples required for model construction, a desampling factor and a model order.

**Selection of training sequence.** Selection of the segment to be used for training of the AR model is described in detail in [2]. In general the original FDTD record is divided into early and late time responses. The first part, dominated by transients, is discarded and only the other part is used for building model.

**Desampling factor.** Due to stability conditions of the FDTD algorithm the sampling period $\Delta t_{FDTD}$ is much smaller that it is required by signal processing methods or the Nyquist formula. Leaving the value of $\Delta t_{FDTD}$ unchanged entails problems with order selection and may lead to numerical instability of the method. This is because the model based on the oversampled sequence requires additional terms to extract the signal components situated outside the band. In our case the sampling period was increased by the factor:

$$ k = \frac{1}{2\Delta t_{FDTD}\left(f_{max} + (t_0)^{-1}\right)}, \qquad (4) $$

where $t_0$ corresponds to the time shift in the FDTD sequence. It can be shown that sampling the band-limited signals at exactly twice their maximum frequency is not sufficient, hence the additional factor $1/t_0$ in the formula (4).

**Model order selection.** Once the training sequence and desampling factor have been chosen one can pass on to the determination of the exact number of poles contained in the data. There are two commonly used statistics for selection of model orders the Akaike information criterion (AIC) and the minimum description length (MDL) [5]. Both of them are based on calculation of the predication error between the model and the data samples, using digital filtering as a result of modeling. The model order that ensures reaching the minimum of one of these measures is regarded as the best one. In our case the criteria are regarded as general guidelines for selecting model order and serve as a starting point for determination of the exact number of poles contained in the data. In order to investigate the possibility of model order reduction, the afore-mentioned criteria were modified in the following way. All terms outside the bands of interest were discarded. Thus the model order was lowered to the number of poles which lie in the band of interest. The approach, called a band limiting, considerably improved the efficiency of the model construction algorithm.

## 3. Numerical results

The method was verified by modeling of the three previously mentioned filters. In all cases model parameters were selected using the methods described above. The

frequency-domain responses of the investigated structures were calculated directly from the filter coefficients of the AR model using an analytical formula. The error norms given in Table 1 were evaluated in the frequency-domain with reference to the Fourier transform of the original FDTD sequence.

In all cases, with model orders selected automatically (Figs. 1, 3, 5), the Fourier transforms obtained by combining the FDTD algorithm and the AR model were almost indistinguishable from those obtained directly from the FDTD record of samples.
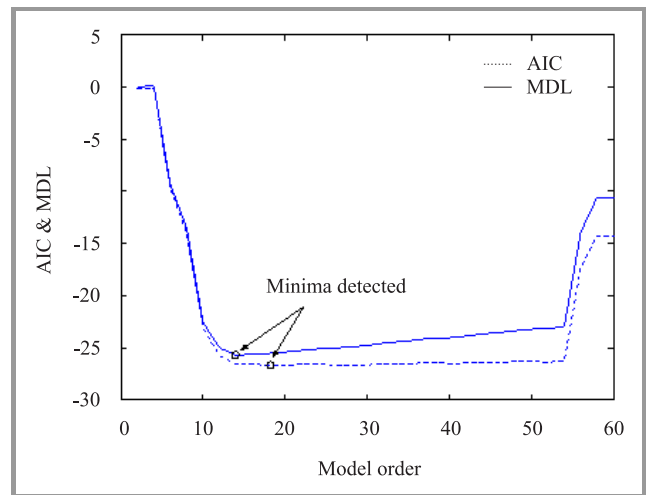


*Fig. 1.* Determination of the model order for the microstrip pass-band filter.
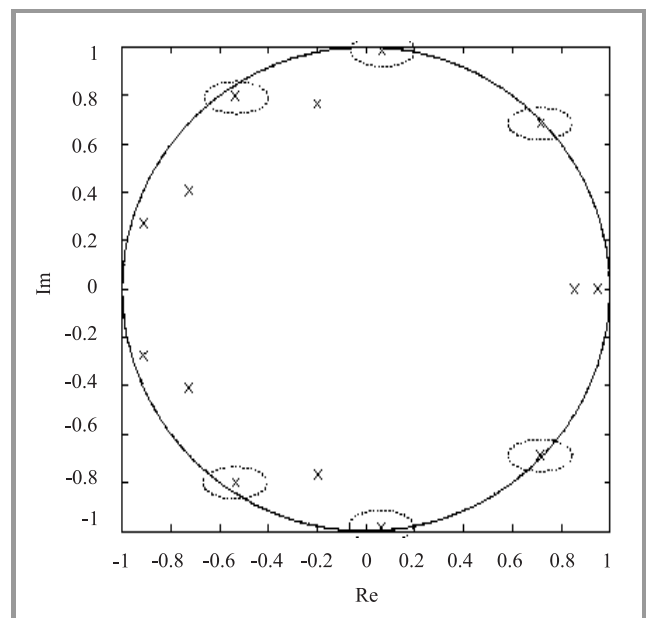


*Fig. 2.* Pole locations in complex plane for the microstrip pass-band filter (poles in band of interest are circled).

After reduction of filter orders (only poles from the band were taken into account (Figs. 2, 4, 6)) the original spec-

Table 1
Results of modeling

| Parameters | Filter | | |
|---|---|---|---|
| | low Q | medium Q | high Q |
| Frequency range | $0 - 12$ GHz | $33 - 38$ GHz | $10 - 12$ GHz |
| Desampling factor | 56 | 25 | 27 |
| First/last sample | 3192/6832 | 3650/6150 | 5400/10044 |
| Order selected automatically | 14 | 28 | 56 |
| Order selected after band limiting | 6 | 6 | 8 |
| Error norm with model (order selected automatically) | $2.0 \cdot 10^{-5}$ | $2.35 \cdot 10^{-5}$ | $2.74 \cdot 10^{-4}$ |
| Error norm with model (order selected after band limiting) | $3.7 \cdot 10^{-5}$ | $2.36 \cdot 10^{-5}$ | $5.4 \cdot 10^{-2}$ |



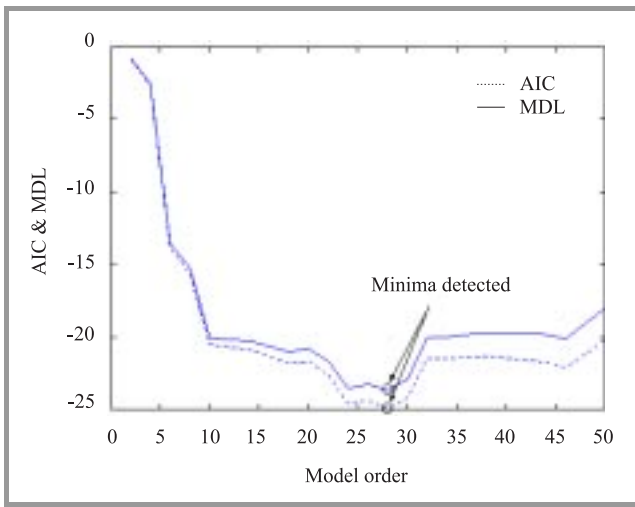*Fig. 3.* Determination of the model order for the three-section waveguide filter.
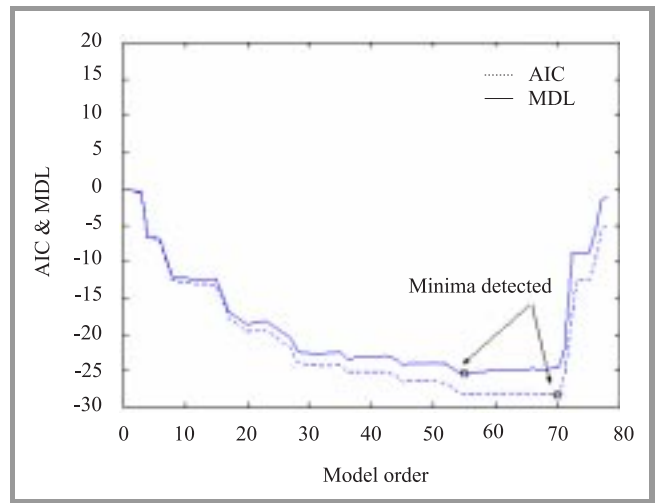


*Fig. 5.* Determination of the model order for the dual-mode waveguide filter.
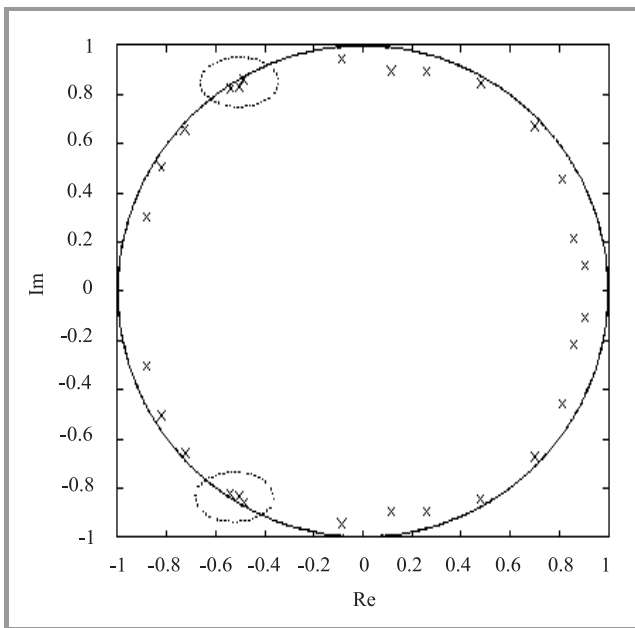


*Fig. 4.* Pole locations in complex plane for the three-section waveguide filter (poles in band of interest are circled).
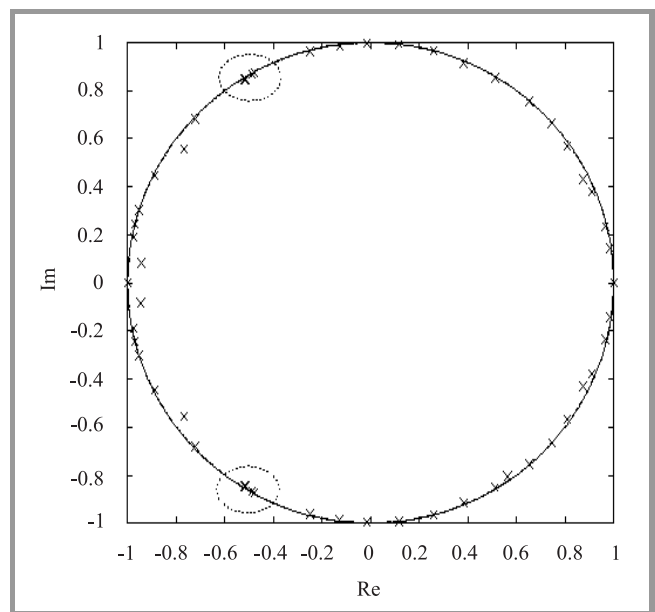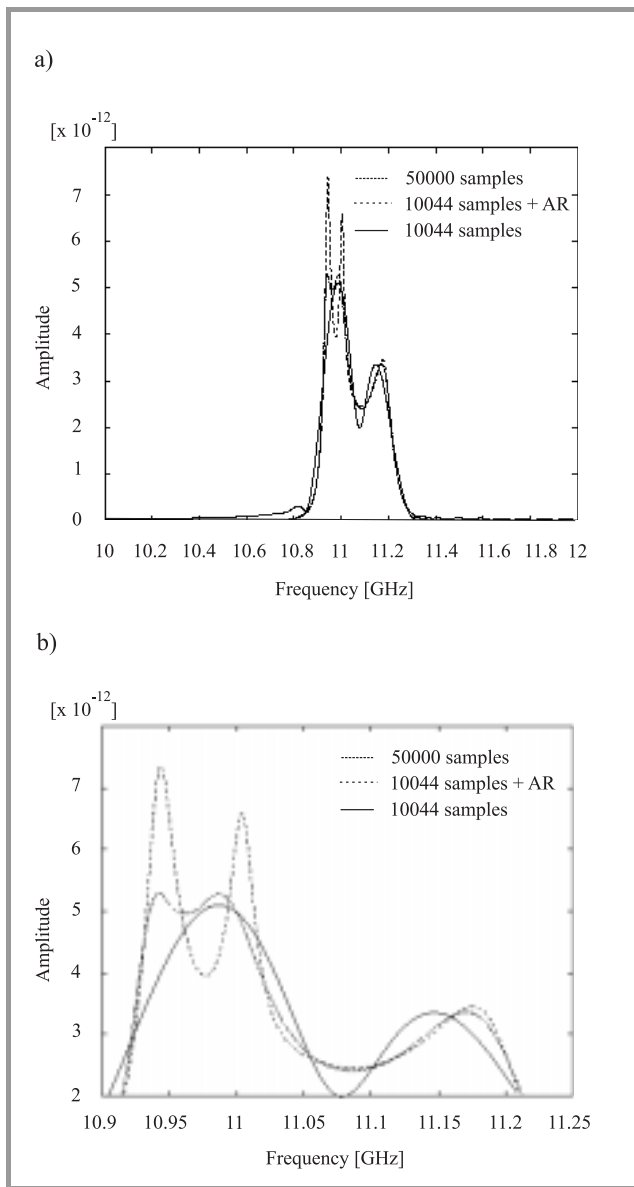


*Fig. 6.* Pole locations in complex plane for the dual-mode waveguide filter (poles in band of interest are circled).

**Fig. 7.** (a) Amplitude spectrum of the dual-mode waveguide filter; (b) exploded view of the amplitude spectrum of the dual-mode waveguide filter.

orders we were able to achieve good agreement between spectra.

## 4. Conclusions

The contribution demonstrated that using some simple techniques of the model parameters selection it is possible to considerably reduce model orders for low and medium Q circuits. The numerical results showed that, for the considered structures, extrapolation of signal signatures using the forward-backward AR with afore-mentioned parameters selection techniques yielded superior results to those obtained by other authors [3, 6]. Furthermore, in our case, the frequency spectra were calculated with an analytical formula involving the digital filter coefficients. This approach eliminates the need of the use of the Fourier transform and therefore it further reduces the numerical costs of the method as a whole.

## References

[1] W. L. Ko and R. Mittra, "A combination of FD-TD and Prony's method for analyzing microwave integrated circuits", *IEEE Trans. Microw. Theory Techn.*, vol. MTT-39, no. 12, pp. 2176–2181, 1991.

[2] M. Mrozowski, "Criteria for building Prony models for time domain CAD", *IEEE AP-S Digest*, pp. 2306–2309, 1998.

[3] J. Chen, C. Wu, T. Lo, K. Wu, and J. Litwa, "Using linear and nonlinear predictors to improve the computational efficiency of the FD-TD algorithm", *IEEE Trans. Microw. Theory Techn.*, vol. MTT-42, no. 10, pp. 1993–1997, 1994.

[4] V. Jandhyala, E. Michielssen, and R. Mittra, "FDTD signal extrapolation using the Forward-Backward autoregressive (AR) model", *IEEE Microw. Guid. Wave Lett.*, vol. 4, no. 6, pp. 163–165, 1994.

[5] S. L. Marple, *Digital Spectral Analysis*. Prentice Hall, Inc. Englewood Cliffs, 1987.

[6] C. Eswarappa and W. J. R. Hoefer, "Autoregressive (AR) and autoregressive moving average (ARMA) spectral estimation techniques for faster TLM analysis of microwave structures", *IEEE Trans. Microw. Theory Techn.*, vol. MTT-42, no. 12, pp. 2407–2411, 1994.

[7] W. Gwarek, M. Celuch-Marcysiak, M. Sypniewski, and A. Więckowski, "QuickWave – 3D manual", http://www.qwed.com.pl

tra were still predicted quite well in the cases of the low and medium Q circuits. The error norms, given in the last row of the table, are almost equal to those computed using the models with higher orders. For the low and medium Q structures the AR method together with the proposed parameters selection techniques yields superior results to those reported in [3, 6], where the model orders were established on the level of 50 for both the microstrip band-pass filter and the three-section waveguide filter. However, for the case of the high Q filter, the comparison of original spectrum with the estimated one showed some discrepancy (Fig. 7). The error norm is much higher compared to the case of the model of the 56 order. Thus only for low and medium Q structures with reduced model

**Piotr Kozakowski**
e-mail: piotek@task.gda.pl
Department of Electronics, Telecommunications
and Informatics
Technical University of Gdańsk
Narutowicza st 11/12
80-952 Gdańsk, Poland

**Michał Mrozowski**
e-mail: mim@pg.gda.pl
Department of Electronics, Telecommunications
and Informatics
Technical University of Gdańsk
Narutowicza st 11/12
80-952 Gdańsk, Poland

# Propagation in rectangular waveguides with a pseudochiral Ω slab

Jerzy Mazur and Krzysztof Dorko

**Abstract — The transfer matrix approach is applied for analysis of waveguides loaded with a uniaxial pseudochiral Ω slab. In particular a pseudochiral parallel plate and rectangular guides are investigated. Based on the numerical analysis the influence of the pseudochirality on propagation characteristics and field distribution are examined. Other feature such as a field displacement phenomenon appearing in the both considered structures due to the pseudochirality is also discussed.**

*Keywords — waveguides, propagation, pseudochiral media.*

## 1. Introduction

A thorough characterization of a wave propagation and scattering in complex media allows to investigate their potential usefulness in various applications. Among complex media we can find a new pseudochiral medium [1], called Ω media. The pseudochiral Ω material contains small omega shaped metal particles mostly ordered along a preferred direction. Although the concept of Ω media has arisen from the chiral media and both materials are characterized by the similar constitutive relations their interactions with electromagnetic wave are considerable different. In particular the chiral medium exhibits the effect of optical activity that refers to the rotation of the wave polarization plane while the pseudochiral medium yields the field displacement effect. Recently, the propagation properties of the pseudochiral guides were intensively studied [2 − 4]. These behaviors in particular depend in particular on the arrangement of the Ω particles in the medium inserted to the structure. For example the direction of the field displacement in the cross-section of the guide is changed when the Ω particles in the medium are reversed [3, 4]. The electromagnetic wave interaction with pseudochiral media have recently suggested their potential applications, e.g.: phase shifter [2], nonradiative Ω guides [5] nonreflecting shields [6]. Moreover, the scattering properties of pseudochiral guides have been utilized in [7] to reconstruction of the Ω medium parameters. In this letter we consider the problem of the electromagnetic wave propagation in a rectangular guide containing a slab of Ω medium as shown in Fig. 1. This structure completes the class of pseudochiral guides presented in [4]. The problem is solved by using transfer matrix approach (TMA) proposed in [8] for ferrite filled guides. Here the TMA is modified to the cases where pseudochiral materials, such as Ω media, are involved. It is shown that except of hybrid modes the considered guides supports also the TE$_n$ modes. The main feature of the guide is that the
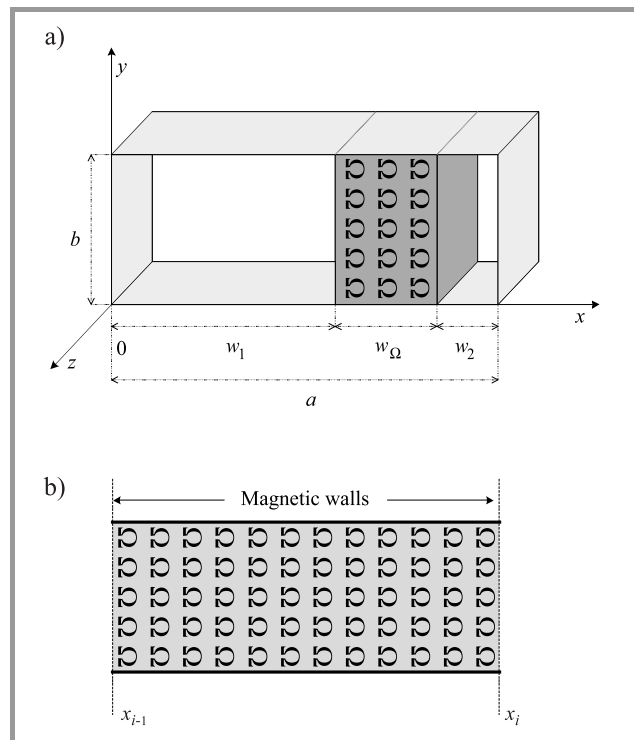


**Fig. 1.** Structures under examination (a) a rectangular waveguide containing pseudochiral Ω slab; (b) a parallel – plate pseudochiral guide.

field displacement occurs along the *x* axis and the magnitude of the phenomenon depends on the Ω medium parameters. Considerable differences in field distribution are observed when the slab is reversed in the guide.

## 2. Transfer matrices formulation

Let us consider a structure shown in Fig. 1b, where pseudochiral material is located between two parallel metal plates. The Ω particles lie in the guide cross-section and the stemps are perpendicular to the metal plates of the guide. For this medium, the relative electric permittivity and magnetic permeability tensors are of the diagonal form:
$\overline{\varepsilon} = \varepsilon(\vec{i}_x\vec{i}_x + \vec{i}_z\vec{i}_z) + \varepsilon_y\vec{i}_y\vec{i}_y$ and $\overline{\mu}_c = \mu(\vec{i}_x\vec{i}_x + \vec{i}_y\vec{i}_y) + \mu_z\vec{i}_z\vec{i}_z$.
The magnetoelectric coupling tensors have the following dyadic representation $\overline{\Omega}_{yz} = \Omega\vec{i}_y\vec{i}_z$ and $\overline{\Omega}_{zy} = \Omega\vec{i}_z\vec{i}_y$, where Ω is a coupling admittance between electric and magnetic field along *y* and *z* axis, respectively. In fact, the polarization vectors induced in Ω inclusions increase the values of $\varepsilon_y$ and $\mu_z$. Thus it follows that $\varepsilon < \varepsilon_y$ and $\mu < \mu_z$.

In general, the unbounded pseudochiral medium in Fig. 1 supports hybrid modes. However, if we assume that the field is uniform in the $y$ direction, then the hybrid field is decoupled into TE and TM modes. Therefore the TE$_n$ modes appear in the guide. Hereafter, the propagation characteristics of these waves are determined applying TMA. We get a following transfer matrix equation that defines the relation between the tangential fields components $\underline{F} = (H_z, E_y)^T$ at the side inter faces $x_i$ and $x_{i-1}$:

$$
\begin{bmatrix} H_z \\ E_y \end{bmatrix}_{x_i} = \begin{vmatrix} T_{11}^\Omega & T_{12}^\Omega \\ T_{21}^\Omega & T_{22}^\Omega \end{vmatrix} \cdot \begin{bmatrix} H_z \\ E_y \end{bmatrix}_{x_{i-1}} , \qquad (1)
$$

where

$$
T_{11}^\Omega = \cosh(pw_\Omega) + k_0 \kappa \mu_z \frac{\sinh(pw_\Omega)}{p} ,
$$

$$
T_{12}^\Omega = j \frac{\beta^2 - k_0^2 \varepsilon_y \mu \left(1 + \frac{\mu_z}{\varepsilon_y}\kappa^2\right)}{k_o \eta_0 \mu} \frac{\sinh(pw_\Omega)}{p} ,
$$

$$
T_{21}^\Omega = -jk_o \eta_0 \mu_z \frac{\sinh(pw_\Omega)}{p} ,
$$

$$
T_{22}^\Omega = \cosh(pw_\Omega) - k_o \kappa \mu_z \frac{\sinh(pw_\Omega)}{p} .
$$

Here, $\beta$ is the propagation constant in $z$ direction, the eigenvalue $p$ is found from relation: $p = \sqrt{(\mu_z/\mu)\beta^2 - k^2 \mu_z \varepsilon_y}$, $k_0$ and $\eta_0$ are the wavenumber and intrinsic impedance of the free space, respectively, $\kappa = \eta_0 \Omega$ is the coupling coefficient. The structure containing $n$ regions is defined by total transfer matrix relation determined as follow: $F_{x_i} = T^n T^{n-1} T^1 F_{x_{i-1}}$.
Note that the TMA solution can be easily derived for any combination of the regions and boundary conditions at the side walls of the guide. If the transfer matrix for dielectric regions needed then it can be determined by introducing in Eq. (1) the $\kappa = 0$ and scalar values of the material electric permittivity and magnetic permeability.

## 3. Propagation in $\Omega$ waveguides

As a first example we consider a parallel plate pseudochiral guide shown in Fig. 1b. Using Eq. (1) together with magnetic wall conditions at the side planes $x_i$ and $x_{i-1}$, the dispersion relation $T_{12}^\Omega = 0$ is determined.
It can be shown that the dominant wave in the guide is the TEM mode. This mode propagates in the guide with the propagation constant $\beta = \sqrt{k_0^2 \mu \mu_z \kappa^2 + \mu \varepsilon_y k_0^2}$ and distribution of the transverse field components $E_y$, $H_x \sim \exp(-px)$, where $p = k_0 \mu_z \kappa$. Note that the eigenvalue $p$ is a real quantity so the dominant mode is a surface wave. The coupling coefficient $\kappa$ is small, in a typical $\Omega$ material $\kappa \leq 1$. Hence, $\beta$ slightly depends on coupling coefficient variation.

In spite of this, the coupling coefficient strongly affects the field distribution inside the waveguide. The effect observed is similar to the field displacement phenomena appearing in a ferrite parallel plate guide with perpendicular magnetization [9]. Contrary to the ferrite guide, the phenomenon in the pseudochiral structure is reciprocal. It means that the field distribution in the $\Omega$ guide does not depend on the propagation direction. However, the field energy is concentrated at the one edge of the guide in dependence on the $\kappa$ sign. Note that the change of the sign occurs when the $\Omega$ particles are reversed. It relates to the $\pi$ turn of the pseudochiral sample in the guide. This operation causes the change of the propagation properties when the $\Omega$ sample is asymmetrically placed in the guide.
Therefore, we now consider the pseudochiral rectangular waveguide which cross-section is subdivided into three regions (one pseudochiral and two isotropic) as shown in Fig. 1a. The TMA is now used to determine the total transfer matrix. At this point it only remains to apply the electric wall boundary conditions at the edge planes of the guide to obtain the dispersion relation:

$$
\mu \mu_z k_0 \kappa \tanh(p_\Omega w_\Omega) \left[ p_1 \tanh(p_2 w_2) - p_2 \tanh(p_1 w_1) \right] +
$$
$$
+ p_\Omega p_2 \mu \tanh(p_1 w_1) + p_1 p_\Omega \mu \tanh(p_2 w_2) +
$$
$$
+ \left[ \beta^2 - k_0^2 \mu \varepsilon_y \left(1 + \frac{\mu_z}{\varepsilon_y}\kappa^2\right) \right] \tanh(p_1 w_1) \times
$$
$$
\times \tanh(p_2 w_2) \tanh(p_\Omega w_\Omega) = 0 . \qquad (2)
$$

Let us consider two $\Omega$ guides depicted as $R^{+\Omega}$ and $L^{+\Omega}$ in Fig. 2a. The $L^{+\Omega}$ guide arises from the $R^{+\Omega}$ structure when the $\Omega$ slab in this guide is displaced symmetrically to the opposite side. We can infer from Eq. (2) that the propagation properties of these two guides are different. The another situation is shown in Fig. 2b where $R^{+\Omega}$ and $L^{-\Omega}$ guides are considered. The $L^{-\Omega}$ structure appears when the $\Omega$ slab is turn of $\pi$ in the $L^{+\Omega}$ guide. Now we can note from Eq. (2) that both guides shown in Fig. 2b preserve invariant wave properties. The rotation of the guide by $\pi$ with respect the $y$ or $z$ axis leads to the $L^{-\Omega}$ structure as shown in Fig. 3 while the identical structure appears after rotation of $R^{+\Omega}$ with respect the $x$ axis. It means [10]
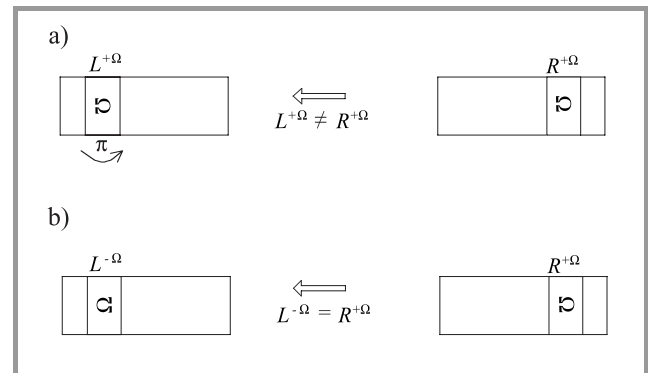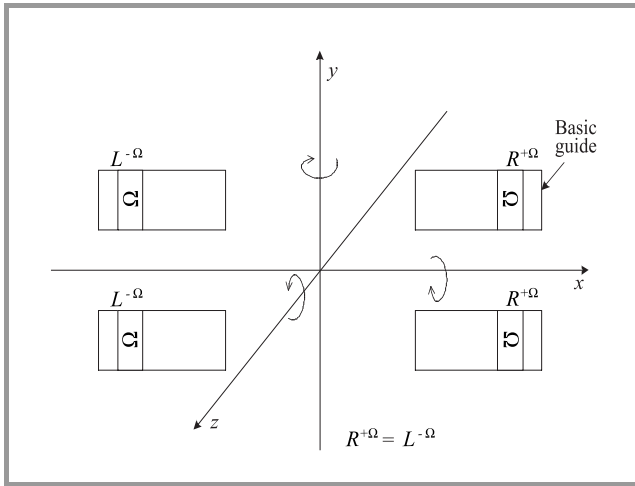


**Fig. 2.** Examples of pseudochiral guides after symmetrical displacement of the $\Omega$ slab in the basis structure.

**Fig. 3.** Complementary guides arising from rotation of the basis structure by $\pi$ about any axis of the rectangular coordinate system.

that the considered pseudochiral guide has symmetry with respect to the rotation by $\pi$ about any $x$, $y$, $z$ axis.

To discuss the influence of the reversing of $\Omega$ slab on the guide propagation properties we have displayed in Fig. 4 dispersion characteristics of the dominant mode, TE mode calculated from Eq. (2) against the change of $\kappa$ sign. One of the most important features shown in Fig. 4 is that the difference between the characteristics depends only on parameter $\kappa$. The variation of the dominant mode cutoff frequency with $\kappa$ parameter is shown in Fig. 5 for different localizations of the pseudochiral sample in the guide cross-section. As one can see, the cutoff frequency of the dominant mode varies with the displacement of the pseudochiral slab. However if the slab reaches the symmetrical position
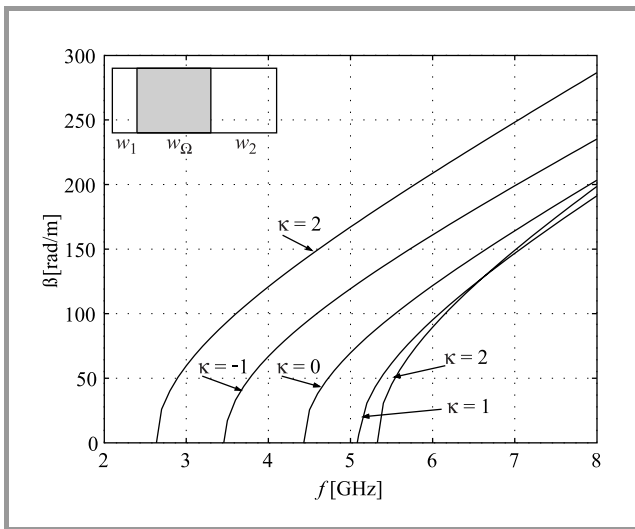


**Fig. 4.** Dispersion characteristics of the dominant mode in the pseudochiral waveguide shown in Fig. 1. Rectangular waveguide is WR-90. Dimensions in millimeters are, $w_1 = 2$, $w_\Omega = 10$, $w_2 = 10.86$, $\Omega$ slab; $\varepsilon = 2$, $\varepsilon_y = 2.5$, $\mu = 1$, $\mu_z = 1.5$, $\kappa$ is a parameter.

with respect to first one and the slab is reversed then the cutoff frequencies in the both cases are equal. It confirms the predicted symmetry properties of such $\Omega$ guide. Finally, Fig. 6 shows the power density distribution of dominant mode in the cross-section of the guide with symmet-
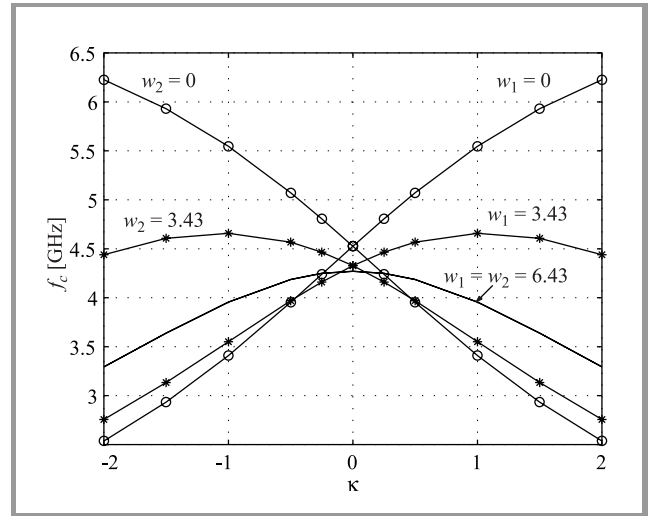


**Fig. 5.** Cutoff frequency characteristics of the dominant mode in the $\Omega$ guide shown in Fig. 1a. Parameters follow from Fig. 4.
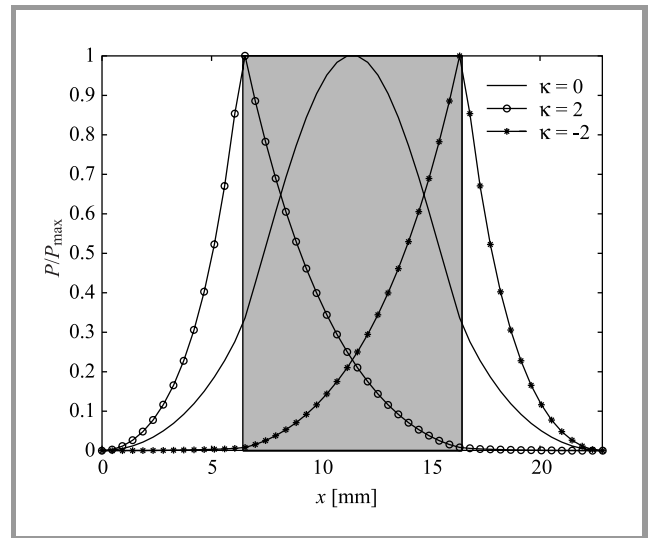


**Fig. 6.** The change of $n$ power density distribution of dominant mode in the symmetrical $\Omega$ guide with respect to the sign of $\kappa$. The guide dimensions and parameters of the $\Omega$ slab are as in Fig. 4.

rical localization of the pseudochiral slab. Note that the field displacement phenomenon can be observed when the pseudochirality is introduced. The intensity of the effect becomes greater due to a greater value of the $\kappa$ parameter. The field energy is concentrated at the one or the other side of the slab in depending on the sign of $\kappa$. This phenomenon can be recognized as an effect complementary to this one appearing in the ferrite guide when the magneti-

zation direction is reversed. However, in contrary to the ferrite structure the field distribution in the pseudochiral guide does not depend on the propagation direction.

## 4. Conclusion

We have examined a rectangular guides with a slab of pseudochiral Ω medium. Several unique and notable features associated with the considered structure were presented. It has been shown that the $TE_0$ wave can propagate in the guide as a dominant mode. The significant influence of the pseudochiral medium on the propagation characteristics and field distribution in the guide was observed. It has been shown that in such structure the field displacement phenomenon occurs. This effect depends on the coupling parameter $\kappa$. The direction of the field displacement is changed when the Ω slab in the guide is reversed. The similar phenomenon appearing in the ferrite guide depends on the magnetization or propagation directions. However, contrary to the ferrite structure the field displacement phenomenon in the pseudochiral guide is reciprocal. Future studies will focus on examination of scattering characteristics of the Ω guides to determine their prospective application.

## References

[1] N. Engheta and M. M. Saadoun, "Novel pseudochiral or Ω-medium and its applications", in *Proc. PIERS'91*, Cambrige, MA, July 1991, p. 339.

[2] M. M. Saadoun and N. Engheta, "A reciprocal phase shifter using novel pseudochiral or Ω-medium", *Microw. Opt. Technol. Lett.*, vol. 5, pp. 184–188, 1992.

[3] J. Mazur and D. Pietrzak, "Field displacement phenomenon in a rectangular waveguide containing a thin plate of an Ω-medium", *IEEE Microw. Guid. Wave Lett.*, vol. 6, pp. 34–36, 1996.

[4] J. Mazur and J. Michalski, "Pseudochiral omega medium in rectangular waveguides", in *7th Int. Conf. Compl. Media, Bianisotropic'98*.

[5] A. L. Topa, C. R. Paiva, and A. M. Barbosa, "Full-wave analysis of a nonradiative dielectric waveguide with a pseudochiral Ω slab", will be published in *Trans. MTT*.

[6] S. Tretyakov and A. Sochava, "Proposed composite material for non-reflecting shields and antenna radomes", *Electron. Lett.*, vol. 29, pp. 1048–1049, 1993.

[7] M. Norgren and S. He, "Reconstruction of the constitutive parameters for an Ω material in a rectangular waveguide", *IEEE Trans. Microw. Theory Techn.*, vol. 43, pp. 1315–1321, 1995.

[8] F. E. Gardiol, "Propagation in rectangular waveguides loaded with slabs of anisotropic materials", Universite Catholique de Louvain, 1969.

[9] M. Hines, "Reciprocal and nonreciprocal model of propagation in ferrite strip line and microstrip devices", *IEEE Trans.*, vol. MTT-19, no. 5, pp. 442–451, 1971.

[10] M. Mrozowski, *Guided Electromagnetic Waves – Properties and Analysis*. Tauton, Somerset: England Research Studies Press, 1997.
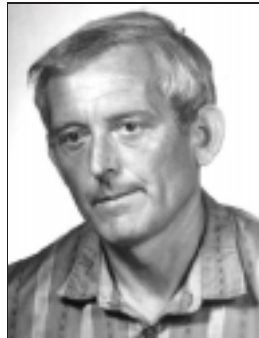
**Jerzy Mazur** was born in Brno, Czechoslovakia, on March 23, 1946. He graduated from the Technical University of Gdańsk (TUG), Poland, in 1969. He received the Ph.D. and habilitation degrees in electrical communication engineering from TUG in 1976 and 1983, respectively where he is currently a Full Professor. Since 1992, he has been also a consultant at Research Telecommunication Institute, Gdańsk, Poland. His research interests are concerned with electromagnetic field theory and integrated circuits for microwave and millimeter-wave applications.
e-mail: jem@pg.gda.pl
Faculty of Electronics, Telecommunication
and Informatics (ETI)
Technical University of Gdańsk
Narutowicza st 11/12
80-952 Gdańsk, Poland

**Krzysztof Dorko** was born in Łomża, Poland, on September 5, 1972. He received the M.Sc.E.E. degree from the Technical University of Gdańsk (TUG), Poland, in 1997. He is currently pursuing a Ph.D. degree in TUG, Poland. His research interests are in wave propagation in complex materials and nonreciprocal planar microwave devices.
Faculty of Electronics, Telecommunication
and Informatics (ETI)
Technical University of Gdańsk
Narutowicza st 11/12
80-952 Gdańsk, Poland

# Recognition of narrowband radio signals using autoregressive models and pattern comparison approach

Jerzy Łopatka

**Abstract** — **This paper presents an improved spectral recognition method for digitally modulated radio signals. It is based on a signal autoregressive (AR) model. Model poles are used as signal features for neural network based on recognition process. To reduce an influence of the signal noise and distortions introduced by the digital receiver, a nonlinear $Z$ plane transformation is proposed.**

*Keywords* — *signal models, modulation recognition.*

## 1. Introduction

Automatic radio signal recognition and classification is an essential problem in adaptive radio links, radio monitoring and electromagnetic compatibility analysis. Many authors focused on this problem during last years, but usually they take a lot of simplifying assumptions. They assume that the center frequency is known [8], data rate is given [3], perfect bit synchronization is performed [3] or data stream is known [1]. Unfortunately, in real system these assumptions are invalid.

In this paper, we propose an asynchronous approach, i.e., we assume that there is no a priori knowledge about signal parameters. The proposed method enables fast and reliable recognition of signals with unknown parameters. It is based on spectral analysis, but the number of parameters for signal description is minimized to reduce computational effort and memory requirements. For this purpose, a parametric model of the signal is used. It is an adaptive filter described by a set of parameters corresponding to the analyzed signal. To achieve a precise description of the signal, both model parameters, order and structure should be selected properly according to the structure of the signal under consideration. For narrowband radio signals, AR models can be used because AR spectral estimates have sharp peaks that correspond with carriers in radio signals. The AR method is computationally effective and has high spectral resolution for short data sequences. To achieve precise carrier frequency estimation and to avoid spectral peaks splitting, the LS method [9] has been chosen.

## 2. Selection of parameters used for signal recognition

To use model parameters in the recognition process, they must be complete and distinctive, i.e., contain the main part of information concerning the signal and enable signal recognition. The parameters should be also resistant to radio signal distortions and frequency offset caused by inaccurate receiver tuning or the Doppler shift. Algebraic relations between parameters of the original signal and distorted or shifted one should be easy to determine, the shift should be easy to calculate and some simple transformations should enable correcting the shift.

Adaptive AR filter, being a signal model, is usually described by its transfer function parameters, reflection coefficients (for lattice structure) or poles layout:

$$H(z) = \frac{1}{b_1 z^{-n} + .. + b_{n-1} z + b_n} = \frac{A}{\prod\limits_{k=1}^{n} \left(1 - d_k z^{-1}\right)}, \quad (1)$$

where: $b_i$ – filter parameters, $d_k$ – filter poles, $A$ – constant.

In previous works [7] it was proved that the values of transfer function parameters $b_i$ depend strongly on the signal frequency, initial phase and frequency shift. The distances between these parameters for uncorrelated realizations of the same signal are so large, that recognition on their basis is impossible. Dissipation of reflection coefficients for the lattice structure is much smaller, but relations between coefficients change in the case of the frequency shift. These parameters cannot be used for radio signals recognition either. As an alternative it is possible to use the poles $d_k$ layout. This enables control and correction of the filter stability. If any of poles is outside the unit circle, it can be simply reflected inside to correct the problem [5]. In the case of the frequency shift, the poles are simply rotated on the **Z** plane. The phases of all poles are changed by the same value, whereas the poles magnitudes remain unchanged [7]. This enables simple correction of poles' locations to eliminate the frequency shift.

## 3. Model order selection

Some standard methods can be used to select the AR model order [5], but these methods are inaccurate. If the model order is underestimated, some part of information may be lost. In the case of overestimation, additional, false spectral peaks may occur in the spectral estimate. One or two additional poles may cause a considerable change of the spectral estimate. Moreover, the radio signals change continuously and it would be necessary to estimate the model order after each realization.

**Fig. 1.** FSK signal spectrum estimate and poles location for AR model of order 8.



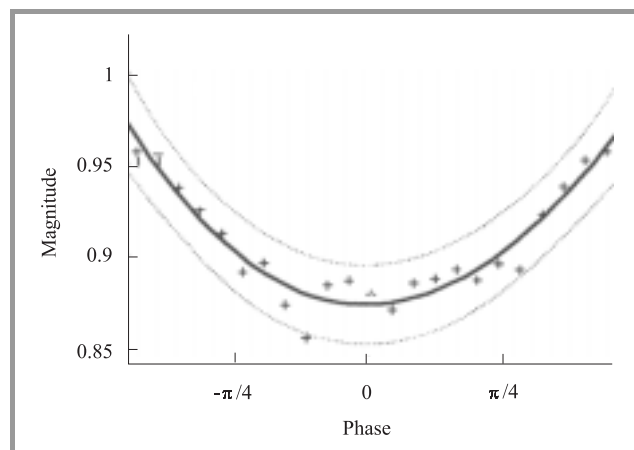**Fig. 2.** Location of poles for narrowband noise and interpolating polynomial.

tion is invalid, because they realize complex processing of the signal. They use digital downconversion, decimation and lowpass filtration. To provide good selectivity they also use an oversampling, equal minimum 1.7 for the 3 dB output bandwidth [2]. This causes the channel noise to become a narrowband noise, and magnitudes of "noise" poles depend on their phases (Fig. 2). To compensate the filtration problem, the average magnitudes of poles versus their phases were calculated and interpolated using the 4th order polynomial. The calculated values of the polynomial for phase values $[-\pi; \pi>$ were used to create a normalized correction table $C(\varphi)$. Its maximum value equals 1. The calculated magnitudes of poles are multiplied by correction coefficients from this table:

$$\left|\tilde{d}_k\right| = C\left(arg\left(d_k\right)\right) \left|d_k\right|. \qquad (2)$$

This correction gives approximately the same magnitudes for all "noise" poles.

## 5. Poles location transformation

The model poles can be divided into "signal" and "noise" poles. The "signal" poles are located on or near to the unit circle and have low dissipation for successive realizations of the signal. It is an important advantage from recognition point of view. The "noise" poles located along the unit circle but nearer its center have much larger dissipation. They depend on the noise components which are not very important. Moreover, the influence of poles on the signal spectral estimate becomes lower for larger distance from the unit circle. Thus the influence of "noise" poles on final spectrum is lower then "signal" poles. Because pattern recognition consists in calculation of distances between stored patterns and the received one, distances between all corresponding poles should be taken into consideration. From this point of view, "noise" poles have too high weight. Distances between them should be smaller to decrease their dissipation and decrease their influence on the final decision. It can be

On the other hand, radio signals are usually noisy because of influence of the radio channel, so the received signal consists of determined components and the noisy background. After a number of tests, an overestimated, the constant model order equal 8 was selected. Usually 1, 2 or 3 "signal" poles with magnitudes near to 1 correspond to the analyzed signal, whereas the several additional "noise" poles (lying near to the circle centre) create a quite good model of the noisy, spectrally flat environment of the useful signal (Fig. 1).

## 4. Correction of the receiver distortions

According to the previous works [4], the noisy environment may be modeled by equally spaced poles located along the unit circle. It means that poles magnitudes should be approximately equal to each other and should not depend on the pole phase. In real digital radio receivers this assump-
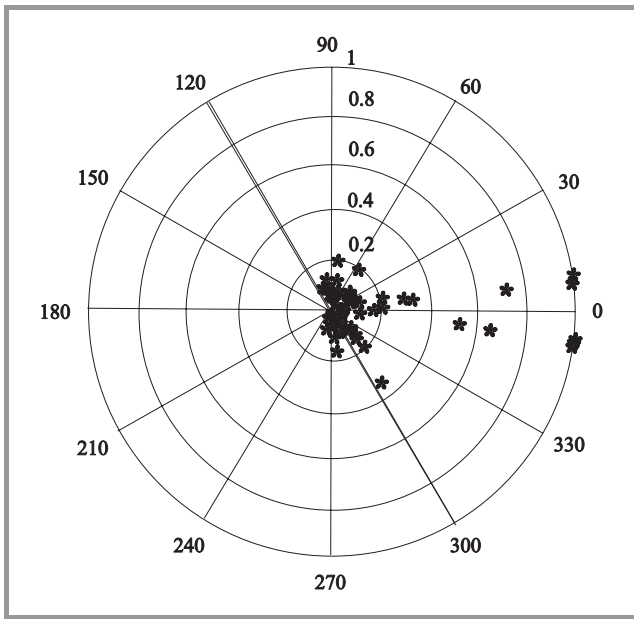
**Fig. 3.** FSK signal poles after compensation of narrowband noise and transformation.

done by shifting them towards the **Z** plane origin, without changing their phases:

$$|\hat{d}_k| = \frac{|\tilde{d}_k|}{1 - |\tilde{d}_k|} \left[ \max \left( \frac{|\tilde{d}|}{1 - |\tilde{d}|} \right) \right]^{-1}. \tag{3}$$

After transformation, the filter poles are shifted towards the **Z** plane origin according to the distance of each pole from the unit circle and from another side this decreases the distance between "noise" poles and increases the distance between "signal" and "noise" poles (Fig. 3).

## 6. Pattern recognition

Determination of distances between received and stored patterns is the next step of the recognition process. The minimum distance indicates the type of the received signal. Its value is a confidence rate defined as:

$$D = min \left( \sum_{j=1}^{w} \sum_{i=1}^{k} |\hat{d}_j - d_i|^2 \right), \tag{4}$$

where: $p$ – number of poles, $w$ – number of classes, $\hat{d}_j$ – received pattern poles, $d_j$ – stored pattern poles.

Distances should be calculated between corresponding poles. It is a nontrivial problem if the errors of receiver tuning occur. To diminish these errors, a 3-step preprocessor is proposed. First the preprocessor performs a shift procedure:

$$d'_k = Re(d_k) - Re(d_{med}) + j(Im(d_k) - Im(d_{med})), \tag{5}$$

where: $d_{med}$ – the gravity center of the pattern. This operation eliminates errors of overlaying of the stored and

received patterns. The second and the third step is scaling and rotation:

$$d''_k = \frac{d'_k}{Ke^{j\Phi}}, \tag{6}$$

where: $K$ – scaling factor, $\Phi$ – rotation factor.

$$K = \frac{1}{p} \left( \sum_{i=1}^{p} |d'_j| \right); \quad \Phi = arg(d_{med}). \tag{7}$$

Scaling factor $K$ corrects changes of the pattern size, that can be caused e.g. by changes of the SNR. Rotation eliminates the frequency shift.

## 7. Efficiency analysis

To check the efficiency of the proposed method some measurements were made. Selected digitally modulated signals: 2FSK, 2PSK, 4PSK, 8PSK and 16QAM with known S/N ratios, data rates and deviation (for FSK) were recorded using a digital receiver. The signals were divided into short, 40 sample segments and for each segment the layout of its poles was calculated. On the basis of the transformed poles pattern on the **Z** plane, neural network training for pattern recognition was performed. The network consisted of 2 layers and 60 neurons with the log-sigmoid transfer function. It was trained using the back propagation learning algorithm. The training set consisted of 20 records for each type of the signal, with SNR varying from 0 dB to 20 dB. The achieved results are shown in Fig. 4.
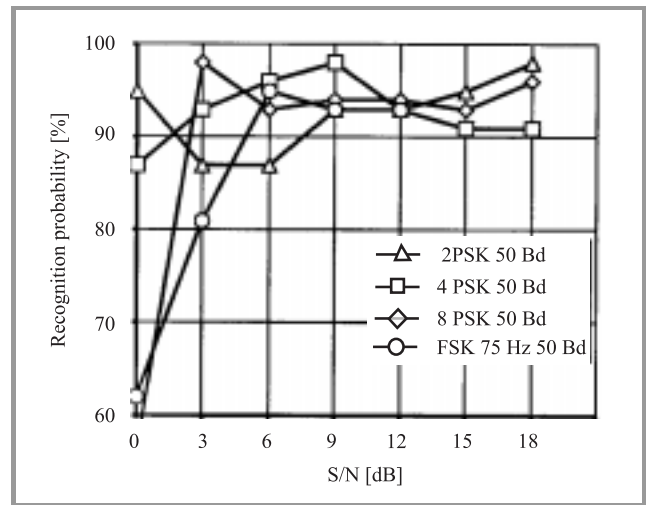


**Fig. 4.** Percentage efficiency of signal recognition versus S/N ratio for: 2, 4, 8 PSK 50 Bd and FSK 50 Bd with frequency shift 75 Hz.

The computational effort for proposed method is a sum of computations for AR parameters estimation $C_{AR}$ [9], necessary corrections $C_C$ and neural network operation $C_N$:

$$\begin{aligned} C = C_{AR} + C_C + C_N = (MN + 6M^2) + \\ + 17M + (2MF + 2F + 2FS + 2S), \end{aligned} \tag{8}$$

where: $N$ – length of signal record, $M$ – order of the model, $F$, $S$ – number of neurons in the first and the second layer.

For values of parameters used in the simulation, a single recognition calculation required less than 2000 operations that makes the method suitable for real time applications.

# 8. Conclusions

The autoregressive models with neural networks can be used for recognition of the digital radio signals. The description of each signal is very concise. The method is useful for discrimination signals with different spectral shapes. It performs well for SNR better than 3 dB. Identification of signals with similar spectral shapes or different data rates can be performed in the next stage using additional distinctive features. This method may be also implemented as the initial step of selection in intelligent multipurpose demodulators and radio monitoring systems.

# References

[1] B. Dongming, Z. Gengxin, and Y. Xinying, "A maximum likelihood based carrier frequency estimation algorithm", in *Conf. ICSP*, Beijing, China, 2000.

[2] *HSP 50214 Programmable Downconverter*. Harris Corporation, 1998.

[3] P. Hua, G. Lindong, and L. Zhongxin, "Non-decision-aided carrier frequency estimator for digital radio", in *Conf. ICSP*, Beijing, China, 2000.

[4] S. Kay, "The effects of noise on the autoregressive spectral estimator", *IEEE Trans. ASSP*, no. 27, pp. 478–485, 1979.

[5] S. B. Kesler, *Modern Spectrum Analysis II*. New York: IEEE Press, 1986.

[6] I. Kollar, *Frequency Domain Identification Toolbox for use with MAT-LAB*. The MathWorks, 1994.

[7] J. Lopatka, "A use of spectral analysis for radio-signals recognition", in *II Conf. Signal Proc.*, Liptovski Mikulas, 1994.

[8] M. Luise and R. Reggiannini, "Carrier frequency recovery in all-digital modems for burst-mode transmissions", *IEEE Trans. Commun.*, vol. 43, no. 2/3/4, pp. 1169-1178, 1995.

[9] L. Marple, *Modern Spectrum Estimation*. Prentice-Hall, 1988.

**Jerzy Łopatka** received the M.Sc. and Ph.D. degrees in communications from the Military University of Technology (MUT), Warsaw. At present he is a Head of Radio and Electronic Warfare Section in the Communication Systems Institute (MUT). His main research interests include digital signal processing in wireless systems.
e-mail: jlopatka@wel.wat.waw.pl
Communication Systems Institute
Military University of Technology
Kaliskiego st 2
00-908 Warsaw, Poland

# Optical gain in one-dimensional photonic band gap structures with *n-i-p-i* crystal layers

Igor S. Nefedov, Victor N. Gusyatnikov, Marian Marciniak, Valerii K. Kononenko, and Dmitrii V. Ushakov

**Abstract** — The gain enhancement in a layered periodic photonic band gap structure containing active medium based on GaAs *n-i-p-i* superlattices separated by AlGaAs layers is analyzed. The dependences of extinction coefficient and refractive index on excitation level and wavelength are presented. Transmission characteristics of a probe light versus excitation level are calculated. It is shown that the threshold of generation can be essentially reduced if the wavelength of probe light falls to the band gap edge.

**Keywords** — *photonic crystal, doping superlattice, optical gain, tunable source.*

## 1. Introduction

The interest in multilayer periodic structures forming a photonic band gap (PBG) is increasing because of their attractive application for controllable optical switches and other various nonlinear optical devices [1, 2]. All nonlinear phenomena are enhanced at the PBG edge due to strong delay of the energy velocity and electric field concentration within certain areas of PBG structures. Besides, the optical gain can be enhanced at the band edge in one-dimensional (1D) PBG structures due to the same reasons [3].
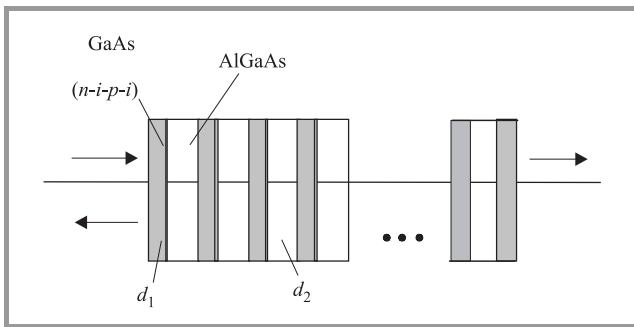


**Fig. 1.** 1D PBG structure with the GaAs *n-i-p-i* crystal layers.

In the present work, the possibilities to use of *n-i-p-i* superlattices as optically controllable active layers in PBG structures are investigated. We consider such a photonic structure in the GaAs-AlGaAs system where the absorption layers with optical controllable parameters are the GaAs *n-i-p-i* crystal layers (see Fig. 1). In certain spectral range the absorption in *n-i-p-i* layers disappears and the light amplification occurs. The gain coefficient in *n-i-p-i* layers depends on the wavelength and the difference in the quasi-

Fermi levels $\Delta F$. The model, where a pump, which can be electrical or optical, excites uniformly all active layers, is considered. Light transmission characteristics versus $\Delta F$, which is assumed to be the same all over the active layers, are calculated. As shown, the described photonic structures with the *n-i-p-i* layers are attractive to make narrow-band tunable radiation sources.

## 2. Dispersion characteristics of *n-i-p-i* layers

We consider the optical properties of the GaAs-AlGaAs photonic structures where the absorption layers are the GaAs *n-i-p-i* crystal layers (Fig. 1). In particular, the active *n-i-p-i* layers can be in the form of $\delta$-doped semiconductor superlattices. In this case, the donor and acceptor concentrations are assumed to be $N_a = N_d = 10^{20}$ cm$^{-3}$, width of doped *n*- and *p*-type regions $d_n = d_p = 1$ nm, thickness of *i*-layers $d_i = 8$ nm. Under optical excitation, the concentration of charge carriers in the *n-i-p-i* layers increases. Therewith, the difference in the quasi-Fermi levels $\Delta F$ grows and conditions of radiation absorption and refraction change as well.

Dispersion characteristics of the *n-i-p-i* layers are shown in Fig. 2. Dependencies of the extinction coefficient $\kappa$ and change in the refractive index $\Delta n$ at different wavelengths $\lambda$ on the excitation level $\Delta F$ have been calculated according to the Kramers-Krönig relation taking into account the transformation of the potential relief of the doping superlattice under optical or electric excitation. Effects of the density state tails, screening of the impurity electrostatic potential, and shrinkage of the energy band gap are included too [4, 5]. The quantizied change in the refractive index $\Delta n$ is related to the filling of the subband levels by current carriers at the excitation of the layers. At definite values of $\Delta F$, the extinction coefficient $\kappa$ becomes negative, i.e., light amplification occurs in the certain interval of wavelengths. Here, the normalized parameter $\kappa_0(\lambda)$ is the initial extinction coefficient at the thermodynamic equilibrium ($\Delta F = 0$). The index of refraction of the *n-i-p-i* layers is estimated as a sum of the quantity $\Delta n$ and the value of the refractive index for the GaAs host material.

To find connection between $\Delta F$ and the exciting radiation power $P$ in the layers under uniform optical excitation of the structure, the following approach is used. It is assumed

a)



b)
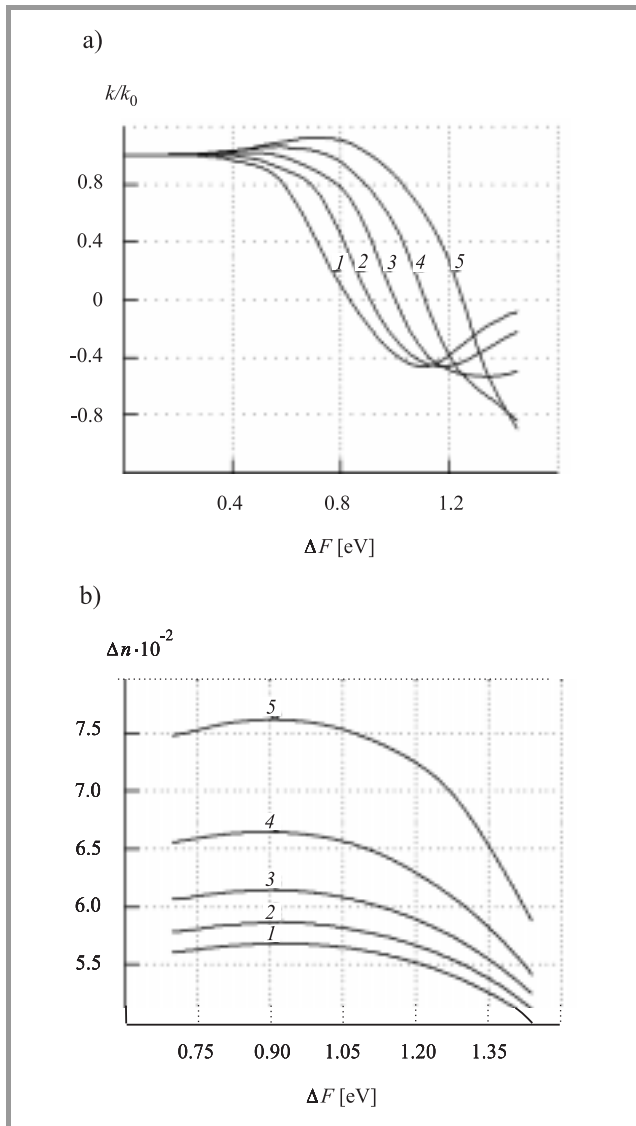


**Fig. 2.** Dependencies (a) of the extinction coefficient $\kappa$ and (b) quantizied refractive index $\Delta n$ at different wavelengths $\lambda$ on the excitation level $\Delta F$. $1 - \kappa_0 = 9.50 \cdot 10^{-6}$, $\lambda = 1500$ nm, $2 - \kappa_0 = 3.70 \cdot 10^{-5}$, $\lambda = 1375$ nm, $3 - \kappa_0 = 1.68 \cdot 10^{-4}$, $\lambda = 1250$ nm, $4 - \kappa_0 = 8.71 \cdot 10^{-4}$, $\lambda = 1125$ nm, $5 - \kappa_0 = 4.60 \cdot 10^{-3}$, $\lambda = 1000$ nm.

that the quantum yield at the excitation of the controllable layers in the 1D PBG structure equals 1, i.e., every absorbed quantum produces one electron-hole pair. Concentrations of non-equilibrium carriers are found from the stationary continuity equation that determines the simple relation between the excitation level $\Delta F$ and the generation rate at the absorption of excitation quantum. The rate of the carrier generation per unit volume in a definite *n-i-p-i* layer is equal to $kP/h\nu_{exc}$, where $k$ is the absorption coefficient and $h\nu_{exc}$ is the energy of excitation quantum. The spectrum of absorption $k(\lambda)$ is connected with the spectrum of the extinction coefficient as $k = 4\pi\kappa/\lambda$.

The increase of the two-dimensional concentration of electrons $n$ versus the difference in the quasi-Fermi levels $\Delta F$ is

a)



b)
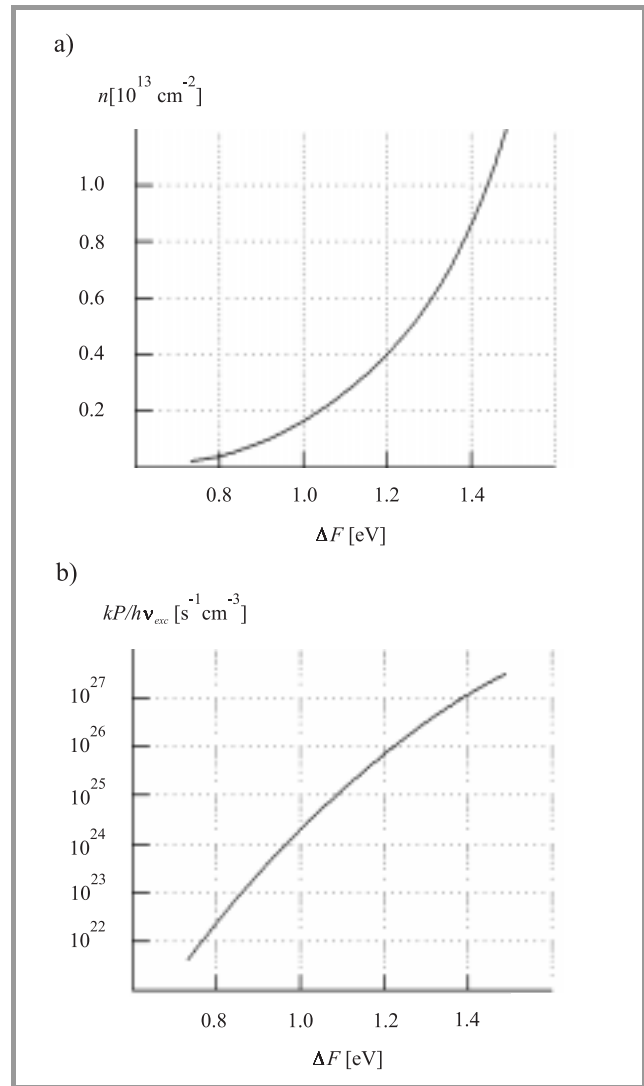


**Fig. 3.** Dependencies (a) of the electron concentration $n$ and (b) rate of excitation $kP/h\nu_{exc}$ on the quasi-Fermi level difference $\Delta F$ in the *n-i-p-i* layers of the photonic structure.

shown in Fig. 3a. Using the dependence $n(\Delta F)$, from the relation between $kP/h\nu_{exc}$ and $\Delta F$, which is given in Fig. 3b, one can evaluate the effective life-time of carriers at the radiative recombination. For the *n-i-p-i* structure examined, values of the effective life-time of carriers cover a wide range from 1 ms at a low-intensity excitation to10 ns at the high excitation levels.

## 3. Gain in the PBG structure

The spectral range where the absorption coefficient in *n-i-p-i* layers is negative at the high excitation levels can be seen in Fig. 2a. The 40-period structure, whose parameters are taken in such a way as the PBG edge falls within the region of maximal gain, was considered. Thicknesses of GaAs and $Al_{0.3}Ga_{0.7}As$ layers are $d_1 = 64.5$ nm and $d_2 = 72.9$ nm, respectively.

Igor S. Nefedov, Victor N. Gusyatnikov, Marian Marciniak, Valerii K. Kononenko, and Dmitrii V. Ushakov

The transmission characteristics in a suitable spectral range are presented in Fig. 4, where $T$ is the amplitude transmission coefficient. The maxima of transmission peaks correspond to the band edges, both of them are within the region of negative absorption coefficients. Thus, the PBG structure with the active *n-i-p-i* layers allows considerably to
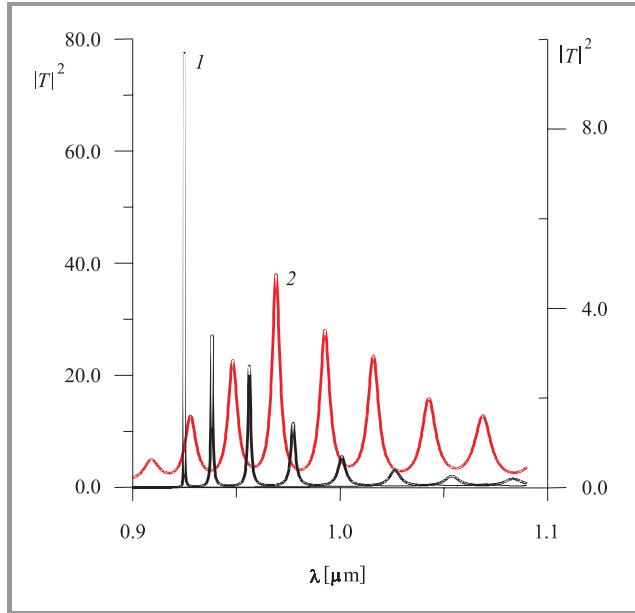


***Fig. 4.*** Transmission coefficient $|T|^2$ versus the wavelength $\lambda$ for the 40-period structure (curve 1, left $Y$-axis) and for the 1-period structure (curve 2, right $Y$-axis), having the same optical thickness, at $\Delta F = 1.348$ eV.



***Fig. 5.*** Surfaces of the transmission coefficient $|T|^2$ versus the wavelength $\lambda$ in microns and difference in the quasi-Fermi levels $\Delta F$ for (a) the 40-period and (b) 1-period structures of the same optical thickness.

enhance the light amplification and to reduce the necessary level of excitation.

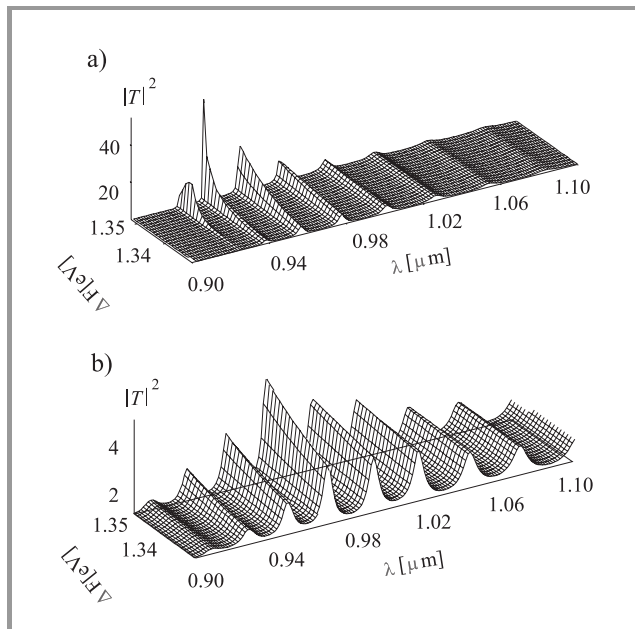Next two-dimensional surfaces of the transmission $|T|^2$ versus the difference in the quasi-Fermi levels $\Delta F$ and the wavelength $\lambda$ are presented for the 40-period (Fig. 5a) and for the 1-period (Fig. 5b) structures. (One-period structure has the 2582 nm GaAs *n-i-p-i* layer and the 2916 nm $Al_{0.3}Ga_{0.7}As$ layer). One can see that the gain is achieved for the 40-period structure exceeds in an order the gain in 1-period structure having the same optical length of active medium. If the excitation level $\Delta F = 1.348$ eV, that corresponds to the peak of transmission $|T|^2 = 5$ for the 1-period structure (Fig. 4), we obtain $|T|^2 \approx 80$ for the 40-period structure at the wavelengths corresponding to the band edges. The gain starts to rise markedly from some a threshold level of excitation. This threshold level for the 1-period structure significantly exceeds the respective values for the 40-period structure.

## 4. Discussion

Thus, the results obtained show that 1D PBG structure with the active *n-i-p-i* layers can be promising for creating miniaturized light sources. The main advantage of the resonator with active medium embedded into periodic multilayer is caused by strong delay of the energy velocity in comparison with the energy velocity in a bulk material or in DFB structure with a slight index modulation [6]. Comparison with one-period structure shows that application of the multiperiod structure allows to reduce the resonator length where threshold of generation can be achieved at the same parameters of active medium and the excitation level. Thus, a laser used the resonator considered can be alternative to the DFB laser whose fabrication is too complicated, quite expensive and low-reproducible.

## Acknowledgement

## References

[1] M. Scalora, J. P. Dowling, C. M. Bowden, and M. J. Bloemer, "Optical limiting and switching of ultrashort pulses in nonlinear photonic band gap materials", *Phys. Rev. Lett.*, vol. 73, pp. 1368–1371, 1994.

[2] I. S. Nefedov and V. N. Gusyatnikov, "Optically controlled GaAs-GaAlAs photonic band gap structure", *J. Opt. A*, no. 2, pp. 344–347, 2000.

[3] J. P. Dowling, M. Scalora, M. J. Bloemer, and C. M. Bowden, "The photonic band edge laser: a new approach to gain enhancement", *J. Appl. Physt.*, vol. 75, pp. 1896–1994, 1994.

[4] V. K. Kononenko, I. S. Manak, and D. V, Ushakov, "Optoelectronic properties and characteristics of doping superlattices", *Proc. SPIE*, vol. 3580, pp. 10–27, 1998.

[5] V. K. Kononenko and D. V. Ushakov, "Carrier transport and screening in *n-i-p-i* crystals", *Phys. Stat. Sol. (B)*, vol. 211, pp. 743–749, 1999.

[6] J. E. A. Whiteaway, B. Garrett, G. H. B. Thompson, A. J. Collar, C. J. Admistead, and M. J. Fice, "The static and dynamic characteristics of single and multiple phase-shifted DFB laser structures", *IEEE J. Quant. Electron.*, vol. 28, pp. 1277–1293, 1992.

**Igor S. Nefedov** graduated from Saratov State University, Saratov, Russia in 1972 and received the M.Sc. degree in radio physics and electronics. He received the Ph.D. and Doctor of Science (habilitation) degrees in radio physics in 1981 and 1998, respectively. From 1981 to 1992 he was a researcher at the Research Institute of Mechanics and Physics, Saratov State University. From 1992 he is a Leading Researcher at the Institute of Radio Engineering and Electronics of Russian Academy of Sciences, Saratov, Russia. In 2001–2002 I. Nefedov is a Visiting Professor of Radiolaboratory at Helsinki University of Technology. His research interests are in area of electrodynamics of anisotropic and gyrotropic media and photonic band gap structures as well as optical switching. He has published about 100 scientific papers.
Institute of Radioengineering and Electronics, RAS
Saratov Department
Zelyonaya st 38
410019 Saratov, Russia

**Victor N. Gusyatnikov** graduated from Saratov State University, Saratov, Russia, in 1977 and received the M.Sc. degree in semiconductor physics. He received the Ph.D. degree in semiconductor physics from the Nizhni Novgorod State University, Nizhni Novgorod, Russia. From 1993 to 1998 he was a manager of laboratory of physics of semiconductors at the Research Institute of Mechanics and Physics, Saratov State University. Now, he is a senior lecturer at the Saratov State Social and Economic University. His research interests are electronic processes in semiconductor structures in strong electrical and electromagnetic fields, optical, photoelectric, kinetic properties of classical semiconductor superlattices, theory of photonic band gap structures, computing and scientific programming. He has published more than 50 papers. Dr. Gusyatnikov is a Soros Associate Professor (2001).
Institute of Radioengineering and Electronics, RAS
Saratov Department
Zelyonaya st 38
410019 Saratov, Russia

**Marian Marciniak** Associate Professor has been graduated in physics from Marie-Curie Sklodovska University in Lublin, Poland, in 1977. From 1985 to 1989 he performed Ph.D. studies in electromagnetic wave theory at the Institute of Fundamental Technological Research, Polish Academy of Sciences, followed by Ph.D. degree (with distinction) in optoelectronics received from Military University of Technology in Warsaw. In 1997 he received his Doctor of Science (habilitation) degree in optics from Warsaw University of Technology. From 1978 to 1997 he held an academic position in the Military Academy of Telecommunications in Zegrze, Poland. In 1996 he joined the National Institute of Telecommunications in Warsaw where he actually leads the Department of Transmission and Fibre Technology. His research interests include photonics, terabit networks, IP over WDM networks, optical waveguide theory and numerical modelling, beam-propagation methods, and nonlinear optical phenomena. He is an author or co-author of over 160 scientific publications in those fields, including three books. He is an active member of the IEEE – Lasers & Electro-Optic Society, IEEE – Communications Society, New York Academy of Sciences, Optical Society of America, SPIE – The International Society for Optical Engineering and its Technical Group on Optical Networks, and American Association for the Advancement of Science. He was the originator of accession of Poland to European Research Programs in the optical telecommunications domain: COST 240 *Modelling and Measuring of Advanced Photonic Telecommunication Components*, COST 266 *Advanced Infrastructure for Photonic Networks*, COST 268 *Wavelength-Scale Photonic Components for Telecommunications*, and COST P2 *Applications of Nonlinear Optical Phenomena*. He has been appointed to Management Committees of all those Projects as the Delegate of Poland. He has been appointed as the Evaluator of the European Union's 5th Framework Program proposals in the Action Line *All-Optical and Terabit Networks*. He is a Delegate to the International Telecommunication Union, Study Group 15: *Optical and Other Transport Networks*, and to the International Electrotechnical Commission, Technical Committee 86 *Fibre Optics* and its sub-Committees. He served as a Delegate to the *World Telecommunication Standards Assembly* WTSA 2000. He is the originator and the Chairman of the Topical Commission on *Fibre Technology* of the National Committee for Standardisation. In early 2001 he originated the IEEE/LEOS Poland Chapter and actually he serves as the Interim Chairman of that Chapter. He participates in Program Committees of several international conferences, and he is a reviewer for several international scientific journals. In addition to that, he serves as a Member of the Editorial Board of *Microwave & Optoelectronics Technology Letters* journal, Wiley, USA,

and the *Journal of Telecommunications and Information Technology*, National Institute of Telecommunications, Poland. He was the originator and the organiser of the 1st, 2nd and 3rd *International Conferences on Transparent Optical Networks ICTON'99*, 2000, and 2001. Recently he has been appointed by the *World Scientific and Engineering Society* to act as the originator and Chairman of the *WSES International Conference on Wireless and Optical Communications* 2002. His biography has been cited in Marquis *Who's Who in the World*, *Who's Who in Science and Engineering*, and in the *International Directory of Distinguished Leadership* of the *American Biographical Institute.*
e-mail: M.Marciniak@itl.waw.pl
National Institute of Telecommunications
Szachowa st 1
04-894 Warsaw, Poland

of Sciences of Belarus, where he currently heads the Scientific Group at the Laboratory of Optics of Semiconductors. His present research interests concern nonlinear optical properties of low-dimensional systems including quantum-well lasers and wide-band gap semiconductor superlattices. He is the author of three books, holds five technical patents, and has published more than 110 journals articles and a number of reviews. Dr. Kononenko is a member of the SPIE, International Technical Working Groups on Optical Materials, Belarussian and European Physical Societies, and Polish Society of Sensor Engineering.
e-mail: lavik@dragon.bas-net.by
Stepanov Institute of Physics, NASB
220072 Minsk, Belarus

**Valerii K. Kononenko** graduated in radiophysics from the Byelorussian State University, Minsk, BSSR, in 1965. He received the Ph.D. degree in quantum electronics from the Institute of Physics, Academy of Sciences of the BSSR, in 1972, the D.Sc. degree in physics of semiconductors and dielectrics in 1992, and the academic status of Professor in physics in 1997. In 1965 he joined Stepanov Institute of Physics, National Academy

**Dmitrii V. Ushakov** received the M.Sc. and Ph.D. degrees in Radiophysics and Electronics Department of Belarussian State University, Minsk, Belarus. His research interests and experience include physics of semiconductor doping superlattices, hetero-*n-i-p-i* structures, quantum cascade lasers, and photonic band gap crystals. He has published more than 20 papers.
Stepanov Institute of Physics, NASB
220072 Minsk, Belarus

# New multimedia and telematic tools for asynchronous distance learning

Jolanta Chęć, Mariusz Pajer, and Bogdan A. Galwas

**Abstract** — **New tools of modern education, connected mainly with Internet, are described in the paper. Their characteristics, principles of application were discussed in succession. Evaluation trail of their usefulness was done. Possibilities of carrying on laboratory experiments and distance designing were described. Probe to foresee directions of further development of Internet tools in the educational process was done.**

*Keywords — Internet, open and distance learning, multimedia, compact disc, e-mail.*

## 1. Introduction

Education is a complex and multi-element process. The well-known, traditional tools used in education when there is a face-to-face contact between a lecturer and students, as in case of lectures, design and accounting classes and the laboratory training, still retain their big value. Similarly a book, a manual and a set of lectures have kept their high usefulness in the self-education process. However, the necessity of the development of the new techniques has become evident, together with the dissemination of education and the development of postgraduate continuing education. The techniques of open and distance learning, which facilitate work and education for participants, were originated this way.

The development of multimedia and teleinformatics techniques contributed to the creation of very useful didactic means for the educational and self-educational processes. The practice of the past few years shows that during training courses as well as postgraduate studies at first some educational tools are chosen, and then they are applied at appropriate level to achieve the best results. The process of education at both higher and postgraduate levels requires the new kinds of didactic means and their purposeful use. The multimedia and electronic techniques of the preparation of the new generations of the didactic materials will be discussed in succession and at the end they will be evaluated.

## 2. Electronic books

Books in the electronic format can be prepared on CD-ROMs or offered by the Internet. The electronic books are computerised versions of paper manuals with multimedia elements. They are provided with strong search and presentation tools and they contain a large amount of information. E-books can be based on the contents of traditional paper books and offer more possibilities than the text itself. They also involve various human senses in the educational process. The presentation of the material takes into account different techniques of message transfer. It is the acknowledgement of the thesis that data collected with the use of a computer are more useful. The learning process with the use of electronic books is more effective and more pleasant. Users have also the possibility to check their knowledge by the use of tests for self-control. In the case of wrong answers the users have a possibility to learn the appropriate material by the use of a given entry.

The multimedia reference products provide learners with the text information enabling to hear it and also see in motion. A large number of well-organised references enables the learners to study the material more thoroughly. Both experience and practice are also very important, especially in case of complex systems where the interoperation of various coefficients can be understood by the directly gained experience. Simulation programmes are very useful to gain such practical experience.

Electronic books may contain the following multimedia elements:

- text (fundamental text, dictionaries, helpful comments, notices);

- tables, graphs, illustrations, interactive maps, photos (coloured, panoramic);

- animations, films (video sequences);

- 3D objects, sound track (wordy commentary, music, special effects); electronic books, by the use of multimedia and search tools, enable interaction for students.

Information in electronic books can be arranged in the following ways:

- chronologically (according to the event sequence);

- thematically (after selection one of branches of thematic references its sub-themes are presented; after selecting one of sub-themes, references to it are presented; an entry text can be presented after clicking the mouse in such a sub-theme reference);

– text, music and images stored in database can be sorted.

Search of information in electronic books is very easy in comparison with paper books. Electronic books present a completed list of references, within a given thematic entry, into other entries connected with a given training material and supplementary information. These entries have usually the possibility to come back to previous entries. A graphical presentation of thematic links facilitates the learning process. Didactic material can also contain glossaries with the explanation of the terms used in the material.

Paper materials have some limitations as a medium for information transfer:

– description of reality is limited to words and static illustrations, photographs and graphs;

– they are passive (it is difficult to learn e.g. in case of learning a foreign language one cannot check pronunciation);

– feedback and interaction are weak.

The Internet is a very useful tool for education purposes. The didactic materials can be accessible in the real time (by using chat rooms, audio or video conferences, white boards) and in the asynchronous mode (news groups, discussion groups and forums, hyperlinks with other resources). The Internet also offers rich graphics, multimedia and hipermedia. File formats accessible through the Internet are as follows: graphic formats (GIF, JPEG, BMP, TIFF), audio formats (WAV, AU, MPEG, MIDI, MP3, RA), video formats (MOV, AVI, MPEG, MPEG-2), animations formats (GIF89a, Java, Shockwave, FLI and FLC), 3D formats (VRML). Multimedia programs can be created with the use of the following programming languages: C++, Pascal and Visual Basic. The content of CD-ROMs can be updated through the Internet by the use of the plug-in technique connected to the Internet browsers.

In distance learning an electronic book contains the didactic material in the form friendly to users. Such materials have the following advantages: a very high degree of interaction, a very quick search of information, rich presentation technologies (multimedia and simulation programs, a large capacity, a possibility of self-learning and self-evaluation). All these advantages facilitate the learning process considerably. The didactic materials can be accessible in the Internet with the use of the educational portal.

There are a lot of examples of electronic books. One was prepared in the National Institute of Telecommunications in Poland [7]. The electronic books in the *Academic Multimedia Books* series of Warsaw University of Technology (WUT) in Poland are similar in form to them. The books of the *Academic Multimedia Books* series constitute a basis for studies in the distance learning program model SPrINT, which is used at WUT. In the SPrINT model electronic books are provided on CDs and through the Web service using the Lotus Learning Space platform [10]. Experiences gathered in the field of using electronic books in distance learning at WUT shows it is useful for students to illustrate lectures with rich examples (for example solutions of tasks in the field of mathematics).

## 3. Simulations illustrating lectures

Lectures can be enriched by the use of simulations, which can be applied to real devices, physical phenomena, systems, etc., and which include an imitation, reproduction, and modelling. Particular aspects of systems or phenomena are imitated in simulations. The main purpose of a simulation is to give a user some assistance to understand the simulated systems and phenomena. The appropriate way of presentation is ensured by good multimedia simulations (simulations that use multimedia elements such as video sequences), sound track (voice, music), graphics (3D objects), etc. A good simulation contains many characteristics of a modelled phenomenon. Simulations may be used to foresee the results of phenomena. They are usually quite large so supercomputers have to be used for their realisation. Simulations are used to give a user some better knowledge of a modelled phenomenon. Simulation programs to serve complex relations of mutually dependent coefficients. Graphics, easy in use, is a key for the creation of attractive simulations. Music, sound effects, graphics and animations are elements used for the presentation of the actual state of a modelled phenomenon. Simulations have many common features but most of them are hidden (a user does not see them). The most visible element is the interface form, which results from the popularisation of software for the sake of simple users. Both the organisation and presentation of a large amount of information is important for the realisation of a simulation. Sound effects, graphics and animations add a multimedia background to dry, uninteresting formulae and equations.

There are different forms of simulation programs: from very simple ones without a user's engagement up to the complex ones, in which a user can actively participate by setting up variable parameters of a process and next observing the progress of a phenomenon.

Simulation programs have various degrees of complexity. At the basic level the complexity of a problem can be simplified or eliminated. At next levels when the complexity is higher and simulations are disseminated in large electronic books, the sizes of such books depend on the complexity and depth of simulation. Educational value of such material is often very high. Simulation programs develop the ability to solve problems, to take decisions and to deduct. The analysis of a current user's activity can be done with the use of an option that enables the repetition of a situation.

Good examples of simulations are included in the electronic book *Physics I* which has been published by WUT in the *Academic Multimedia Books* series. Simulations provided in that book were prepared in the MS Excel. The book includes forms which allow students to change parameters of simulations and graphs which illustrate the results.

Other good examples are Java applications and applets prepared by the FernUniversität (Hagen, Germany) for their students [8]. These simulations show e.g. the changes in time of the voltage and the intensity of current in a capacitor.

## 4. Distance laboratory

The experiments in a real student laboratory is an important component of the educational process at a higher level. At a first sight the educational process, based on the use of the Internet, makes it impossible to carry out laboratory experiments. The analysis of solutions used in the ODL systems shows that some interesting qualities were developed, which can replace traditional technique of preparation and carrying out laboratory experiments. Three basic techniques of carrying out the distance laboratory training have been distinguished:

- **Simulation of measurement results**, by the mathematical model of an experiment, is a simple solution. The development of the mathematical model of an experiment and the description of the system of equations are the starting point. The next step: the selection of the software, accessible for a student, that may give a solution of the system of equations for conditions assumed by the student. The use of the appropriate software for the presentation of calculation results in the form of characteristics and graphs is also very important.

- Another solution is to prepare an environment to **carry out real distance experiment**. The measurement system, controllable by a computer, should be prepared for measurements usually at a school laboratory. Student requests and conditions concerning the experiment are sent to the computer that controls the system by the use of the Internet. In succession the computer realises measurements, records the results, and sends them to students (using for example e-mail).

- In some cases there is a possibility to create **home laboratory** by a student, using his computer and a set of elements (laboratory kit) sent to him by the school. The kind of experiments in which student should show his own self-dependence is especially useful. Unfortunately, only a few experiments can be realised this way because the cost and complexity of many laboratories makes their realisation in home conditions impossible.

FernUniversität Hagen provide a remote laboratory for their students [9]. In these laboratory students can e.g. control and watch a mobile robot through the Web service. The Distributed European Lab prepared by the University Bordeaux 1, the Fachhochschule of Münster and the University of Madrid in the RETWINE (*RemoTe Worldwide Instrumentation Network*) project [11] supported by the European Community is very interesting. Students can make real remote experiments in the field of electrical engineering through the RETWINE with the use of the Java Applet which presents the full front panel of a remote instrument and provides the full control of experiment.

## 5. Distance designing

In the practice of engineering, the education leading to designing complex constructions, electronic circuits and informatics systems is a necessity. In such cases some complex software (ORCAD, AutoCAD, etc.) can be of assistance to a designer. A student's task is to get knowledge concerning work with this kind of software and learn about its possibilities.

Students studying in the asynchronous mode, far-away from the university centre, may have problems connected with getting appropriate knowledge because the software mentioned above is expensive and requires installation on a computer with high quality parameters (workstation), so it is impossible to install it on a personal computer.

There is a possibility of a student's distance work with software installed on the university server, by the use of the Internet. Although work in the on-line mode is not possible due to the limited capacity of links, a student may send appropriate instructions to the computer that serves the software and will receive after a short time, the results of the calculations. The time of waiting for a reply should not be greater than a few hours.

The problem of "distance designing" has no appropriate solution yet in the way that is appropriate for its standing in the educational process. In some cases it could be possible to make the professional software available to students in their computers during limited time of study (e.g. 3 months). An other way is to use terminal services, e.g. with the Citrix MetaFrame platform. This platform allows to use any remote applications through the real slow connection (20 kbit/s). In this way students can remotely use any designing tool and any simulation environment, too.

## 6. Asynchronous communication techniques

### 6.1. Electronic mail

The electronic mail is the classic tool of asynchronous communication between users of the Internet network. The correspondents situated in different places and having an access to the network at different time can exchange the letters and information. A letter can be sent to a single person or to a selected group of correspondents. Annexes can be added to the letter in the form of some files with text, pictures, calculations, etc.

The electronic mail is based on the post servers and SMPT protocol. Letters to users are put into personal boxes that each should have a unique address. Popular post programs

(Netscape Messenger, Outlook), operating on the basis of POP3 or IMAP protocols, are used for remote reading or sending of messages. The service of accounts, by the use of interactive WWW services (Hotmail, Yahoo), is also given. E-mail is an easy, quick and rather cheap form of contact between students, lecturers and administration. An electronic mail should be accessible by post boxes of universities and training centres not only for lecturers and administration but also for students. This service should be a part of an educational portal.

### 6.2. News groups and discussion groups

News groups are arranged for publication of advertisements and messages directed at the largest number of recipients. An access to the news server is a condition for participation in news groups. A user must personally connect with a news server and take messages from a selected group. The access to groups may be completely anonymous or controlled and admitted selectively for reading and writing of messages to a specified group. Messages are disseminated by the use of servers through the NNTP protocol. It is rather difficult to speculate about the confidentiality and privacy of a correspondence.

News groups could be successfully used in distance learning for the propagation of the common messages and for exchanging the information between students and lecturers. Discussions groups (or discussion lists) are a form of an electronic mail system for simultaneous transmission of messages to many users. Their proper operation requires some special servers.

In order to participate in a discussion group it is necessary to enter it. Most often it is done by sending a letter with the specified content to the addresses of the discussion group's participants. Discussions list and news group are very popular, but discussion list seems to be more interesting.

### 6.3. Messaging and discussion systems, discussion forums

In web-based education systems special subsystems are created and used for sending, reception, storage and management of messages and news groups. They can replace e-mail and classical news servers in communication between administration, lecturers and students. They are based on WWW interactive applications. Messages subsystems ensure confidentiality protection and privacy for correspondence nearing a classical e-mail, but they do not offer such big functionality as e-mail because they are closed.

In practice all mentioned above asynchronous communication techniques are used in distance learning as a way to communicate with students. The National Institute of Telecommunications uses electronic mail and discussion forums for communication between students and teachers. The servers use the typical software, for example MS Exchange, Qmail, Sendmail, Dnews or MS Internet Information Server. The discussion forum is in practice provided as

part of all distance learning platforms, for example Lotus LearningSpace, WebCT, Top Class.

## 7. Synchronous tools as a support for asynchronous distance learning

### 7.1. A chat

A chat is the simplest form of remote discussion for two or more persons at a distance and at the same time. Exchange of information is based on sending text messages. Quick typing on a computer is very useful. A chat enables to organise virtual class meetings, exchange of questions, answers and comments. It is a good form for improvised distance meetings. Low needs concerning the quality of telecommunication links are its important advantage. Modem connection using 9.6 kbits/s is enough for it.

### 7.2. Audio conferences

In comparison to chats the audio conferences are a more convenient and more natural form of the Internet based meetings. They allow to ask the questions, to discuss material, to solve problems very quickly. Of course the text, pictures and illustrations may be also presented. The audio conferences require better parameters of the communication links, than in case of a chat. Modem connection using 28.8 kbits/s is enough for them.

### 7.3. Audio-video conferences

Audio-video conferences are the most complete method for arranging regular distance lectures. The important disadvantage of audio-video conference is the requirement concerning a very high speed of the communication links. For fluent transfer 384 kbits/s is needed. For this reason a wider use of the audio-video conference technique in the Internet might be necessary in the future.

### 7.4. A white board

A white board is a very interesting form of a group's work at synchronous mode. It enables remote work simultaneously for a few people, concerning the same presentation or application, for instance an editor enabling common writing of notes, formulae, tasks solution. Participants can not only observe performed activities (e.g. marking part of a text) but also can make them themselves. Owing to it, participants can give questions, comments and notices currently, which significantly adds value to this form of work. A white board, (particularly together with chats or audio conferences) is a fine tool for carrying out distance lectures, as well as audio-video conferences. In practice it is even better because it needs significantly smaller speed of connection. In most cases 56 kbits/s modem connection could be enough for it.

All the techniques mentioned above can be used to complete the list of tools for successful distance learning. Chats and audio conferences can be used for an exchange of opinions, solving problems, giving answers for student questions. On a limited scale, lectures can be replaced by the use of audio conferences. The virtual experiments can be carried out by the use of audio-video conferences or a white-board together with a chat or with audio conferences.

Special requirements concerning communications network parameters and high costs of connections are the main reasons that synchronous tools are used on a very limited scale now. It is important that the educational portal should enable synchronous work at least in a chat form, next in an audio conference and white board forms. Possibilities of that kind are offered by a some platforms supporting distance learning (Centra, FirstClass, Learning Space 4).

# 8. Requirements for computer equipment and networks

The present-day education, especially in case of scientific and technical areas, requires the involvement of more and more modern educational equipment. Computer laboratories that should be connected to Internet, arise at universities and schools. The quick development of various techniques, especially in the electronics and informatics, as well as audio-visual technologies bring impetuous changes to telecommunications networks, computer and audio-visual equipment.

Requirements concerning computer equipment and its connection to the Internet network are different and they depend on the level of technologies being used. It is necessary to have at least processor units of Intel Celeron/Pentium III/IV or AMD Duron/Athlon classes with the operating store of about 64/128 MB for the reproduction of advanced multimedia materials. The contemporary PC systems satisfy the above requirements without any problems.

For distance education purposes a computer should be equipped with a sound card and also loudspeakers. For the purpose of carrying out audio and audio-video conferences a microphone and camera are needed. A CD-ROM reader is also necessary to reproduce materials from CDs. Requirements, concerning the band of a communications line for connection with the Internet for the purpose of distance education, also strongly depend on the type of tools being used. Connection cost is also a very important element. The slow lines of 14.4 kbits/s of the analogue modem can be already used for distance learning if it serves only for the an electronic mail, news, discussion groups and for the review of WWW services not very rich in graphics elements and without multimedia elements.

The enlargement of the band to 28.8 or 33.6 kbits/s (analogue modem) allows to review web services rich in graphics, to use chats, audio conferences or even to work on remote servers by the use of a white board. However, the good work conditions are really ensured by the use of line of about 128 kbits/s speed (ISDN, HIS modem, xDSL modems, TV modems). A further increase of connection speed to the 384 kbits/s (xDSL modems, cable, TV modems) will give better comfort of work sufficient for carrying out audio-video conferences.

Now many video conferences are carried out by the use of the ISDN because this solution is not so expensive in comparison with other techniques. The ISDN transmits data almost four times quicker than a modem, so graphics, voice and image are transmitted more quickly in comparison with analogue lines. Video conferences may be also realised in point-to-point and point-to-multipoint communication modes.

The ADSL is a technology for networks that enables broadband and asymmetric access for subscribers to public networks and the Internet. Now the ADSL technology is widely used in distance education in countries that do not have funds for the creation of new optical telecommunications links. Another good solution is using TV modems with the cable TV. This technique has become widely offered in cities as it is cheap and often based on the existing infrastructure.

In academic communities and in companies, distance learning could be based on computer networks. Students could use the Ethernet, Fast Ethernet and even Gigabit Ethernet or ATM technology. Especially the ATM is now one of the most effective technologies of multimedia transfer (voice, image and data) so it is useful for distance learning.

# 9. Conclusions

Multimedia techniques have been developing intensively and together with the Internet are offering new tools for the technology of education. All these new tools have been used for a relatively short time and yet proved their special usefulness in the systems of continuing and distance education. The use of these tools requires knowledge and experience that should be achieved in a very short time, because the development of information technologies seems to be very fast indeed.

# References

[1] D. Minoli, *Distance Learning Technology and Applications*. Boston, London: Artech House, 1996.

[2] T. Kaskine *et al.*, "The great Paella cookbook for online learning", Centro de Formación de Postgrado – CERES Universidad Politecnica de Valencia & Lifelong Learning Institute Dipoli Helsinki University of Technology, Helsinki – Valencia, 1999.

[3] G. Trentin, "Internet: does it really bring added value to education", *Int. J. Educ. Telecommun.*, vol. 2, no. 2/3, pp. 97–106, 1996.

[4] A. G. Picciano, "Developing an asynchronous course model at a large urban university", *J. Asynchr. Learn. Netw.*, vol. 2, issue 1, March 1998.

[5] D. Minoli and R. Keinath, *Distributed Multimedia Through Broadband Communication Services*. Norwood, M.A.: Artech House, 1994.

[6] K. Eichin and G. Soder, "Education and multimedia – interactive teachware for communications engineering", *Int. J. Electron. Commun.*, May 1999.

[7] B. A. Galwas, M. Pajer, and J. Chęć, "Model of e-book for distance learning courses", *J. Telecommun. Inform. Technol.*, no. 2, pp. 46–50, 2001.

[8] S. U. Egarievwe *et. al.*, "Internet application of LabVIEW in computer based learning", http://www1.nks.no/eurodl/icl2000/egarievwe

[9] H. Wupper and V. Kokits, "Interactive multimedia applications for online courses in electronics", Fachbereich Elektrotechnik, Jahresbericht 1999, Annual Report, FernUniversität, Gesamthochschule in Hagen, Germany, pp. 99–103, 1999.

[10] C. Röhrig and A. Jochheim, "Browser-based remote access to laboratory experiments", Fachbereich Elektrotechnik, Jahresbericht 1999, Annual Report, FernUniversität, Gesamthochschule in Hagen, Germany, 1999.

[11] http://www.okno.pw.edu.pl

[12] http://www.retwine.net

**Mariusz Pajer** received the M.Sc. Eng. degree in computer engineering from the Warsaw University of Technology (WUT), Warsaw, Poland, in 1999. In 1997 he joined the National Institute of Telecommuniactions (NIT), Warsaw, Poland when he has been working in IT Center in field of data bases, computer networks and WWW. From 1997 he has been working in WUT as network administrator. In 2000 he joined the SPRiNT, Open and Distance Learning (ODL) program, in WUT when he has been working in field of designing and developing course materials and educational portal. From 2000 he has been co-working whith Training Center in NIT in field of ODL. His main interests are information systems, ODL and computer networks.
e-mail: M.Pajer@itl.waw.pl
National Institute of Telecommunications
Szachowa st 1
04-894 Warsaw, Poland

**Jolanta Chęć** received the M.Sc. degree in electronic engineering (speciality Automatics and Informatics) from the Technical University in Gdańsk. Now she works in the National Institute of Telecommunications (NIT) in Gdańsk (Poland) as a senior specialist. Her research activity is concentrated on information and communication technology (ICT). Since 1994 she has been a member (expert) in the Problem Commission (for Computer Networks and Software) of the Polish Committee for Standardization. In 1995–1996 she took part (research and analytic works) in the international COPERNICUS 1044/STEP Project coordinated by ETSI (European Telecommunications Standards Institute). She is the author of more than twenty published scientific paper (for conferences, symposia, scientific magazines).
e-mail: jolac@il.gda.pl
National Institute of Telecommunications
Jaśkowa Dolina st 15
80-252 Gdańsk, Poland

**Bogdan A. Galwas** – for biography, see this issue, p. 20.

# ICTON 2002

# IEEE Networking the World

# COST

# PCIC

## 4th International Conference on Transparent Optical Networks

### Co-located with: European Symposium on Photonic Crystals ESPC 2002

### CALL FOR PAPERS – Second Announcement

The National Institute of Telecommunications in Warsaw, Department of Transmission and Fibre Technology, and IEEE/LEOS Poland Chapter are pleased to announce the 4th **International Conference on Transparent Optical Networks ICTON 2002**, which will be held at the National Institute of Telecommunications, 1 Szachowa Street, Warsaw, Poland, **April 21-25, 2002**. ICTON 2002 will be technically co-sponsored by the IEEE Lasers and Electro-Optics Society. European Projects COST P2: "Applications of Non Linear Optical Phenomena" and COST 266: "Advanced Infrastructure for Photonic Networks" are associated with the organisation of the Conference. The **European Symposium on Photonic Crystals ESPC 2002** will be organised as a part of ICTON 2002 in association with COST 268: "Wavelength Scale Photonic Components for Telecommunications" Project.

The following European events will be co-located with ICTON 2002:
COST 266 Management Committee Progress Meeting & Workshop on All-Optical Routing, April 22-23, 2002
PCIC Review Meeting on April 23, 2002
COST 268 Working Group and Management Committee Meeting, April 24-27, 2002, with ESPC as a part of WG2 activities.

An **exhibition** of photonic telecommunication industry is planned with the Conference.

**The scope of the Conference** is concentrated on the applications of all-optical technology in transparent networks, systems and components, and includes:

- Terabit Transport Networks
- Ultra-dense WDM transmission
- Optical time domain multiplexing
- Wavelength conversion
- Soliton transmission
- Dispersion management and compensation
- Polarisation Mode Dispersion
- Optical amplifiers
- New fibre types
- New transmission windows
- New light sources
- Fibre gratings
- Arrayed waveguide gratings
- **Photonic Band-Gap structures (ESPC)**

- VCSELs
- All-optical signal regeneration
- All-optical signal processing
- Optical switching
- Optical memory and data storage
- Non-linear waveguide optics
- Analogue transmission systems
- Broadband access networks
- Optical transmission of microwaves
- Modelling of optical systems and components
- Standardisation of optical networks
- IP over WDM
- Network migration

Authors are cordially invited to send their **contributions** (4 pages in electronic form, Word 6.0 or later version accompanied with PDF version) for Regular Sessions and Poster Session to the Organising Committee by **February 28, 2002**. The authors will be notified on the acceptance by March 15, 2002. **Post-deadline contributions** with very recent results are solicited until **April 2, 2002**.

ICTON 2002 Organising Committee:
Marian Marciniak, Doctor of Sciences – Chairman
National Institute of Telecommunications
Department of Transmission and Fibre Technology
Szachowa 1, 04-894 Warsaw, Poland
Tel: (+48 22) 812 00 72, fax: (+48 22) 512 83 47
E-mail: ICTON@ITL.WAW.PL , http://www.itl.waw.pl/icton/

ICTON 2002 Scientific Committee:
Prof. Andrzej P. Wierzbicki – Chairman
National Institute of Telecommunications
Szachowa 1, 04-894 Warsaw, Poland

# ICTON 2002

**4th International Conference on Transparent Optical Networks**, April 21 – 25, 2002
**COST 266 & Workshop on All-Optical Routing: WAOR**, April 22 - 23
**European Symposium on Photonic Crystals: ESPC 2002**, April 24 – 25
**COST 268 Working Group and Management Committee Meeting**, April 25 - 26

**National Institute of Telecommunications, 1 Szachowa Street, Warsaw, Poland**

## Conference Registration Form

Title (Prof./Dr/Mr/Ms): ....................................................................................................

Family name:.......................................................... First name:............................................

Company:..............................................................................................................................

Address:...............................................................................................................................

City:........................................Zip Code:.........................Country:...................................

Phone:...............................Fax:.........................E-mail...................................................

Accompanying person name:.............................................................................................

| REGISTRATION FEE | | | | |
|---|---|---|---|---|
| | | Before March 21 | After March 21 | Amount EUR |
| **ICTON** WAOR | Regular | 160 EUR | 180 EUR | |
| | Students and Ph.D. Students (*) | 80 EUR | 90 EUR | |
| **ICTON** ESPC | Regular | 160 EUR | 180 EUR | |
| | Students and Ph.D. Students (*) | 80 EUR | 90 EUR | |
| **ICTON** WAOR+ESPC | Regular | 280 EUR | 300 EUR | |
| | Students and Ph.D. Students (*) | 140 EUR | 150 EUR | |
| ☐ | COST 268 Meeting | 60 EUR 40 EUR (When attending ICTON and/or ESPC) | | |
| ☐ | Conference Dinner on Wednesday | 30 EUR/person | | |

(*) Students must include a statement from their department head affirming their status of full-time students.

| | | | |
|---|---|---|---|
| ☐ | Accompanying person (social programme) | 50 EUR | |

## Social Programme
**Included in the registration fee for participants** *Please tick as appropriate*

☐ I would like to attend the guided tour around Warsaw on Sunday, 21 April
☐ I would like to attend the Welcome Reception on Sunday, 21 April
☐ I would like to attend the Barbecue Party on Monday, 22 April
☐ I would like to attend the Concert on Tuesday, 23 April

| | |
|---|---|
| *REGISTRATION* **Total (EUR)** | |

## Payment:
The payment can be made by:

☐ **bank transfer**, payable to: **Instytut Lacznosci (ICTON)**
        Bank Przemyslowo Handlowy PBK S.A. III Oddzial
        00-950 Warszawa, ul.Krucza 24/26,
        **Account No 11101053-401050000426**

☐ **bank cheque**, payable to **Instytut Lacznosci (ICTON), 04-894 Warszawa, ul. Szachowa 1, Poland**

  (*Copy of the bank transfer to be mailed or faxed to the Organising Committee*)

========================================================================

Date...................... Signature...........................................

**Please fill in and mail or fax as soon as possible to:**

ICTON 2002 Organising Committee, Marian Marciniak, Doctor of Sciences – Chairman, E-mail: ICTON@ITL.WAW.PL
National Institute of Telecommunications, Szachowa 1, 04-894 Warsaw, Poland, Fax: + 48 (22) 5128 347, Tel.: + 48 (22) 8120 072

# INFORMATION FOR AUTHORS

The *Journal of Telecommunications and Information Technology* is published quarterly. It comprises original contributions, both regular papers and letters, dealing with a broad range of topics related to telecommunications and information technology. Items included in the journal report primary and/or experimental research results, which advance the base of scientific and technological knowledge about telecommunications and information technology.

The *Journal* is dedicated to publishing research results which advance the level of current research or add to the understanding of problems related to modulation and signal design, wireless communications, optical communications and photonic systems, speech devices, image and signal processing, transmission systems, network architecture, coding and communication theory, as well as information technology. Suitable research-related manuscripts should hold the potential to advance the technological base of telecommunications and information technology. Tutorial and review papers are published by invitation only.

Papers published by invitation and regular papers should contain up to 15 and 8 printed pages respectively (one printed page corresponds approximately to 3 double-space pages of manuscript, where one page contains approximately 2000 characters).

*Manuscript*: An original and two copies of the manuscript must be submitted, each completed with all illustrations and tables attached at the end of the papers. Tables and figures have to be numbered consecutively with Arabic numerals. The manuscript must include an abstract limited to approximately 100 words. The abstract should contain four points: statement of the problem, assumptions and methodology, results and conclusion, or discussion, of the importance of the results. The manuscript should be double-spaced on only one side of each A4 sheet (210 × 297 mm). Computer notation such as Fortran, Matlab. Mathematica etc., for formulae, indices, etc., is not acceptable and will result in automatic rejection of the manuscript. The style of references, abbreviations, etc., should follow the standard IEEE format.

*References* should be marked in the text by Arabic numerals in square brackets and listed at the end of the paper in order of their appearance in the text, including exclusively publications cited inside. The **reference entry** (correctly punctuated according to the following rules and examples) **has to contain**.

From journals and other serial publications: initial(s) and second name(s) of the author(s), full title of publication (transliterated into Latin characters in case it is in Russian, possibly preceded by the title in Russian characters), appropriately abbreviated title of periodical, volume number, first and last page number, year. E.g.:

[1] Y. Namihira, "Relationship between nonlinear effective area and modefield diameter for dispersion shifted fibres", *Electron. Lett.*, vol. 30, no. 3, pp. 262–264, 1994.

From non-periodical, collective publications: as above, but after title – the name(s) of editor(s), title of volume and/or edition number, publisher's name and place of edition, inclusive pages of article, year. E.g.:

[2] S. Demri, E. Orlowska, International nnuumtihity. Abstract models verses concrete models" in *Fuzzy Set,*

*Logics and Reasoning about Knowledge*, D. Dubois and H. Prade, Eds. Dordrecht: Kluwer, 1999, pp. 301–314.

From books: initial(s) and name(s) of the author(s), place of edition, title, publisher(s), year. E.g.:

[3] C. Kittel, *Introduction to Solid State Physics*. New York: Wiley, 1986.

*Figure captions* should be started on separate sheet of papers and must be double-spaced.

*Illustration*: Original illustrations should be submitted. All line drawings should be prepared on white drawing paper in black India ink. Drawings in Corel Draw and Postscript formats are preferred. Colour illustrations are accepted only in exceptional circumstances. Lettering should be large enough to be readily legible when drawing is reduced to two- or one-column width – as much as 4:1 reduction from the original. Photographs should be used sparingly. All photographs must be gloss prints. All materials, including drawings and photographs, should be no larger than 175 × 260 mm.

*Page number*: Number all pages, including tables and illustrations (which should be grouped at the end), in a single series, with no omitted numbers.

*Electronic form*: A floppy disk together with the hard copy of the manuscript should be submitted. It is important to ensure that the diskette version and the printed version are identical. The diskette should be labelled with the following information: a) the operating system and word-processing software used, b) in case of UNIX media, the method of extraction (i.e. tar) applied, c) file name(s) related to manuscript. The diskette should be properly packed in order to avoid possible damage during transit.

Among various acceptable word processor formats, TeX and LaTeX are preferable. The *Journal's* style file is available to authors.

*Galley proofs*: Proofs should be returned by authors as soon as possible. In other cases, the article will be proof-read against manuscript by the editor and printed without the author's corrections. Remarks to the errata should be provided within two weeks after receiving the offprints.

*The copy of the „Journal"* shall be provided to each author of papers.

*Biographies and photographs* of authors are printed with each paper. Send a brief professional biography not exceeding 100 words and a gloss photo of each author with the manuscript.